

Physiological effects of trading fatty acids between organellar membranes in salt-treated Arabidopsis seedlings

Dissertation

Zur Erlangung des

Doktorgrades der Naturwissenschaften (Dr. rer. nat.)

der Naturwissenschaftlichen Fakultät I – Biowissenschaften –

der Martin-Luther-Universität

Halle-Wittenberg,

vorgelegt von

Frau Monique Matzner

Geb. am 24.04.1993 in Magdeburg

Gutachter: Prof. Dr. Ingo Heilmann
Prof. Dr. Kristina Kühn
PD. Dr. Rochus B. Franke

Eingereicht am: 14.03.2023

Tag der Verteidigung: 22.06.2023

Table of Contents

Table of Contents	II
Abbreviations	V
Figures	VIII
Tables	X
Summary	XII
Zusammenfassung	XIII
1. Introduction	1
1.1. The complex subcellular organization of plant cells.....	1
1.1.1. Examples for cross-organelle exchange of substances and information in plants.....	5
1.1.2. Cellular membranes control communication and dynamics of plant cell compartments...7	
1.2. Plastidial and extraplastidial membranes differ in their lipid composition.....	8
1.2.1. Plastidial and extraplastidial fatty acid desaturases.	13
1.2.2. <i>Arabidopsis fad</i> mutants prove the exchange of fatty acids between organelle membranes.	15
1.2.3. The role of fatty acid unsaturation in membrane function.	17
1.2.4. Mechanisms for exchange of fatty acids and lipids between cellular membranes.	18
1.3. Photosynthesis as a membrane-localized process	22
1.4. Physiological effects of salt stress in <i>Arabidopsis</i>	24
1.4.1. Effects of salt treatment on photosynthesis.	25
1.4.2. Salt stress can induce dynamic changes in plant membrane biology.....	26
1.4.3. Effects of salt stress on the plasma membrane and other cellular membranes.	26
1.4.4. Membrane lipid unsaturation is important for plant salt tolerance.....	27
1.4.5. Vesicular trafficking and membrane contact sites during salt treatment.	28
1.4.6. Open questions on the links of fatty acid metabolism and plant physiology.	29
1.5. The aims of this work	29
2. Material and Methods	31
2.1. Material	31
2.1.1. Chemicals.....	31
2.1.2. Equipment	31

2.1.3. Single-use Materials	33
2.1.4. Software	33
2.1.5. Plant lines	34
2.2. Methods	35
2.2.1. Sterilization of plant seeds	35
2.2.2. Plant growth conditions	36
2.2.3. Salt stress treatment	37
2.2.4. Analysis of membrane lipids.....	38
2.2.5. Quantification of transcript abundance	41
2.2.6. Quantification of chlorophyll and carotenoid contents.....	46
2.2.7. Analysis of photosynthetic parameters.....	46
2.2.8. Determination of the de-epoxidation state of xanthophyll cycle (XC) pigments in Arabidopsis.....	48
2.2.9. Transmission electron microscopy	52
2.2.10. Statistics.....	53
3. Results	54
3.1. Mild salt treatment of Arabidopsis plants changes membrane lipid composition.	54
3.1.1. Perception of low salt concentrations without macroscopic effects on plant growth.....	54
3.1.2. Extraplasmidial and plastidial lipids increase after short-term salt treatment.	59
3.1.3. Bidirectional exchange of polyunsaturated fatty acids between ER and plastids.	66
3.1.4. Salt treatment of ω -3 <i>fad</i> mutants.....	71
3.2. Plastidial and extraplasmidial FADs influence photosynthesis and photoprotection.	77
3.2.1. Altered chlorophyll and carotenoid amounts in <i>fad</i> mutants.....	77
3.2.2. Photosynthetic performance is affected in <i>fad</i> mutants.	79
3.2.3. Salt application has a dose-dependent effect on photosynthesis.	82
3.2.4. The xanthophyll cycle is inhibited in the <i>fad3</i> mutant.....	85
3.3. Reasons for and consequences of changes in membrane lipid levels.	89
3.3.1. <i>fad</i> mutations do not result in massive changes in plastid ultrastructure.	89
3.3.2. Unaltered jasmonic acid levels and responses in the <i>fad3</i> mutant.	93
3.3.3. Salt-induced lipid changes are linked to the induction of plant senescence.	96
4. Discussion	99
4.1. Salt sensitivity of Arabidopsis.	100

4.2. Salt-induced senescence of plants101

4.3. The role of dynamic changes in PC and MGDG upon stress.....103

4.4. Trans-organellar mobilization of membrane lipid intermediates.....105

4.5. Differences of lipid amounts and fatty acid profiles due to plant culture conditions.....110

4.6. Global changes in *fad* mutants, which might also influence photosynthetic parameters. ...111

4.7. Adjustments for Imaging-PAM measurements and light-exposure experiments.112

4.8. Phenotypes of stacked *fad* mutants suggests an influence of trans-organellar lipid exchange on plant performance.114

5. References 118

6. Supplements XV

Acknowledgement – Danksagung..... XXVIII

Curriculum vitae XXX

Erklärung XXXI

Abbreviations

½ MS	0.5 Murashige and Skoog nutrient mix
16:0	palmitic acid
16:1	palmitoleic acid; 16:1 ^{Δ7} ; 16:1 ^{Δ9}
16:2	hexadecadienoic acid; 16:2 ^{Δ7,10}
16:3	hexadecatrienoic acid; 16:3 ^{Δ7,10,13}
18:0	stearic acid
18:1	oleic acid; 18:1 ^{Δ9}
18:2	linoleic acid; 18:2 ^{Δ9,12}
18:3	α-linolenic acid; 18:3 ^{Δ9,12,15}
20:1	gondoic acid, 11-eicosenoic acid; 20:1 ^{Δ11}
ABA	abscisic acid
Ad	latin, filled "up to"
Arabidopsis	<i>Arabidopsis thaliana</i>
ATP	adenosine triphosphate
Ax	antheraxanthin
Bidist.	double distilled
CCV	clathrin-coated vesicles
cDNA	complementary DNA
Chl	chlorophyll
CL	cardiolipin
CoA	coenzyme A
COP	coat protein complex
DAG	diacylglycerol
DB	double bond
DES	de-epoxidation state
DGDG	digalactosyldiacylglycerol
DNA	desoxyribonucleic acid
ER	endoplasmic reticulum
FA	fatty acid
FAB2	stearoyl-ACP-D9-desaturase
FAD	fatty acid desaturase
<i>fad3</i>	<i>fad3-2</i>
<i>fad3-4c</i>	FAD3 complemented, under cauliflower mosaic virus promoter 35S
<i>fad378</i>	<i>fad3 fad7 fad8</i>
<i>fad78</i>	<i>fad7 fad8</i>
FAME	fatty acid methyl ester
FAX1	fatty acid exporter 1

F _v /F _m	maximum quantum yield of photosystem II
GC	gas chromatography
HPLC	high performance liquid chromatography
IEM	inner envelope membrane of plastids
JA	jasmonic acid, jasmonate
JA-Ile	jasmonoyl-isoleucine
JAZ	JASMONATE ZIM-domain
LACS	long-chain acyl-CoA synthetases
LHC	light harvesting complex
MCS	membrane contact sites
MGD1	monogalactosyldiacylglycerol synthase 1
MGDG	monogalactosyldiacylglycerol
MPK6	mitogen-activated protein kinase 6
NaCl	sodium chloride
NADPH	nicotinamide adenine dinucleotide phosphate
NASC	Nottingham Arabidopsis Stock Center
NPQ	nonphotochemical quenching
OEM	outer envelope membrane of plastids
OPDA	12-oxo-phytodienoic acid
PA	phosphatidic acid
PAM	Pulse-Amplitude-Modulation
PAR	photosynthetic active radiation, $\mu\text{mol m}^{-2} \text{s}^{-1}$
PC	phosphatidylcholine
PE	phosphatidylethanolamine
PEAMT	phosphoethanolamine N-methyltransferase
PG	phosphatidylglycerol
PI	phosphatidylinositol
PIP ₂	phosphatidylinositol bisphosphate
PLC	phospholipase C
PS	phosphatidylserine
PS	photosystem
PsbS	photosystem II subunit S
qE	energy-dependent quenching
qi	photoinhibition (NPQ component)
qPCR	quantitative real time polymerase chain reaction
qZ	zeaxanthin-dependent quenching
RNA	ribonucleic acid
ROS	reactive oxygen species
RT	room temperature, 22 °C

<i>sn</i>	stereo specific numbering
SNARE	N-ethylmaleimide sensitive attachment protein receptors
SOS1	salt overly sensitive 1
SQDG	sulfoquinovosyldiacylglycerol
SYT1	synaptotagmin1
TAG	triacylglycerol
TGD	trigalactosyldiacylglycerol complex
TLC	Thin layer chromatography
UBC	Ubiquitin-conjugating enzyme
VDE	violaxanthin de-epoxidase
VIPP1	protein in plastids 1
Vx	violaxanthin
WT	wild type
<i>x g</i>	multiple of the acceleration due to gravity
XC	xanthophyll cycle
Zx	zeaxanthin
ω 3-FADs	omega-3 fatty acid desaturases; FAD3, FAD7, FAD8
ω 6-FADs	omega-6 fatty acid desaturases; FAD2, FAD6

Figures

Figure 1.1.: Structure of a plant cell.....	2
Figure 1.2.: Main classes of membrane lipids.....	9
Figure 1.3.: Plant lipid classes.....	11
Figure 1.4.: Possible geometric shapes of amphiphilic lipids.....	12
Figure 1.5.: Fatty acid desaturation at membranes of ER and plastids of Arabidopsis plants.	15
Figure 1.6.: Vesicular and non-vesicular transport pathway of lipids.....	20
Figure 3.1.: Influence of low salt concentrations on growth of seedlings and transcript level of salt stress marker and genes involved in lipid biosynthesis.	57
Figure 3.2.: Transcript abundance of salt stress marker genes and genes involved in lipid biosynthesis when treated with 100 mM NaCl.....	58
Figure 3.3.: Lipid analysis of extraplastidial and plastidial lipids in WT after treatment with low salt concentrations.....	61
Figure 3.4.: Analysis of the degree of unsaturation of PC and MGDG in WT plants after long-term treatment with low salt concentrations.	63
Figure 3.5.: Analysis of PC and MGDG levels of WT after short-term treatment with 100 mM NaCl.	65
Figure 3.6.: Fatty acid profile in seeds and green tissue of fad mutants.....	67
Figure 3.7.: Comparison of 18:2 ^{Δ9,12} and 18:3 ^{Δ9,12,15} fatty acid levels between WT and fad mutants.	69
Figure 3.8.: Germination and root growth of WT, fad3, fad78 and fad378 seedlings under salt stress.	72
Figure 3.9.: Relative PC and MGDG levels of WT, fad3, fad78 and fad378 seedlings after short-term treatment with low salt concentrations.....	75
Figure 3.10.: Concentration of chlorophyll a, b and carotenoids in fad mutant lines of Arabidopsis.....	78
Figure 3.11.: The active quantum PSII efficiency of different Arabidopsis fad mutants.	80
Figure 3.12.: The nonphotochemical quenching of different Arabidopsis fad mutants.....	81
Figure 3.13.: Photosynthetic parameters of Arabidopsis WT seedlings treated with different salt concentrations.....	83
Figure 3.14.: De-epoxidation of XC-pigments in WT controls and the fad3 mutant after exposure to different light intensities.....	86

Figure 3.15.: De-epoxidation assay under optimal condition with isolated thylakoids from leaves of WT and fad3 seedlings.88

Figure 3.16.: Ultrastructure of chloroplasts from Arabidopsis fad mutants.....91

Figure 3.17.: Expression level of JAZ10 in roots and shoots under unwounded and 1 h past wounding in Arabidopsis WT, fad3 and complemented FAD3-4c line.94

Figure 3.18.: Level of various oxylipin species in WT, fad3, FAD3-4c and JA-deficient mutant fad378.....95

Figure 3.19.: Expression level of senescence marker S40-3 and SAG13 in Arabidopsis WT seedlings after short term treatment with low salt concentrations.....97

Figure 4.1.: Models of the possible interplay of PC and MGDG during the response to salt-induced osmotic stress.....107

Figure 6.1.: Analysis of PC and MGDG levels of WT after long-term treatment with high salt concentrations..... XV

Figure 6.2.: Images of root growth of WT, fad3, fad78 and fad378 seedlings under salt stress.XVII

Figure 6.3.: Development of fad mutant seedlings..... XVIII

Figure 6.4.: Comparison of plant rosettes between fad mutants..... XVIII

Figure 6.5.: Inflorescence state of WT, fad3 and complemented FAD3-4c line.XIX

Figure 6.6.: Impaired development of siliques in fad378 plant line.XIX

Figure 6.7.: Ratio of chlorophyll a to chlorophyll b in different fad mutants.XX

Figure 6.8.: Effect of salt on root growth of Arabidopsis fad mutants compared to WT.XX

Figure 6.9.: Maximum quantum PSII efficiency in Arabidopsis WT and fad mutant seedlings.XXI

Figure 6.10.: Leaf cross sections of WT, fad3, fad78 and fad378.XXII

Figure 6.11.: The comparison of fatty acid species associated to PC between WT, fad3, FAD3-4c and fad378 plant lines.XXIII

Tables

Table 2.1.: Equipment used for this work.	31
Table 2.2.: Single-use materials used in this work.	33
Table 2.3.: Programs used in this work.	33
Table 2.4.: Plant lines analyzed in this work.	34
Table 2.5.: Solutions and media used for cultivation of plants.	35
Table 2.6.: Solutions and buffers used for RNA extraction and proof of quality and quantity.	42
Table 2.7.: Components of cDNA synthesis.	43
Table 2.8.: Reaction mix for qPCR.	44
Table 2.9.: Used qPCR oligonucleotide (primer) combinations.	44
Table 2.10.: qPCR program for determination of transcript abundance.	45
Table 2.11.: Buffer used for thylakoid extraction according to Casazza et al. (2001).	48
Table 2.12.: Media used for preparation and HPLC eluents for pigment separation according to Kraay et al. (1992).	50
Table 2.13.: Linear elution gradient for HPLC separation of thylakoid pigments according to Kraay et al. (1992).	51
Table 2.14.: Data used to calculate pigments according to Lohr (2001).	52
Table 6.1.: Lipid analysis of WT seedlings after treatment with 50 mM NaCl displayed in Figures 3.3. C, D.	XXIV
Table 6.2.: Saturation degree calculated from measured lipid amounts of PC and MGDG displayed in Figure 3.4. B.	XXIV
Table 6.3.: Fatty composition of seeds from fad3 and complemented line FAD3-4c displayed in Figure 3.6. A.	XXIV
Table 6.4.: Basal lipid level of PC and MGDG in fad mutants displayed in Figures 3.6. B, C and 3.7. A, B.	XXV
Table 6.5.: Lipid analysis of fad3 and fad78 mutants after treatment with 50 mM NaCl displayed in Figure 3.9. A.	XXV
Table 6.6.: Saturation degree calculated from measured lipid amounts of PC and MGDG displayed in Figure 3.9. B.	XXV
Table 6.7.: Basal concentration of Chl a, Chl b and Carotenoids in fad mutans displayed in Figure 3.10.	XXV

Table 6.8.: Photosynthetic parameter of WT and fad mutants from low to high light as displayed in Figures 6.7.; 3.11.; 3.12.	XXVI
Table 6.9.: Photosynthetic parameters of WT under normal conditions and treated with either 50 or 100 mM NaCl as displayed in Figure 3.13. A-D.	XXVI
Table 6.10.: Root length of WT and fad mutants under normal conditions and treated with either 50 or 100 mM NaCl as displayed in Figure 6.6.	XXVI
Table 6.11.: Transcript level of various genes after treatment with 50 mM NaCl displayed in Figures 3.1. B-D and 3.19.	XXVII
Table 6.12.: JAZ10 transcript level in roots and shoots in unwounded and wounded seedlings of fad3 and FAD3-4c displayed in Figure 3.17.	XXVII
Table 6.13.: Basal oxylipin concentrations in WT and fad mutants as displayed in figure 3.18.	XXVII
Table 6.14.: Lipid analysis of WT seedlings after treatment with 100 mM NaCl displayed in Figures 3.5.	XXVII

Summary

The survival of plants exposed to stress depends on fast and efficient physiological responses. Environmental stresses are perceived mostly at the plasma membrane, which defines the contact between the cellular and extracellular space. To maintain membrane integrity under environmental stress, membrane lipid composition can be adjusted, and stress-triggered lipid dynamics have previously been studied for different cellular membranes. However, it is currently not well understood how the distribution of lipid intermediates between cellular membranes is globally coordinated. Therefore, experiments in this thesis addressed salt-induced changes in amounts and fatty acid profiles of membrane lipids, focusing on the extraplastidial lipid phosphatidylcholine (PC) and the plastidial lipid monogalactosyldiacylglycerol (MGDG). The content of both MGDG and PC increased in two-week-old *Arabidopsis* seedlings after 2 h of exposure to 50 mM NaCl, and the proportion of the associated polyunsaturated fatty acid 18:3^{A9,12,15} also increased. These changes in membrane lipid composition reflect membrane adjustments to osmotic stress and possibly also salt-induced senescence, as shown by the analysis of marker transcripts. The hypothesis that increased levels of MGDG might supply lipid intermediates for lipid rearrangements in extraplastidial membranes was tested by analyzing fatty acid desaturase (*fad*) mutants, for which such export has previously been shown. Interestingly, seedlings of the *fad3* mutant displayed basally increased levels of MGDG and PC, similar to the increased levels observed in salt-treated WT controls, and there was no further increase upon salt treatment. A link between plastidial and extraplastidial membranes was tested by analyzing the effects of salt treatment or various *fad* mutants on photosynthesis. When grown on salt media, photosynthesis of WT seedlings was inhibited to varying degrees, depending on the salt concentration. By contrast, ω -3 *fad* mutants showed largely no decreases in photosynthesis, except for the triple mutant *fad3 fad7 fad8* and, interestingly, also the *fad3* knockout mutant of the ER localized FAD3, which displayed decreased nonphotochemical quenching (NPQ) under high light intensities. Subsequent analyses revealed that the xanthophyll cycle component of the NPQ was affected in the *fad3* mutant. The data from stress-treatments and mutant analyses demonstrate a trans-organellar effect of ER-based fatty acid unsaturation on specific aspects of thylakoid function, which might be explained by plastidial membrane rearrangements to supply lipid intermediates for the maintenance of extraplastidial membranes, at the expense of thylakoid function.

Zusammenfassung

Schnelle und effiziente physiologische Reaktionen sind wichtig für Pflanzen, wenn diese einem Stress ausgesetzt sind. Umweltbedingte Stresse werden vor allem an der Plasmamembran wahrgenommen, die den Kontakt zwischen dem zellulären und dem extrazellulären Raum darstellt. Um die Membranintegrität unter Stressbedingungen aufrechtzuerhalten, kann die Zusammensetzung der Membranlipide angepasst werden. Diese durch Stress ausgelöste Dynamik von Lipiden konnte bereits für verschiedene zelluläre Membranen untersucht werden, allerdings ist noch nicht bekannt, wie die Verteilung von Lipid-Intermediaten zwischen den Zellmembranen global koordiniert wird. Die Experimente in dieser Arbeit befassten sich daher mit salzinduzierten Veränderungen der Mengen und Fettsäureprofile von Membranlipiden, wobei der Schwerpunkt auf dem extraplastidären Lipid Phosphatidylcholin (PC) und dem plastidären Lipid Monogalactosyldiacylglycerol (MGDG) lag. Die Behandlung mit 50 mM NaCl führte in zwei-Wochen-alten Arabidopsis-Keimlingen nach 2 h zu einem Anstieg der Mengen an MGDG und PC und dem Anteil der damit veresterten mehrfach ungesättigten Fettsäure 18:3^{Δ9,12,15}. Diese Veränderungen in der Zusammensetzung der Membranlipide sind Teil der Reaktion auf den osmotischen Stress und möglicherweise auch salzinduzierter Seneszenz, wie die Analyse von Marker-Transkripten zeigt. Die Hypothese, dass erhöhte MGDG-Mengen Lipid-Intermediate für Lipidumverteilungen in extraplastidären Membranen liefern könnten, wurde durch die Analyse von Fettsäuresaturase (*fad*) Mutanten getestet, für die ein solcher Export bereits nachgewiesen wurde. Interessanterweise wiesen Keimlinge der *fad3* Mutante im Grundzustand erhöhte MGDG- und PC-Konzentrationen auf, die den erhöhten Konzentrationen in salzbehandelten WT-Kontrollen ähnelten und bei Salzbehandlung nicht weiter anstiegen. Eine Verbindung zwischen plastidären und extraplastidären Membranen wurde getestet, indem die Auswirkungen einer Salzbehandlung oder verschiedener *fad* Mutanten auf die Photosynthese untersucht wurden. Die Photosynthese von WT-Keimlingen wurde auf Salzmedien in Abhängigkeit von der Salzkonzentration unterschiedlich stark gehemmt. Im Gegensatz dazu zeigten ω 3-*fad* Mutanten weitgehend keine Verringerung der Photosynthese, mit Ausnahme der Dreifachmutante *fad3 fad7 fad8* und interessanterweise auch der *fad3 knockout* Mutante des im ER lokalisierten FAD3, die bei hohen Lichtintensitäten ein verringertes nichtphotochemisches Quenching (NPQ) zeigte. Weitere Analysen ergaben, dass die Xanthophyllzyklus-Komponente des

NPQ in der *fad3* Mutante beeinträchtigt war. Die Daten aus Stressbehandlungen und Mutantanalysen zeigen einen trans-organellen Effekt der ER-basierten Fettsäure-Unsättigung auf spezifische Aspekte der Thylakoidfunktion, der durch plastidäre Membranumverteilungen zur Bereitstellung von Lipid-Intermediaten für die Aufrechterhaltung extraplastidäre Membranen auf Kosten der Thylakoidfunktion erklärt werden könnte.

1. Introduction

1.1. The complex subcellular organization of plant cells.

Since the emergence of cellular life, no less than four billion years ago, progressive evolution has shaped cell types with increasing complexity. The eukaryotic cells forming the smallest autonomous building blocks of animals, fungi and plants contain a nucleus and numerous subcellular compartments. This basic structure has stood the test of time and is retained in all multicellular eukaryotic organisms to this day. Multicellular organisms include most animal and plant species with tissues made of specialized cells that fulfil different physiological functions. What all these tissues have in common, however, is that their cells contain similar sets of organelles that enable basic metabolism and energy processing. In addition to a basic structure which is mostly shared with animal cells, plant cells contain plastids as specialized organelles for photosynthesis and some other plant-specific metabolic processes, making plant cells the most complex of all cells structurally. The main research goal of this thesis regards the mechanisms by which substances are exchanged between plant cell organelles. Firstly, the relevant plant organelles will be briefly introduced in the following paragraphs.

The basic cellular organization of a plant cell is illustrated in Figure 1.1. A central organelle for any eukaryotic cell is the nucleus which is delimited by a double bilayer and contains pores that allow rapid and selective exchange of nucleus-specific and small proteins and RNA (Heldt and Piechulla, 2015). Within the nuclear envelope resides the DNA with the nuclear genome. The set of transcribed genes differs between tissues and changes to respond specifically to stress (Shaw and Brown, 2012).

In close proximity to the nucleus is the endoplasmic reticulum (ER) which can be divided into two different types and places of functions: rough ER and smooth ER. While the rough ER is located closely around the nucleus and temporarily attached with ribosomes as the site of biosynthesis of ER-residing or secreted proteins, the smooth ER spans the volume of the cell in a network-like pattern (Heldt and Piechulla, 2015). Synthesized proteins channeled into the ER lumen can be destined for ER residence or directed to the Golgi for modification and distribution by vesicles of the secretory pathway. The smooth ER supplies membrane components for the maintenance of the cellular membrane system such as the assembly of glycerolipids and the modification of fatty

acids by fatty acid desaturases (FADs). The ER is also the site of synthesis of other important membrane lipid compounds such as phytosterols and intermediate products of sphingolipid (ceramide) synthesis (Li-Beisson et al., 2010). Depending on the tissue, specialized organelles, such as oil bodies (also called oleosomes or lipid droplets) can transiently derive from the ER membrane and serve as reservoirs for oil or other lipids (Greer et al., 2020).

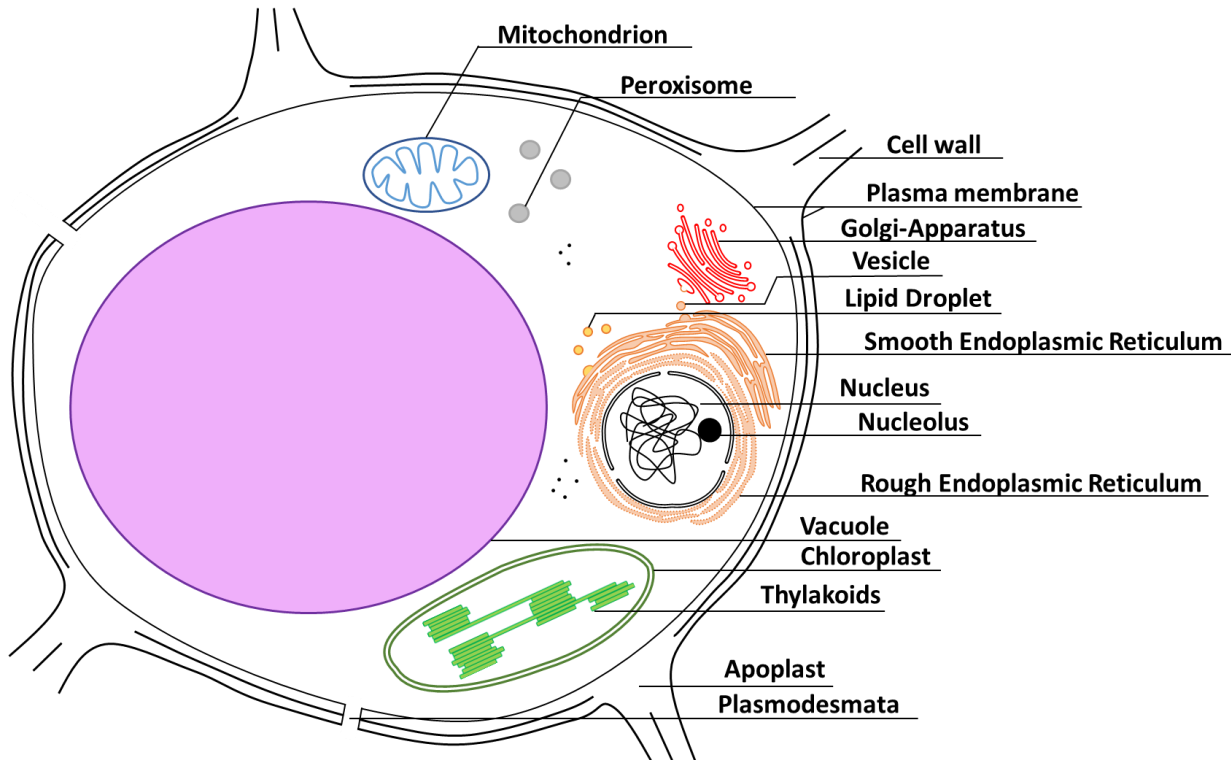


Figure 1.1.: Structure of a plant cell.

Schematic structure of plant cell in green tissue. The illustrated organelles are described in more detail in the main text.

The smooth ER is in contact with the Golgi apparatus and is receiving and collecting the protein cargo from the ER for protein modification, such as glycosylation. Vesicles filled with proteins are split off and distributed to the target sites such as plasma membrane and vacuole (Heldt and Piechulla, 2015). In addition, the Golgi is also involved in important intermediate steps in the biosynthesis of sphingolipids, which are membrane components of ER and plasma membrane (Li-Beisson et al., 2010). Along with the ER, the Golgi is an important element of the secretory pathway, and enables the posttranslational modification and distribution of nuclear-encoded membrane proteins from their site of biogenesis to various membrane systems in the cell, or to the cell surface.

The plasma membrane represents the physiological barrier of every cell and limits the diffusion of water-soluble elements between the inside and outside of the cell. Therefore, it is above all the site of selective and controlled exchange of macromolecules, ions and water by proteins integrated in or associated with the membrane (Heldt and Piechulla, 2015). As the outermost border of the cell, the plasma membrane separates the extracellular apoplastic space and the intracellular cytoplasm where the organelles are located. It is often the first place in which signaling molecules or environmental stresses are recognized, such as pathogens or salt.

Plant cells are encompassed by the cell wall which consists mainly of cellulose but also in smaller amounts of pectin and glycoproteins. The cell wall determines shape and stability of the cell which would otherwise burst due to the internal "turgor" pressure of the vacuole (Schopfer and Brennicke, 2010).

The plant vacuole is a multifunctional organelle and can occur in several small vacuoles or as one central vacuole that takes up about 80 % of the cell volume, depending on the tissue and developmental stage (Marty, 1999). One important physical function of the vacuole is the maintenance of cell turgor which is the driving force for the vital rigidity of the vegetative organs created by the uptake of water, exerting counterpressure against the cell wall. Water uptake and turgor occur through the accumulation of ions and organic acids, which are osmotically active. The vacuole contains not only these factors but can also store diverse other molecules (Marty, 1999). For instance, vacuoles can serve to detoxify the cell, help control redox homeostasis or accumulate pigments, such as anthocyanins during stress. Furthermore, they can contain lytic enzymes for the recycling of proteins, nucleic acids or carbohydrates, which is important especially during senescence (Biswal et al., 2013).

As a common component of metabolic processes of plant cells, such as photosynthesis, H_2O_2 is produced as a toxic by-product, which is directly degraded by catalases to H_2O in peroxisomes (Heldt and Piechulla, 2015). Peroxisomes are involved in several primary metabolic processes, but can be mainly divided into two tissue-specific forms: in vegetative tissues, peroxisomes serve as a node in the plastid-mitochondrial photorespiratory mechanism to convert glycolate to glycine; in oil-rich seeds, glyoxysomes are the site of the glyoxylate cycle where among others fatty acids are degraded by β -oxidation to provide the basis for the formation of all other biomolecules during germination (Hu et al., 2012; Li-Beisson et al., 2010). Peroxisomes are also the site of

intermediate steps for the synthesis of the phytohormones auxin (indole-3-acetic acid, IAA) and jasmonic acid (JA, Schaller et al., 2004; Hu et al., 2012).

In contrast to the previously mentioned elements of the plant cell, mitochondria and plastids are semi-autonomous due to their evolutionary origin as endosymbiotic organelles and contain their own DNA and ribosomes to synthesize some of their proteins autonomously. In mitochondria, the double membrane separates two further compartments from the cytosol - the matrix (inner compartment) and the intermembrane space - which are required for respiration and ATP formation by oxidative phosphorylation through protein complexes localized in the inner mitochondrial envelope membrane (Heldt and Piechulla, 2015). The membranes are not only composed of phosphoglycerolipids, which also form most of the other organellar membranes, but contain diphosphatidylglycerol (cardiolipin, CL) that is found exclusively in mitochondria (and in bacterial membranes) and is thought to improve curvature properties (Ikon and Ryan, 2017). The oxidative respiratory system in the inner membrane and the tricarboxylic acid cycle in the matrix are important ways to generate energy in form of ATP to provide energy for reactions all over the cell (Schopfer and Brennicke, 2010).

Unlike mitochondria, which often have the same shape and function, plastids can differ in size shape and abundance, depending on the type of tissue of a plant (Sakamoto et al., 2008). Plastids are surrounded by two envelope membranes: an outer envelope (OEM) and an inner envelope (IEM) defining an inter-membrane space as well as the inner plasmatic space called stroma. Thylakoids are membrane compartments inside the stroma that derive from the inner envelope membrane. Thylakoids hold the photosynthetic protein complexes to fix light energy into NADPH and ATP to assimilate CO₂ and form carbohydrates in the stroma (Schopfer and Brennicke, 2010). It is important to note that photosynthesis is not the only essential physiological task of plastids, but also serve as the sites of biosynthesis of fatty acids, phytohormones, aromatic amino acids and many intermediates of plant secondary metabolism (Sakamoto et al., 2008).

In sum, each cellular compartment has its physiological tasks, and compartmentalization ensures controlled metabolic reactions without mutual interference. However, the compartmentalization also means that compounds must be exchanged between organelles, relying on specific functional transport mechanisms.

1.1.1. Examples for cross-organellar exchange of substances and information in plants.

Communication and exchange between organelles is an essential requirement for plant metabolism, but also the key for successful recognition of and response to environmental challenges. As mentioned above, the production of cellular compounds regularly involves more than one organelle. Therefore, intermediates must often pass organellar membranes with the help of specific transporters, channels or pores in combination with different transport mechanisms. For instance, photorespiration involves ribulose 1,5-bisphosphate carboxylase-oxygenase (RubisCO)-mediated oxygenation of ribulose 1,5-bisphosphate in the plastid and the formed 2-phosphoglycolate is detoxified in a recycling journey involving peroxisome and mitochondrion, arriving on the same pathway back to the chloroplast as newly formed 3-phosphoglyceric acid for use in Calvin cycle (Bauwe et al., 2010). While this recycling process deprives the cell of energy and loses one fixated CO₂, the cross-organellar interactions with other important cellular processes, such as nitrogen assimilation and respiration, provide a metabolic advantage nonetheless (Dutilleul et al., 2003; Schjoerring et al., 2006).

The secretory pathway of proteins is another example for cross-organellar exchange and involves the ER, the Golgi, and various target membranes, such as the plasma membrane. As a place of protein biosynthesis, the ER controls correct protein folding and the assembly of membrane-integral protein complexes. The transport of proteins from the ER to Golgi is mediated by proteins coating the vesicles containing protein cargo. Proteins, released into Golgi lumen after fusion of vesicles with Golgi membrane, are glycosylated and sorted for further vesicle-dependent or independent trafficking pathways to other organelles or back to the ER (Liu and Li, 2019). Especially the vesicle exchange between ER and Golgi appears to be important for maintenance for cellular homeostasis (Pastor-Cantizano et al., 2018).

The ER also acts in close cooperation with plastids for the production of membrane lipids. The main hydrophobic elements in all glycerolipids are fatty acids. The biosynthesis of all FAs with chain lengths of 16 or 18 carbons takes place by fatty acid synthase (FAS) in the plastids. Still in the plastid, the fatty acid stearic acid (18:0, where the 18 indicates the carbon chain length and the 0 the number of double bonds) is desaturated to oleic acid (18:1^{Δ9}, where the Δ9 indicates the position of the single double bond after the 9th carbon counted from the carboxyl end). The

18:1^{Δ9} (18:1) is the main fatty acid exported from chloroplasts to the ER, where it becomes esterified to the glycerol back bone of phosphatidylcholine (PC; Bates et al., 2007). Monounsaturated fatty acids, such as 18:1 can be further desaturated by the fatty acid desaturases FAD2 and FAD3 localized at the ER, introducing Δ^{12} and Δ^{15} double bonds into the acyl chain, respectively. Upon modification in the ER, fatty acids are distributed throughout all cellular membranes, including some transport back into the plastids. While different membrane lipids or their derivatives are being discussed to partake in this transport between organelles (PC, lyso-PC, phosphatidic acid - PA or diacylglycerol - DAG), the nature of the fatty acid species transported, and the exact mechanism are still unknown. As a result of the interplay between plastids and ER during lipid biosynthesis, typical eukaryotic glycolipids contain combinations of 18:0 or 18:3^{Δ9,12,15} (18:3) at the *sn*-2 position (Kalisch et al., 2016).

All these examples suggest that metabolism requires different organelles to associate closely to allow for an efficient, rapid and controlled exchange of intermediates. Environmental changes can additionally challenge the metabolism of plant cells and perturb the balance of organellar exchange of metabolites, and it is well-established that the recognition of external stimuli not only triggers signaling cascades involving calcium (Ca^{2+}) or reactive oxygen species (ROS), but also the production of phytohormones and specialized signaling lipids, thus changing the lipid composition of membranes. Therefore, it is important to consider the modes by which environmental stresses can be perceived and transduced in plant cells.

The apoplastic space, vacuole and ER lumen contain high concentrations of Ca^{2+} (Stael et al., 2012), which contrasts with the negligible amounts of Ca^{2+} in the cytosol of plant cells. Changes in cytosolic Ca^{2+} levels are perceived by Ca^{2+} -binding proteins, which upon binding Ca^{2+} can interact with other proteins (e.g. Calmodulin, CaM), mediate their phosphorylation (e.g. calcium dependent protein kinases, CDPKs) or exert effects on cellular membranes (e.g. synaptotagmin, Syt), changes in calcium concentration lead to responses to biotic and abiotic stress (Tuteja and Sopory, 2008a; Saheki and Camilli, 2017; Klimecka and Muszyńska, 2007). The release of Ca^{2+} from extracellular or intracellular stores is thought to involve stretch-activated (mechanosensitive) Ca^{2+} channels or the stress-dependent production of second messengers such as inositol polyphosphates, which might be released from membrane lipids by phospholipase C (PLC), as has been described for animal cells (Tuteja and Mahajan, 2007; Tuteja and Sopory, 2008b).

Jasmonates (JA) are important phytohormones produced rapidly after wounding and herbivory (Wasternack, 2017). They are also involved in developmental processes, such as pollen maturation. The biosynthesis of jasmonates starts with the modification of polyunsaturated fatty acids from plastidial glycolipids, mostly from monogalactosyldiacylglycerol (MGDG), 16:3^{Δ7,10,13} (16:3) and 18:3. Several transformation steps are required at the plastidial IEM for the production of jasmonic acid (JA) until 12-oxo-phytodienoic acid (OPDA) is formed (Wasternack and Hause, 2013). This precursor is exported to peroxisomes and is assumed to play a direct role in defense mechanisms and gene expression in the nucleus (Stintzi et al., 2001). In peroxisomes, additional steps lead to the formation of JA and its subsequent export to the cytosol to form jasmonoyl-isoleucine (JA-Ile), which is involved in control of JA responsive genes, and even more derivatives (Vick and Zimmerman, 1984; Schaller et al., 2004).

All these examples from metabolism or signaling have in common that compounds are exchanged that have to cross organellar borders and that the exchange has to be controlled by membrane-bound transport mechanisms between the respective organelles. To better understand these processes, the nature of cellular membranes has to be considered.

1.1.2. Cellular membranes control communication and dynamics of plant cell compartments.

Membranes are barriers that employ numerous integrated or associated proteins for substrate transport through organellar membranes. The function of these proteins is often influenced by the membrane lipid composition. Within membranes, lipids are in fact not equally distributed but can form domains in which certain lipids occur preferentially (Harayama and Riezman, 2018). The size of such domains can vary, and they are termed *membrane regions* with diameters > 10 μm, *microdomains* at diameters up to 10 μm, or *nanodomains* at diameters around or below 1 μm. Membrane lipids define the properties of membranes with regard to their fluidity, charge, curvature and permeability. Even though individual biophysical properties, such as the saturation state of membrane lipids, can lead to a closer arrangement of lipid types, the properties of membranes are a result of the distribution of various elements within membranes and are dependent on lipids and proteins in a cooperative way (Yu et al., 2020b). At the plasma membrane

it is assumed that lipid microdomain-associated proteins like remorins or flotillins can help to organize receptor like kinases within membrane microdomains (Jaillais and Ott, 2020). In rice, OsRemorin4.1 can interact with the receptor kinase OsSERK1 (Somatic Embryogenesis Receptor Kinase) and prevent it from entering certain lipid microdomains (Gui et al., 2016). The microdomains within membranes can be regulated by actin-binding proteins and thus by the cytoskeleton. The attachment of cytoskeletal structures to cellular membranes is not only important for membrane structure but provides an important link to organellar dynamics (Viola and Gupta, 2007). Organelle movement is important for cell growth, development and response to light stimuli and pathogens (Caplan et al., 2015; Savaldi-Goldstein and Chory, 2008; Wada, 2016). The movement of organelles along organellar "track" is mediated by motor proteins, such as myosins. Myosin-driven organellar movement on the actin cytoskeleton is dependent on the interaction of myosin with anchoring proteins on the outside of the membrane of each organelle. The Arabidopsis genome encodes 13 different myosin class XI protein isoforms to ensure specific organelle movement, and these proteins overlap in their function to secure organellar movement under varying conditions. It is not clear how myosin recruitment is regulated, at the level of myosin itself or through the proteins anchored in organellar membranes (Perico and Sparkes, 2018). As the composition of proteins in within membranes change upon stress or according to developmental cues, and these changes are in a part regulated by membrane lipid composition, the lipids must be adjusted in advance.

1.2. Plastidial and extraplastidial membranes differ in their lipid composition.

As stated above, the membranes of organelles serve different and organelle-specific functions. They also differ with regard to their lipid composition. Roughly half of all lipids in cellular membranes belong to the group of amphiphilic glycerolipids, with glycerol forming the basic structure. Acyl chains are esterified to the first (*sn*-1) and second carbon atoms (*sn*-2) of the glycerol backbone, which have hydrophobic properties (Fig. 1.2. A; Li-Beisson et al., 2010). Sphingolipids and sterols represent further important elements of cellular membranes that are mainly localized in the plasma membrane and the ER (Fig. 1.2. B, C; Valitova et al., 2016). Both

lipid groups have a positive effect on membrane rigidity and sphingolipids additionally possess signaling functions essential for the survival of the plant (Li-Beisson et al., 2010).

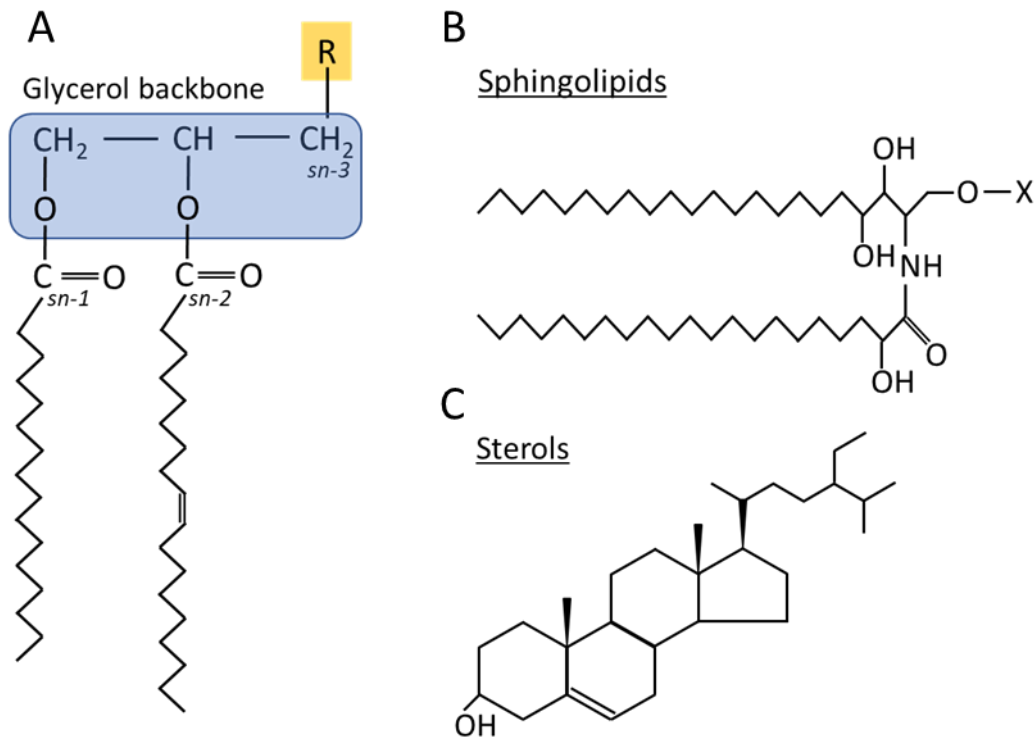


Figure 1.2.: Main classes of membrane lipids.

A. Schematic structure of membrane glycerolipids. The blue box highlights the glycerol back bone to which fatty acids are esterified at the *sn*-1 and *sn*-2 positions, forming the hydrophobic portion of the molecule. At the *sn*-3 position, characteristic polar headgroups are bound (more detailed in Fig. 1.3.), representing the hydrophilic portions of the amphiphilic lipid. B, C, Schematic structures of other membrane lipids, such as sphingolipids with a structure based on ceramide (B); and sterols with a structure based on β -sitosterol (C). The lipid classes are combined in different proportions in cellular membranes, such as the ER or the plasma membrane, influencing diffusion properties, membrane fluidity and the function of membrane-embedded proteins.

The hydrophobic properties of membrane lipids are determined to a large extent by the degree of unsaturation of the associated acyl chains. Cellular membranes are formed through the hydrophobic interactions between lipid molecules, and these interactions are stronger between lipids capable of tight spatial interaction. The interaction between lipids is thus influenced greatly by the degree of fatty acid unsaturation, as the *cis*-double bonds introduce kinks into the molecular shape that sterically hinder intermolecular interactions. In consequence, membranes with lipids containing mostly saturated acyl chains tend to have high melting points and display

rigidity, whereas the presence of unsaturated acyl chains with one or more *cis*-double bonds is responsible for increased membrane fluidity, apparent by a low melting point of the membrane (Heldt and Piechulla, 2015). Within certain boundaries, plants can modulate the degree of membrane lipid unsaturation and thereby control and maintain membrane fluidity even in changing environmental conditions.

The *sn*-3 position of most glycerolipids is occupied by characteristic hydrophilic head groups, such as phosphocholine, phosphoethanolamine, phosphoserine or phosphoinositol, giving rise to the different classes of glycerophospholipids (Fig. 1.3). The plasma membrane, the ER and all other organellar membranes contain different proportions of phosphoglycerolipids, such as phosphatidylethanolamines (PE), PC, phosphatidylinositol (PI), phosphatidylglycerol (PG) or phosphatidylserine (PS) (Fig. 1.3. A). The main lipids of extraplastidial membranes in terms of quantity are the bilayer-forming lipid PC and PE, which has properties of a non-bilayer-forming lipid and is important to facilitate membrane curvature. PI can be phosphorylated at multiple positions of the inositol ring to form phosphoinositides (PIPs). PIPs together with PS can be summarized as anionic lipids, and due to their negatively charged headgroup these lipid play a role in the regulation of various cellular processes (Gerth et al., 2017; Kay and Grinstein, 2013). PA, which can be formed in all membranes, including mitochondria and plastids, appears as an intermediate for the formation of other lipids as well as a signaling lipid during plant stress responses (e.g., salt stress), when it is formed as a degradation product from other phosphoglycerolipids (Fig. 1.3. A, Athenstaedt and Daum, 1999).

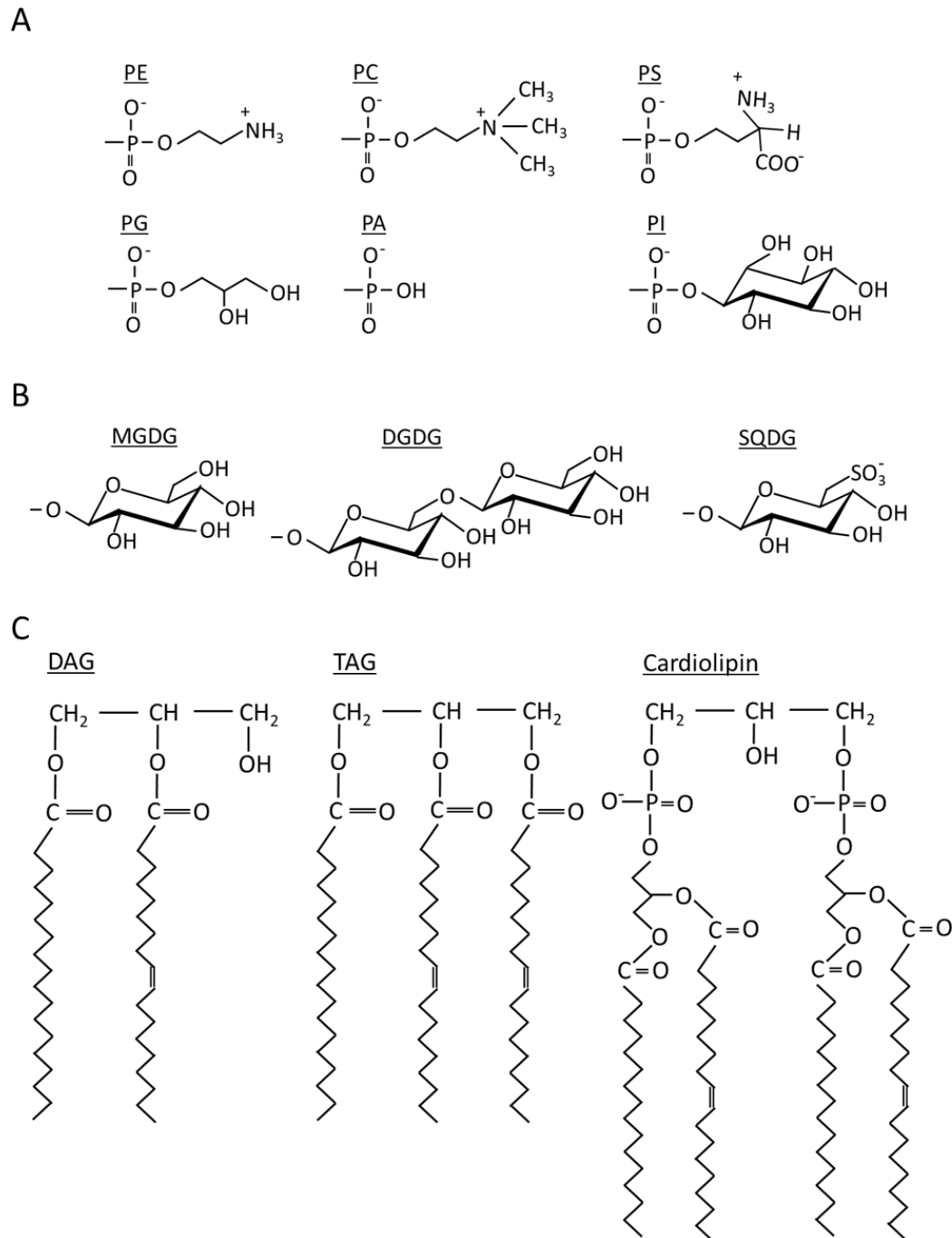


Figure 1.3.: Plant lipid classes.

A. Headgroups of phosphoglycerolipids, PE: phosphatidylethanolamines, PC: phosphatidylcholine, PS: phosphatidylserine, PG: phosphatidylglycerol, PA: phosphatidic acid, PI: phosphatidylinositol. B. Headgroups of galacto- and sulfolipids, MGDG: monogalactosyldiacylglycerol, DGDG: digalactosyldiacylglycerol, SQDG: sulfoquinovosyldiacylglycerol. C. intermediate for synthesis of other glycerolipids and stress signal lipid DAG: Diacylglycerol, storage lipid TAG: triacylglycerol, exclusive mitochondrial membrane phosphoglycerolipid cardiolipin.

In contrast to most other cellular membranes, plastidial membranes consist mainly of glycolipids (galactolipids) that do not contain phosphate, and MGDG accounts for about 50% and digalactosyldiacylglycerol (DGDG) for 25% of the total lipid amount in plastidial membranes of green tissues (Fig. 1.3. B).

The combination of the type of head group and the saturation state of the acyl chains associated with a lipid are decisive for the shape of the lipid molecule, which can either have a cylindrical shape, which naturally tends to form a lamellar structure. In the aqueous environment of the cell, such lipids form planar bilayers, where two lipid layers are oriented facing their hydrophobic acyl chains towards each other and their head groups facing towards the aqueous environment (Fig. 1.4. A; van den Brink-van der Laan et al., 2004). Other lipids may have conical or inverse-conical shapes and may arrange not in planar bilayers, but form inverted hexagonal phases with their head groups facing each other, forming a small, enclosed space, while their acyl chains point towards the aqueous phase (Fig. 1.4. B).

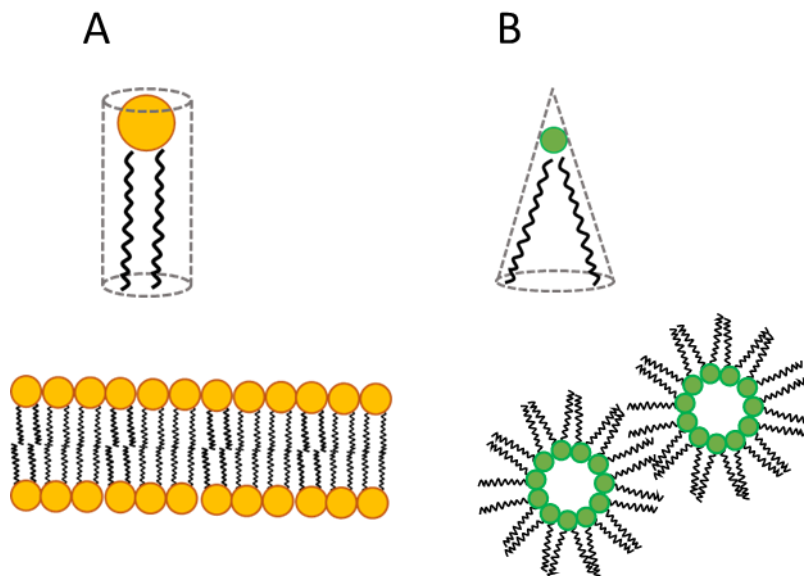


Figure 1.4.: Possible geometric shapes of amphiphilic lipids.

Geometric shapes of lipid molecules based on the ideal diameters of headgroup (green or yellow dots) and the degree of unsaturation of the fatty acids, resulting in cylindrical shapes (A) which preferably form lamellar structures (bilayers) or conical shapes (B) mediating negative membrane curvature and the formation of inverted hexagonal phases.

Due to its assumed geometric shape, MGDG belongs to this latter group of non-bilayer forming lipids. As a main constituent of thylakoids, MGDG mediates the formation of inverted hexagonal

phases thought to play an important role for the function of complexes of the photosynthetic apparatus. DGDG as a neutral bilayer-forming lipid of thylakoids is also important for the function of some photosynthesis proteins. Plastidial membranes furthermore contain the sulfolipid sulfoquinovosyldiacylglycerol (SQDG) and the phospholipid, PG, which are both bilayer-forming lipids thought to be necessary for thylakoid organization, because they can consistently be found in all photosynthetic organisms (fig. 1.3. A, B; Kobayashi, 2016).

Similar to the situation in plastids, mitochondrial lipids are also tightly connected to organelle function, here mostly of the respiratory pathway in the IM. Mitochondrial membranes consist of phosphoglycerolipids, such as PC, PE or PG and additionally contain the mitochondrial-specific lipid, cardiolipin (CL), a dimeric phosphoglycerolipid esterified to four fatty acids. CL is a non-bilayer-forming lipid probably located together with PE at the inner leaflet of the IM to facilitate the formation of mitochondrial cristae architecture (Basu Ball et al., 2018). Diacylglycerol (DAG), like PA, is an intermediate from which storage lipids, such as TAG, but also other membrane lipids can be formed (Fig. 1.3. C, Li-Beisson et al., 2010; Tuteja and Mahajan, 2007).

Even though organelles surrounded by membranes consisting of phosphoglycerolipids outnumber the plastid as the only organelle containing glycolipid membranes, the number of plastids in green tissue and the abundance of thylakoid membranes in each plastid makes glycolipids the most abundant of all lipid classes in green plant cells. While phospholipids and galactolipids differ in chain length and degree of unsaturation of their associated fatty acids, the metabolism of extraplastidial phospholipids and plastidial glycolipids is intrinsically linked through the bidirectional exchange of lipid metabolites between plastids and ER.

1.2.1. Plastidial and extraplastidial fatty acid desaturases.

Fatty acid biosynthesis in plant cells takes place in the plastidial stroma. The main products of the fatty acid synthase complex are 18:0 and palmitic acid (16:0). The plant-specific soluble stearyl-ACP- $\Delta 9$ -desaturase FAB2 (also known as SAD or SS12) can introduce a first double bond at the $\Delta 9$ position of 18:0 in the plastidial stroma, forming 18:1 ^{$\Delta 9$} . For plastidial lipid biosynthesis, 16:0 and 18:1 ^{$\Delta 9$} are used and introduced into glycolipids, such as MGDG or DGDG. FADs located at the IEM (FAD5-FAD8) introduce further double bonds into the acyl chains of these glycolipids.

Alternatively, 18:1^{Δ9} and 16:0 can be exported to the ER. At the ER membrane, these fatty acids are introduced into phosphoglycerolipids, such as PC or PE, and further FADs (FAD2 and FAD3) introduce double bonds into the acyl chains. The extraplastidial fatty acid modification enables the fine-tuning of lipid biosynthesis independently of the plastids. Even though various FADs are localized in two different organelles they overlap in their function, substrate preferences and the products formed (Dar et al., 2017). The functionality of all FAD enzymes is based on the monooxygenation mediated by a di-iron-oxo center of the protein. One oxygen atom of an O₂ molecule will be reduced to form water and the other atom is used to form a hydroxy group at a specific position of the acyl chain which will be cleaved at the next step to result in the release of another water molecule and a carbon double bond in *cis*-configuration in most cases (Heldt and Piechulla, 2015). While the donor of electrons for activation of oxygen can be NAD(P)H+H⁺ for all FADs, the pathway of electron transfer differs. The electron transfer in plastids is ferredoxin-dependent, whereas ER localized FADs use NADPH-cytochrome b₅-reductase and cytochrome b₅ (Heldt and Piechulla, 2015). With the notable exception of the soluble stromal FAB2, FADs are integral membrane proteins and act in sequence to introduce double bonds to form polyunsaturated fatty acids. The step-wise desaturation of 18:1^{Δ9} by the sequential action of the plastidial enzymes FAD6 and the mutually redundant FAD7 and FAD8 yields MGDG and DGDG species carrying mostly 18:3 in both the *sn*-1 and *sn*-2 positions (Fig. 1.5.). In Arabidopsis (a "16:3 plant"), the *sn*-2 position of MGDG or DGDG can also be occupied by hexadecatrienoic acid (16:3^{Δ7,10,13}; 16:3). This fatty acid derives from 16:0, which is desaturated first in the Δ7 position by FAD5, and then further by FAD6 and FAD7/8 (Li-Beisson et al., 2010). The formation of polyunsaturated fatty acids is essential for plastidial membrane lipids, as the thylakoid membrane is highly saturated with photosynthetic proteins, which are thought to require particular biophysical properties of glycolipids associated with polyunsaturated fatty acids.

At the ER, monounsaturated fatty acids exported from plastids are the substrate for a sequence of FAD2 and FAD3 generating 18:2^{Δ9,12} (18:2) and 18:3^{Δ9,12,15} (18:3), respectively (Fig. 1.5.).

The plastidial sequence of fatty acid modification is known as the "prokaryotic pathway", whereas the ER-located sequence of fatty acid modification is termed the "eukaryotic pathway" (Li-Beisson et al., 2010). As shown in Fig. 1.5., the functions of FADs in the plastid and the ER partially overlap. Interestingly, besides the export of fatty acids from the plastids, it has been shown that fatty acids

modified in the ER-based eukaryotic pathway are reimported via lipid intermediates into plastids (Hölzl and Dörmann, 2019). Moreover, the respective plastidial and ER-localized FADs can functionally compensate for each other despite their localization in different cellular compartments, indicating the presence of effective transfer mechanisms for the respective fatty acid and or lipids. These transfer mechanisms are still not well understood.

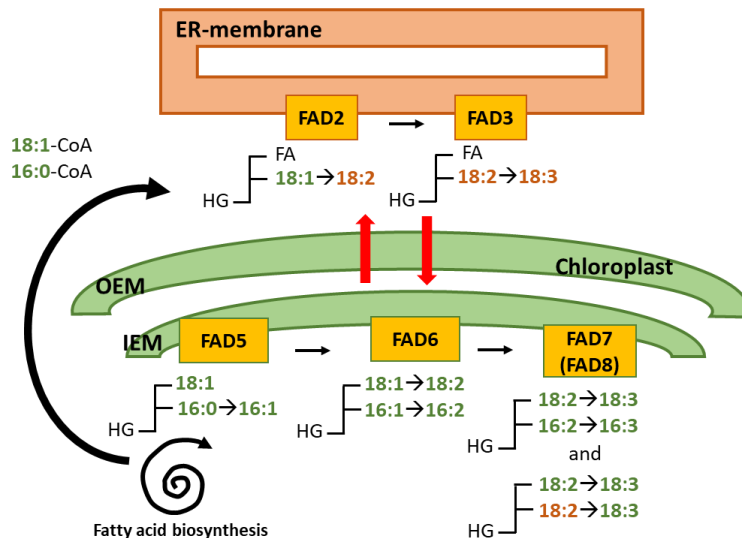


Figure 1.5.: Fatty acid desaturation at membranes of ER and plastids of Arabidopsis plants.

Fatty acid biosynthesis (whirl) takes place in stroma of plastids. Fatty acid (FA) species 18:1^{Δ9} (18:1) and 16:0 are either exported to the membrane of endoplasmic reticulum (ER, big black arrow), where they are first bound to coenzyme A (CoA) before esterified to phosphoglycerolipid (possibly phosphatidylcholine, PC) and fatty acid specie 18:1 is subsequently (small black arrows) desaturated to 18:2^{Δ9,12} (18:2) and 18:3^{Δ9,12,15} (18:3) by fatty acid desaturase (FAD) 2 and FAD3, respectively. Or fatty acids are esterified to plastidial membrane lipid and where is 16:0 desaturated to 16:1^{Δ7} (16:1) by FAD5 and monounsaturated fatty acids are similar to the steps at ER subsequently (black small arrows) desaturated to 16:2^{Δ7,10} (16:2)/ 18:2 and 16:3/ 18:3 by FAD6 and FAD7/FAD8, respectively. Import of extraplastidial 18:2 results in formation of lipids with combination of the fatty acids 18:3/18:3 by FAD7/ FAD8. Fatty acids produced at the ER are marked in orange and plastidial fatty acids in green. HG: headgroup, OEM: outer envelope membrane of plastids, IEM: inner envelope membrane of plastids; FA: fatty acids.

1.2.2. Arabidopsis *fad* mutants prove the exchange of fatty acids between organellar membranes.

Since the stepwise discovery of fatty desaturases in Arabidopsis three decades ago, spearheaded by the group of Prof. Somerville at Stanford University, it is known that fatty acids are exchanged between plastids and the ER (McCourt et al., 1987; McConn and Browse, 1998, 1996; Kunst et al.,

1989, 1988). The movement occurs in both directions and is probably mediated by certain lipids, such as lyso-PC which can efficiently shuttle between the organellar membranes (Browse and Somerville, 1991). Fatty acid transfer is the basis for ER-based lipid biosynthesis using fatty acids derived from plastids, and for the return of fatty acids desaturated in the ER-located eukaryotic pathway into plastids and the incorporation into plastidial glycolipids (Li-Beisson et al., 2010). Under standard growth conditions, individual *fad* mutants with fatty acid desaturation defects in either the plastid or the ER display no drastic changes in the fatty acid composition associated with plastidial or extraplastidial membrane lipids, indicating, that FADs with equivalent function can effectively compensate the nonfunctional FAD even though they are located in another organelle. The range of fatty acids exchanged between organelles is probably broader than only the proposed 18:2 (Wallis and Browse, 2002). In green *Arabidopsis* tissues, *fad2* or *fad3* mutants display major differences in proportion of 18:1 and 18:2, respectively, but still have sufficient amounts of associated 18:2 and 18:3, indicating that loss of function of these enzymes can be compensated by moving fatty acids from the plastid to the ER (Browse et al., 1993; James and Dooner, 1990). Loss of function of any of the plastidial FADs, such as in a *fad7 fad8 (fad78)* double mutant, results in decreased chlorophyll (Wallis and Browse, 2002). Interestingly, a *fad3 fad7 fad8 (fad378)* triple mutant, which cannot form 18:3, neither in the ER nor in the plastids, does not show a visible growth defect. This observation suggests that the respective phenotypes observed for *fad3* mutants might be linked to the modes of inter-organellar exchange of fatty acids rather than with the failure to produce 18:3. By contrast, a *fad2 fad6* double mutant displays perturbed photosynthesis and chlorosis and is only viable on media with added sucrose (McConn and Browse, 1998). Thus, while plants have evolved to contain plastidial glycolipids rich in polyunsaturated fatty acids, such as 18:3, and there are effective means to maintain perturbed 18:3 biosynthesis by enabling inter-organellar transport, it appears that substantial growth defects only occur when the formation of ω 6-fatty acids, such as 18:2, is additionally defective (McConn and Browse, 1998, 1996). Of course, perturbation of fatty acid metabolism that requires the exchange of metabolites between organelles occurs not only in *Arabidopsis* mutants but is a part of regular metabolic processes and acclimation to environmental conditions. For instance, physiological effects on FADs are induced at high and low temperatures when fatty acid adaptation is crucial and the accumulation of saturated or unsaturated fatty acids at high or low

temperatures, respectively, is essential to maintain fluidity and integrity of membranes (Wallis and Browse, 2002).

1.2.3. The role of fatty acid unsaturation in membrane function.

Membrane lipid composition influences the functionality of membrane-associated physiological processes, and the functionality of several protein complexes is known to be dependent on the degree of fatty acid unsaturation of the surrounding membrane lipids. For instance, the activity of plasma membrane localized H⁺-ATPase in *Chorispora bungeana* (a mustard species) is dependent on the double bond index within the membrane (Shi et al 2008). Furthermore, Arabidopsis Na⁺/ H⁺ exchangers are inhibited in *fad2* mutants treated with salt, correlated with a low unsaturation state of extraplastidial phosphoglycerolipids (Shi et al., 2008; Zhang et al., 2012a).

To explain these effects, the influence of fatty acid unsaturation in membrane lipids on the biophysical properties of the membranes must be considered. The fatty acids associated with membrane lipids determine membrane fluidity, because with increasing numbers of *cis*-double bonds the tight molecular packing of lipids within the membrane becomes sterically hindered. For the membrane as a platform for biological processes, fluidity is the basis for lateral protein diffusion within the membrane, and therefore an increase of the ratio of unsaturated fatty acids in membrane lipids enables modulating membrane fluidity during low temperatures, or in membranes with a high density of integral membrane proteins. In consequence, knockout mutants of ω 6-FADs, such as Arabidopsis *fad2* or *fad6*, are sensitive to low temperatures due to the limited capability to form polyunsaturated fatty acids that could be incorporated into membrane lipids (Miquel et al., 1993).

Compared to the plasma membrane, which has a balanced protein/lipid ratio of approx. 1, the thylakoids and inner membrane of mitochondria are more highly occupied by proteins, reaching protein/lipid ratios of 1.6 and 1.9; respectively. Possibly as an adaptation to this situation, each of these membranes contains specific, non-bilayer-forming lipid classes that contain polyunsaturated fatty acids, probably to ensure membrane fluidity with the high protein content

of the membrane (Matos et al., 2007; Chapman et al., 1983; Quartacci et al., 1995; Shishova and Yemelyanov, 2021). To maintain the functionality of cellular membranes over the course of development or during acclimation to changing environmental conditions, such as ambient temperature, it is therefore essential for plant cells to be able to modulate the degree of unsaturation in their membrane lipids according to shifting cellular requirements. The mechanisms by which fatty acids are exchanged between organelles for acyl-editing are currently not well defined.

1.2.4. Mechanisms for exchange of fatty acids and lipids between cellular membranes.

Cellular membranes are diffusion barriers that limit and control the exchange of substances between cellular compartments. Moreover, each cellular membrane has a characteristic lipid composition that is appropriate for its function and provides its biochemical identity. Since all organellar membranes consist of lipid bilayers, but the formation of fatty acids or specific lipid classes is restricted to certain organelles, the formation of most cell membranes depends on specific and efficient lipid transport pathways, as lipophilic compounds cannot cross the cytosolic space autonomously.

There are at least two principal modes, by which lipids can be distributed within the cell, the vesicular and the non-vesicular transport. As the ability to form vesicles is limited to certain organelles, such as the ER or Golgi, non-vesicular transport at membrane contact sites (MCS) might be an important means to connect different cellular membranes (Liu and Li, 2019; Hurlock et al., 2014; Schapire et al., 2008; Zang et al., 2020; Michaud and Jouhet, 2019).

Exchange of molecules between membranes by the vesicular pathway.

Vesicles are associated with protein transport from the ER to the Golgi apparatus and mediate the distribution of integral membrane proteins between cellular membranes as well as the secretion of biomolecules at the cell surface. As membraneous structures that can bud off and fuse with membranes, vesicles are also well suited to distribute lipids throughout the cell. The vesicle trafficking from a donor membrane to an acceptor membrane requires a certain set of

protein complexes to define the target organelle and the ability to merge with the membrane and thereby release the cargo. Vesicle transport of proteins begins in the ER at specific ER export start sites where proteins are collected in certain membrane areas that are then pinched off from the ER. The intermediate membrane structures are covered by various coat proteins (COPs) for stabilization (Zeng et al., 2015). When no further modification of the transported proteins is necessary, vesicles can be directly transported from the ER to various organelles. Vesicles with proteins intended for further modification, such as glycosylations, are transported by vesicular trafficking from the ER to the Golgi. In either case, the transport vesicles fuse with their target membranes with the help of soluble N-ethylmaleimide sensitive attachment protein receptors (SNAREs). The recovery of vesicles after cargo release occurs in a state covered by additional COP proteins and these vesicles are fused again with the ER by SNARE proteins located at the ER membrane (Heldt and Piechulla, 2015). Proteins modified in the Golgi are further distributed to the trans-Golgi network and from there either to the plasma membrane or to the vacuole. This route is also assumed to be involved in the distribution of n-glycosylated proteins into plastids (fig. 1.6. A, Jarvis and López-Juez, 2013).

Vesicle formation is not only part of cellular housekeeping but also occurs at an enhanced rate upon external stimulation. For instance, during periods of osmotic stress, when the cell shrinks as a result of plasmolysis and water efflux, excess plasma membrane is internalized by bulk-flow endocytosis, in which a large number of vesicles coated with clathrin-protein complexes (clathrin-coated vesicles, CCVs) are formed (Zwiewka et al., 2015).

Within plastids, the transport of lipids from the IEM to thylakoids is probably also mediated by vesicle transport implemented by the vesicle inducing protein in plastids1 (VIPP1). This goes as far as that even the formation of the thylakoid membrane system itself and the transport of photosynthesis proteins within the plastid is largely dependent on vesicles, and this mechanism is also used for the repair of thylakoid membrane complexes and in chloroplast adaptation processes during stress (McDonald et al., 2017; Zhang et al., 2012b).

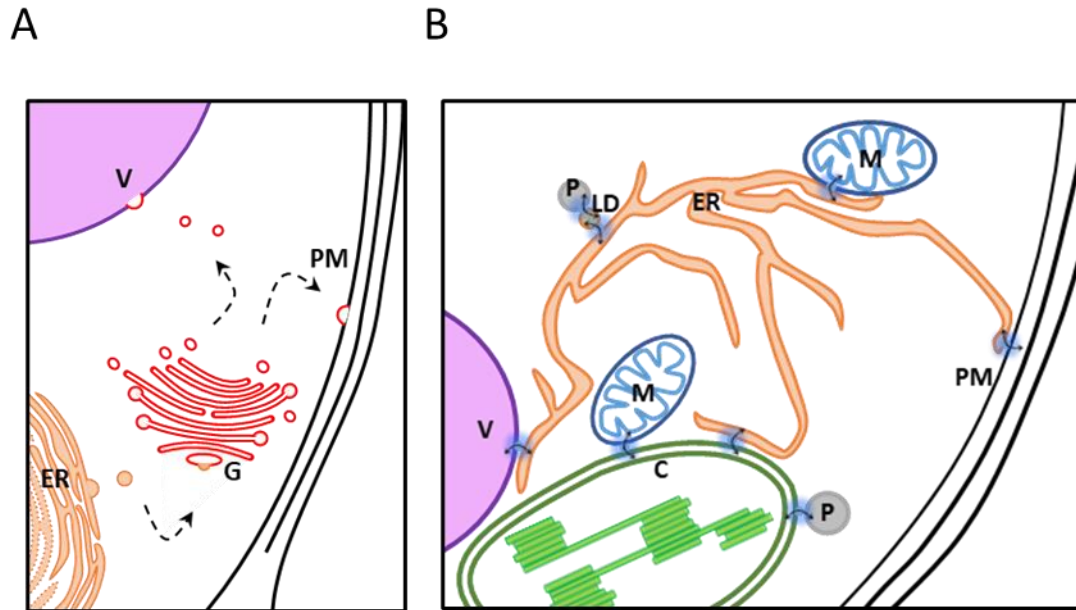


Figure 1.6.: Vesicular and non-vesicular transport pathway of lipids.

A. Vesicular transport of lipids mainly occurs between endoplasmic reticulum (ER) and Golgi-apparatus (G) to vacuole (V) and plasma membrane (PM). In addition, vesicle formation in other organelles and transport of vesicles from Golgi to other organelles is also possible but not displayed here. B. Lipid trafficking mediated by membrane contact sites has been described between most organelles of the plant cell. P: peroxisome, M: mitochondrion, V: vacuole, LD: lipid droplet; C: chloroplast.

Exchange of molecules between membranes by the non-vesicular pathway: Membrane contact sites.

Various studies in recent years show that trafficking can also occur at membrane contact sites (MCS). MCS are membrane regions of two organellar membranes which are in close proximity to one another, probably mediated by tethering proteins. The close spatial proximity of membranes or organelles facilitates the transient formation of specialized transitory structures that represent a physical link. Thereby, compounds can move directly between or across organellar membranes. For the exchange of lipids between organellar membranes this means that transport across the hydrophilic space can be avoided, and lipids may integrate directly into the membrane of the other organelle. The function of MCSs is to date not fully understood, neither in plants nor in other model systems. Proteins locating to MCS regions include flippases and lipid transfer proteins (LTPs), flipping the glycerolipids from one leaflet to another and managing the remodeling of glycerolipids to transportable structures as it is assumed for lyso-PC (Mongrand et

al., 2000; Michaud and Jouhet, 2019). AT MCSs, lipids can be precisely and efficiently transported to other organelles, as is required for lipid biosynthesis pathways, which involve more than one compartment. The steps for the synthesis of ceramides take partially place in ER and in the Golgi and intermediate compounds in animal cells are exchanged with the help of a ceramide transfer protein (CERT, Hanada et al., 2003). A similar candidate for the lipid transfer of ceramides in plants has not yet been found. Also, the biosynthesis of extraplastidial and plastidial membrane lipids rely on efficient exchange between plastids and ER, which even seem to be physically strong connected (Andersson et al., 2007). For plastidial export and import, several proteins are being discussed as parts of possible plastid-ER contact sites, including the previously described machinery for exporting 18:1- and 16:0-ACP from the plastid stroma, such as fatty acid exporter1 (FAX1) at the IEM or the trigalactosyldiacylglycerol complex (TGD) consisting of subunits 1-5, stretched over OEM and IEM and able to bind PA, which is one of the lipids pronounced for the shuttling of fatty acids used for the eukaryotic pathway (Wang et al., 2013; Li et al., 2015). Other proteins contributing to such contact sites are likely long-chain acyl-CoA synthetases (LACS) 9 and 4 at the OEM and at the ER membrane, respectively, which activate transported fatty acids by forming fatty acid-CoA esters. The flippase Aminophospholipid ATPase10 (ALA10) at the ER membrane is connected to the plastidial formation of MGDG in the eukaryotic pathway by flipping PC as a substrate at the ER membrane (Botella et al., 2016). MCS are used by almost every organelle and are often formed during stress conditions (fig. 1.6. B, Michaud and Jouhet, 2019). Salt stress induces MCS between ER and plasma membrane, possibly to facilitate the rapid exchange of lipids, and these ER-plasma membrane contacts are mediated by calcium dependent synaptotagmin1 (SYT1), a protein required to maintain the integrity of the plasma membrane under stress conditions (Lee et al., 2019; Schapire et al., 2008). Peroxisomes and plastids are also thought to enter into a close proximity in a stress-dependent manner when OPDA, a JA precursor, is formed in plastids from MGDG-associated fatty acids, and the close organellar association may enable efficient transfer of OPDA to peroxisomes for further steps of JA biosynthesis (Bobik and Burch-Smith, 2015). Overall, recent evidence supports an important role for MCSs in mediating organellar exchange, including the exchange of lipids, and such exchange may be critical not only for plant development but also during plant responses to changing environmental conditions.

1.3. Photosynthesis as a membrane-localized process

In plants, the maintenance of a specific and optimal lipid composition is especially relevant for thylakoids, the membranes where key steps of photosynthesis take place. Thylakoids are the basis for photoautotrophic sustenance of every plant. The photosynthetic apparatus within thylakoid membranes consists of protein-pigment complexes using light energy to form NADPH and ATP required for the fixation of CO₂. NADPH is the product of the PSI complex in cooperation with stroma localized ferredoxin and ferredoxin-dependent NADP reductase, and the formation of ATP is catalyzed by ATP-synthase (ATPase) using the ensuing proton-motive force. The PSII complex is responsible for forwarding electrons from the dissociation of water, releasing O₂ and protons. The fourth main complex of photosynthesis is the cytochrome b₆/f complex transmitting electrons between PS-complexes by receiving electrons from PSII via plastoquinones and forwarding electrons to PSI via plastocyanin. The electron transport is linked with a proton flow from the stromal to the luminal side of the thylakoids, where protons accumulate due to membrane-mediated spatial separation. The resulting proton-motive force is used by the ATPase to generate ATP. Further associated processes include the photon-capturing and transmission by light harvesting complexes (LHC) I and II, which occupy membrane positions in close spatial proximity to PSI and PSII, respectively (Heldt and Piechulla, 2015).

Experiments in this thesis regard stress-induced changes in plant membrane lipid composition and the ensuing physiological consequences, with a particular focus on the function of photosynthetic membranes. Therefore, the effects of stress on thylakoid function are briefly introduced. The photosynthetic apparatus is at constant risk of accumulating an excess of excitation energy, either under high light conditions or through biotic and abiotic stress factors, which leads to a reduction in the photosynthetic performance of individual complexes and the formation of ROS (Heldt and Piechulla, 2015). Photosynthetically active organisms therefore have various mechanisms to on one hand prevent uneven excitation of PS complexes (e.g., light fluctuations) by enhancing the excitation ability of the respective PS complex through reversible association with a mobile LHCI (= state transition, qT) or on the other hand quench excessive photons by releasing energy in form of heat (= nonphotochemical quenching, NPQ). The processes contributing to NPQ represent energy dependent quenching and involve core

components of PSII subunit S (PsbS), which is activated at low pH by forming monomers. These monomers can associate with the PSII-LHCII super complexes, resulting in a rearrangement of the complexes within the thylakoids and the formation of the carotenoid zeaxanthin (Zx) which interacts with PsbS to mediate additional aggregation of antenna complexes with the PSII-LHCII super complexes (Kaiser et al., 2019). Energy dissipation can also be achieved by the targeted destruction of PSII subunit D1 by ROS and the subsequent inactivation of the PSII complex. This process is called photoinhibition (qi) and occurs at the expense of maintaining efficient photosynthesis. All these different NPQ components differ in the timing of their onset after stress induction and also in their relaxation back to normal functionality (Steen et al., 2020). Within minutes of high light conditions, the PsbS component already mediates a substantial proportion of NPQ, and it also can go back to normal as it started within a short dynamic time frame. By contrast, the formation of Zx within the xanthophyll cycle (XC) takes longer due to several reasons. The XC comprises the stepwise conversion of violaxanthin (Vx) to antheraxanthin (Ax) as an intermediate of the formation of Zx used for adaptation to different light conditions. In high light conditions, the ability of Zx to dissipate energy is used, while in low light the epoxidized, Vx, can expand the capacity of the LHCs.

A key enzyme of this process is violaxanthin-de epoxidase (VDE), which is activated by forming dimers when the thylakoid lumen acidifies (Hallin et al., 2016). It is assumed that in order to reach its substrate Vx within the thylakoid the VDE dimer has to integrate into the membrane, and that this process requires the presence of inverted hexagonal phases formed by the non-bilayer lipid MGDG (Garab et al., 2016). For green algae *Mantoniella squamata* it was shown that enzymatic conversion from Vx to Ax takes longer than from Ax to Zx due to a higher substrate affinity of VDE to Ax (Goss, 2003). Although it is established that Zx-related NPQ plays a delayed role after the induction of high light stress and also takes longer to relax, it is still debated exactly how Zx synthesis contributes to NPQ (Kaiser et al., 2019).

In any case, the dynamic processes of photosynthesis within the membrane as well as thylakoid adaptation for optimal light utilization and light protection are equally dependent on maintaining the integrity and fluidity of the thylakoid membrane, even under challenging conditions.

1.4. Physiological effects of salt stress in *Arabidopsis*.

One such challenging condition is salt stress, which is also studied in this thesis. In light of progressive environmental change towards climatic extremes, a global rise in temperature, increased incidence of drought conditions and in consequence enhanced salinity all present challenges for plant growth and survival. As plants provide the basis for securing the growing global demand for food for an ever-increasing population, it is essential to gain a better understanding of plant mechanisms involved in efficient adaptation responses to stresses such as drought, heat, evolving pests, parasites or pathogens and salt. The salinization of arable areas, caused by a combination of drought and unsuitable irrigation techniques, is a growing problem for maintaining a minimal necessary level in crop yields (Zörb et al., 2019). One of the commonly used model organisms to unravel salt stress responses is the well-known species *Arabidopsis thaliana*. In general, when plants are confronted with salt stress, they respond simultaneously to at least three different types of stress: osmotic stress, specific ion toxicity and oxidative stress (Munns and Tester, 2008).

The uptake and accumulation of the surrounding salt ions sodium (Na^+) and chloride (Cl^-) leads to an imbalance of mineral nutrients, with a high Na^+ concentration in particular causing damage due to its similarity to potassium ion (K^+), which is involved in enzymatic processes such as protein biosynthesis but cannot functionally replace them (Tester and Davenport, 2003). To prevent Na^+ ions interfering with plant metabolism one responsive mechanism leads to channeling of toxic ions out of cytoplasm into vacuole which comes with advantage in increase of salt concentration in plants to induce water flux towards plants cells and recovery of turgor pressure (Hasanuzzaman et al., 2019). For most plants it is a long way to achieve this level of stress management, if it is at all possible to achieve this state, as it depends on the concentration of salt.

Salt stress causes high production of toxic metabolites such as ROS, which is an oxidative threat to nucleic acids, proteins and membrane lipids and lead to reduced maintenance of the plasma membrane or thylakoid membrane when scavenging mechanisms are ineffective (Munns and Tester, 2008). In addition, ROS lead to an impairment of photosynthesis, which is affected in many ways by salt stress anyway. In worst case, strong ion toxicity and high production of ROS induce

stress related senescence and result in cell death or death of the whole plant. When seeds are exposed to high salt concentration, their germination is also strongly delayed.

Besides their toxic effects, high salt concentrations cause a low osmotic potential in the roots, which makes water uptake physically difficult and results in dehydration. In addition, the stomata of the green tissues close to prevent the plants from losing water through transpiration. However, at the same time this blocks the gas exchange important for maintaining CO₂ fixation, negatively impacting growth (Munns and Tester, 2008). During salt stress conditions, the vacuole loses water, resulting in shrinkage of vacuoles and loss of turgor and plasmolysis. At the level of membranes, the loss of turgor means that now excessive plasma membrane area must be internalized (König et al., 2008; Leshem et al., 2007; Hasanuzzaman et al., 2019). Other cellular membranes are also impacted by salt stress, including the photosynthetic thylakoids.

1.4.1. Effects of salt treatment on photosynthesis.

The reduced ability of roots to take up water as a result of the low osmotic potential already leads to a signal to close the stomata in order to reduce transpiration (Munns, 2002). As a physiological consequence, the now limited access to CO₂ results in a decreased efficiency of the Calvin cycle, with negative impact on photosynthetic performance. More direct effects of salt stress on thylakoid function include an increased cyclic electron flow due to a high number of active PSI centers mediating electron transport from ferredoxin at the stromal side to plastoquinone and cytochrome_{b₆}f complex, enabling the formation of the proton gradient for ATP synthesis to skip the PSII complex (Stepien and Johnson, 2009). High ROS production in plastids causes oxidation of membrane lipids and membrane proteins. In this way especially the PSII is damaged, leading to an enhanced turnover rate of the associated proteins and increased photoinhibition. These effects manifest in a reduced maximum quantum yield of PSII (F_v/F_m), a result of reduced active reaction centers and changes in photobiochemistry promoting high NPQ (Stepien and Johnson, 2009). The inability to compensate the production of ROS with antioxidants favors membrane lipid oxidation and the subsequent degradation of thylakoids and even the plastidial envelope membranes. The lipid elements of these membranes accumulate in plastoglobuli, intra-plastidial

lipid droplets, which are a clear indication of senescence (Hasanuzzaman et al., 2019). During salt stress conditions, the Chl a/ Chl b ratio increases due to conversion of Chl b to Chl a. Moreover, chlorophyll production is directly inhibited by Na⁺ toxicity and results in a general reduction of chlorophyll (Li et al., 2010).

1.4.2. Salt stress can induce dynamic changes in plant membrane biology.

Under stress conditions, plants alter their gene expression to respond specifically and appropriately to the stress situation. Transporters that facilitate the entry of Na⁺ ions are suppressed and degraded, whereas ion exchangers and transporters that support the restoration of Na⁺ homeostasis are synthesized and activated. As such changes in membrane proteins require a change in the properties of the surrounding membrane lipids, and the lipid composition of membranes throughout the cell has been found to change substantially upon salt treatment. In this context it is relevant to note that salt stress poses a risk for increased permeability of membranes due to lipid oxidation and degradation (He and Ding, 2020). As will be explained in the following paragraphs, during salt stress plants implement changes in membrane composition at different levels, with effects on the content of individual lipid classes, on the fatty acid composition in lipids, on the ratio of bilayer to non-bilayer forming membrane areas, and on the abundance of signaling lipids required to form stress-induced specialized membrane structures, such as MCSs or control membrane permeability.

1.4.3. Effects of salt stress on the plasma membrane and other cellular membranes.

The expression and integration of ion exchangers and ion transporters into the tonoplast membrane and the plasma membrane is an important step towards maintaining ion homeostasis and salt tolerance in plants. In one of the initial responses, phospholipase (PLD) α 1 is activated and converts PC to PA, which is a second messenger thought to trigger a signaling cascade involving mitogen-activated protein kinase 6 (MPK6, Yu et al., 2010). MPK6 can phosphorylate the protein salt overly sensitive 1 (SOS1), a Na⁺/ H⁺ antiporter. The plant SOS pathway consists of

five different proteins involved in sensing salt dependent increases in cytosolic calcium (Ca^{2+}), triggering protein kinase activity, and mediating the recovery of Na^+ homeostasis and a decrease in the Na^+/K^+ ratio (Isayenkov and Maathuis, 2019). In maize, the production of PA positively influences the activity of H^+ -ATPase at the tonoplast to support vacuolar accumulation of Na^+ ions (Zhang et al., 2006). Several studies reported rapid decreases in PC abundance after salt stress, which is mainly associated with the ER and the plasma membrane, coinciding with increased formation of PIP_2 (Tasseva et al., 2004; Pical et al., 1999; König et al., 2007). The size of the plastids also shrinks due to salt-induced dehydration, and increasing the ratio of DGDG to MGDG improves salt tolerance and stabilizes the plastid membranes (Wang et al., 2014). These cellular responses require mechanisms by which membrane lipids can be degraded, altered or mobilized. A fast mechanism to turnover lipids for alteration of membrane properties is the breakdown of lipids to form TAG, which can be transiently stored during stress conditions as plastoglobules in plastids, or as lipid droplets in the cytosol (Xu et al., 2020). An example is given by the plastid localized protein sensitive to freezing 2, which is an enzyme involved in the transformation of galactolipids and refers enhanced salt tolerance in tomato (Wang et al., 2016).

1.4.4. Membrane lipid unsaturation is important for plant salt tolerance.

As mentioned above, the functionality of Na^+/H^+ -exchangers and plasma membrane-localized H^+ -ATPases is dependent on the degree of unsaturation of the surrounding membrane lipids (Shi et al., 2008; Zhang et al., 2012a). Reciprocally, the nature of changes in fatty acid unsaturation of membrane lipids is dependent on the type and degree of required stress tolerance and can reflect the oxidation state of lipids with increased unsaturation upon salt exposure (He and Ding, 2020). However, increased unsaturation of lipids in the plasma membrane or in thylakoids enhances salt stress tolerance, possibly due to an efficient mechanism for unsaturated fatty acid adaptation. Halophytes display high levels of unsaturated fatty acids in MGDG and PG, which are related to the protection of PSI and PSII, leading to reduced PSII inhibition upon exposure to salt and an overall improved salt stress tolerance (Meng et al., 2018; Sui and Han, 2014). In the cyanobacterium *Synechocystis sp.* a high content of unsaturated fatty acids in membrane lipids was beneficial for the salt tolerance of the photosynthetic machinery and had a positive effect on

Na⁺/ H⁺-antiporter (Allakhverdiev et al., 2001). Similarly, the functionality of certain FADs is beneficial and decisive for salt tolerance in Arabidopsis or other dicot plants. An antisense *fad7* expression line in tobacco, producing lower amounts of ω₃-fatty acids in plastids, showed increased salt sensitivity (Im et al., 2002). This was also the case when single Arabidopsis mutants of *fad2* and *fad6* were treated with salt, reflecting the importance of unsaturated fatty acids for salt tolerance in these plant species (Zhang et al., 2009; Zhang et al., 2012a). Evidently, the degree of membrane lipid unsaturation is a factor contributing to salt tolerance in plants.

1.4.5. Vesicular trafficking and membrane contact sites during salt treatment.

Hyperosmotic stress results in the dynamic redistribution of membrane lipids to reduce excessive plasma membrane after plasmolysis of the cell (Leshem et al., 2007; König et al., 2008). Severe and efficient membrane changes are necessary to eliminate the possibility that turgor-related change of volume leads to collapse of the cell (Zwiewka et al., 2015). In this context, the process of bulk-flow endocytosis was observed in which unnecessary membrane area is internalized by formation of endomembrane vesicles to restore turgor pressure. The formation of the CCVs involved is linked to an increased abundance of PIP₂ in the plasma membrane (König et al., 2008; Ischebeck et al., 2013). Moreover, MCS are used for membrane lipid remodeling and enhancement of salt tolerance. AtSYT1 seems to be connected to enhance salt tolerance and was not only observed to initiate the salt-induced MCS between ER and plasma membrane, but plasma membrane integrity of *syt1* knockout plants is compromised easier than in wild type controls when confronted with salt (Lee et al., 2019; Schapire et al., 2008). The relevance of other lipid transport proteins and MCS tethers during salt stress still needs to be explored. While the temperature-dependent tolerance or sensitivity of Arabidopsis knock-out mutants or overexpressors of fatty acid desaturase genes can be explained by the physical properties of saturated and desaturated fatty acids, the contribution of unsaturated membrane lipids to salt tolerance is not as well defined. Biophysical studies indicate that membrane properties change with regard to permeability, inter-molecular forces and deformability when the degree of membrane lipid unsaturation is changed, and these properties can greatly influence membrane-associated processes such the budding or fusion of vesicles, the function of integral membrane

proteins such as channels or ATPases, or the overall stability of a membrane challenged by salt or osmotic stress (Barelli and Antony, 2016). As many such studies have been performed using artificial membranes, it is now mandatory to analyze the dynamic changes in membrane composition in intact plants.

1.4.6. Open questions on the links of fatty acid metabolism and plant physiology.

The current understanding of membrane lipid remodeling in plants during salt stress leaves a number of key questions:

- Are there physiological links between the dynamic changes that were previously observed for membrane lipids residing in different compartments?
- If there is a connection between dynamic changes of PC and MGDG, how are hydrophobic elements exchanged between these lipids?
- If there is no connection between dynamic plastidial and extraplastidial lipid changes, how are dynamic lipid changes coordinated?

1.5. The aims of this work

Previous studies with salt sensitive and salt tolerant plant species have focused on changes in the abundance of PC and MGDG and their associated fatty acid profiles and suggest that important steps of plant salt responses occur at the plasma membrane and thylakoid membranes. Plant responses to salt challenges require changes in membrane properties (Guo et al., 2019). A previously reported temporal dependence of changes in PC and MGDG content suggests a connection between the dynamic changes of these lipids (König et al., 2007). However, there has not been a focused study addressing intercompartmental exchange of lipids between plastids and other organelles upon salt stress, nor is the physiological relevance of such an exchange understood.

Therefore, my research was focusing on the following aims:

1. Establish an experimental system to study dynamic changes in PC and MGDG levels during mild salt stress
2. Analyze PC and MGDG dynamics during salt stress and in Arabidopsis mutants with altered fatty acid fluxes between plastidial and extraplastidial membranes
3. Analyze and compare the impact of salt stress on perturbed ER or plastidial fatty acid desaturation on photosynthetic parameters in Arabidopsis
4. Determine the effects of modified lipid metabolism on the survival of plants during salt treatment

2. Material and Methods

2.1. Material

2.1.1. Chemicals

The chemicals used for the experiments described in this thesis were obtained from the following companies, unless otherwise stated: Sigma-Aldrich (Taufkirchen, Germany), AppliChem (Darmstadt, Germany) and Carl Roth (Karlsruhe, Germany).

2.1.2. Equipment

The equipment used for this work is listed in Table 2.1. and is linked to the corresponding methods. All centrifugation steps were performed using either Eppendorf 5424 R or 5810 R depending on type and size of reaction tube and speed requirement.

Table 2.1.: Equipment used for this work.

Equipment	Manufacturer	Used for following methods (sections)
Eppendorf 5424 R or 5810 R centrifuges	Eppendorf SE, Hamburg, Germany	Regularly
Thermomixer comfort 5355 heating block	Eppendorf SE, Hamburg, Germany	2.2.5.2.
Adaptis A1000 phyto chamber	Conviron, Winnipeg, MB, Canada	2.2.2.
Parasonic Lumix DMC-FZ150 camera	Parasonic Corp., Hamburg, Germany	
Zoom-stereo microscope Stemi 508 MAT doc	Carl Zeiss, Jena, Germany	2.2.3.1.
TS-18824 Reacti-Therm triple-block heating module evaporator	Thermo Fisher Scientific, Dreieich, Germany	2.2.4.1.

gas chromatograph Shimadzu GC-2010 Plus, auto-injector AOC-20i	Shimadzu Europe GmbH, Duisburg, Germany)	2.2.4.6.
DB-23 column	Agilent Technologies, Waldbronn, Germany	2.2.4.6.
NanoDrop 2000 photometer	Thermo Fisher Scientific, Dreieich, Germany	2.2.5.1.
Electrophoresis chamber	cti, Idstein, Germany	
Rotor-Gene Q thermocycler	Qiagen, Hilden, Germany	2.2.5.3.
Ultrospec 2100 pro photometer	Biochrom, Holliston, MA, USA	2.2.6.
IMAGING-PAM chlorophyll fluorometer IMAG-L LED-Ring-Array; IMAG-K CCD camera	Heinz Walz, Effeltrich, Germany	2.2.7. 2.2.8.2.2.
Dionex UltiMate 3000 HPLC system; Dionex WPS-3000SL autosampler; Dionex LPG-3400A system; Dionex photodiode array detector PDA-3000; Dionex column thermostat TCC-3000	Thermo Scientific, Dreieich, Germany	2.2.8.3.
ET 250/4 Nucleosil 120-5 C18 chromatography column	Macherey-Nagel, Düren, Germany	
EM 900 transmission electron microscope	Carl Zeiss Microscopy, Jena, Germany	2.2.9.
Ultracut R ultramicrotome	Leica, Wetzlar, Germany	
Variospeed SSCCD camera SM-1k- 120	TRS, Moorenweis, Germany	

2.1.3. Single-use Materials

The experiments were performed with autoclaved pipet tips and sterile tubes (Sarstedt, Nümbrecht, Germany). Table 2.2. lists all materials used in the following methods.

Table 2.2.: Single-use materials used in this work.

Material	Manufacturer
Square petri dishes	Sarstedt, Nümbrecht, Germany
15 ml reaction tubes	Sarstedt, Nümbrecht, Germany
Solid Phase Extraction (SPE)-column	Agilent Technologies, Waldbronn, Germany
TLC-silica coated glass plates (silicagel 60)	Merck, Darmstadt, Germany
Whatman filter paper	VWR, Darmstadt, Germany
GC-inserts	Agilent Technologies, Waldbronn, Germany
GC-screw caps	Agilent Technologies, Waldbronn, Germany
Glass beads (0.85-1.23 mm)	Carl Roth, Karlsruhe, Germany

2.1.4. Software

Table 2.3. lists programs used to record, calculate or convert data.

Table 2.3.: Programs used in this work.

Program	Manufacturer	Used in following methods (sections)
ImageJ Fiji software, version 1.51	(Schindelin et al., 2012)	2.2.3.1.
Shimadzu Postrun Analysis Program	Shimadzu, Europe GmbH, Duisburg, Germany	2.2.4.6.
QUANTUM-Capt image software	BIOTECH, Madrid, Spain	2.2.5.1.
NANODROP 2000	Thermo Scientific, Dreieich, Germany	2.2.5.1.

Rotor-Gene Q Series software	Qiagen, Hilden, Germany	2.2.5.3.
LinRegPCR program	Heart Failure Research Center, Amsterdam, Netherland	2.2.5.3.
ImagingWin	Heinz Walz, Effeltrich, Germany	2.2.7.
Chromeleon Version 6.80 SP2	Thermo Scientific, Dreieich, Germany	2.2.8.4.

2.1.5. Plant lines

All plant lines used for this work were in the *Arabidopsis thaliana* Columbia-0 (Col-0) background (ecotype) and are listed in Table 2.4. Col-0 plants will be referred to as wild type (WT) throughout the text and were used for salt stress experiments and as a control to which other (mutant) lines were compared. For plant lines carrying genetic modifications, the modification method originally used to create the lines is indicated, as well as the Arabidopsis Genome Initiative (AGI) locus code for the gene(s) affected. For most mutant lines, the Nottingham Arabidopsis Stock Centre (NASC) number has also been added, along with information who originally related the lines. If any information is not known, it is marked as not available (n.a.).

Table 2.4.: Plant lines analyzed in this work.

Line	Genetic modification	AGI identifier	NASC Number	Obtained from/ Reference
Columbia, Col-0/ WT	n.a.	n.a.	n.a.	NASC
FAD3-4c	T-DNA, complemented	AT2G29980.1	n.a.	Dr. Larissa Launhardt, MLU
<i>fad2-1</i>	EMS	AT3G12120.1	N8041	(Miquel and Browse, 1992)

<i>fad3-2</i>	EMS	AT2G29980.1	N8034	Prof. Dr. Ivo Feussner, University of Göttingen/ (James and Dooner, 1991)
<i>fad5-1</i>	EMS	AT3G15850.1	N206	(Kunst et al., 1989)
<i>fad6-1</i>	EMS	AT4G30950	N207	Dr. Georg Hölzl, University of Bonn/ (Browse et al., 1989)
<i>fad7-1 fad8</i>	EMS	AT3G11170 AT5G05580	N8036	(McConn et al., 1994)
<i>fad3-2 fad7-2 fad8</i>	EMS	AT2G29980.1 AT3G11170 AT5G05580	n.a.	Dr. Debora Gasperini, IPB Halle/ (McConn and Browse, 1996)

2.2. Methods

2.2.1. Sterilization of plant seeds

Seeds were sterilized by submerging for 10 min in bleaching solution (Tab. 2.5.) and afterwards washed six times with sterile bidist. water. Before sowing on square petri dishes containing ½ Murashige and Skoog (½ MS) solid media (Tab. 2.5.), seeds were resuspended in 0.01 % sterile agarose solution (w/v; Biozym, Hessisch Oldenburg, Germany).

Table 2.5.: Solutions and media used for cultivation of plants.

Media	components
Bleaching solution	6 % (v/v) sodium hypochlorite (NaOCl)

	0.1 % (v/v) Triton X-100
½ MS solid media	0.22 % (w/v) Murashige and Skoog, including modified vitamins (Duchefa, Haarlem, Netherlands) 1 % (w/v) sucrose, SERVA, Heidelberg, Germany) 0.8 % (w/v) micro agar (Duchefa, Haarlem, Netherlands)
½ MS media containing sodium chloride (NaCl)	0.22 % (w/v) Murashige and Skoog 1 % (w/v) sucrose 0.05/ 0.1/ 0.25 or 0.4 M (w/v) NaCl 0.8 % (w/v) micro agar

2.2.2. Plant growth conditions

Sterilized seeds, sown on ½ MS solid media, were kept in the dark at 4 °C for 2-4 days before placed in an Adaptis A1000 phyto chamber and grown under short-day conditions (8 h light/ 16 h dark, 21 °C/ 18 °C, 170 $\mu\text{mol m}^{-2} \text{s}^{-1}$). The duration of growth was two-weeks for all lines listed in Tab 4, except for *fad3*, which was grown for three weeks to account for its developmental delay. Petri dishes with seeds sown in one row of 15 seeds were incubated vertically. Alternatively, petri dishes with seeds sown in five to seven rows of 15 seeds each were incubated horizontally.

Plants to be grown on soil were cultivated first on ½ MS agar plates for two weeks under short-day conditions. Plants were then transferred to pots containing soil and grown for seven weeks under short-day conditions. Then plants were transferred to long-day conditions (16 h light at 21 °C/ 8 h darkness at 18 °C, 170 $\mu\text{mol m}^{-2} \text{s}^{-1}$) and grown five or seven weeks until plants were flowering. Phenotypes of plants were documented before and after exposure to long-day conditions using a Parasonic Lumix DMC-FZ150 camera.

2.2.3. Salt stress treatment

Vertically grown plants were transferred to ½ MS soli media containing 0.05 M or 0.1 M NaCl (Tab. 2.5.). After 0, 0.5, 1, 1.5 and 2 h, plants were photographically documented and harvested for further analysis into 15 ml reaction tubes. The samples contained pools of 13-15 individual plants and were frozen in liquid N₂.

For measurements of photosynthetic parameters (see 2.2.7.), seedlings were grown horizontally for two weeks on ½ MS solid media under control conditions or with either 0.05 M or 0.1 M NaCl added under short-day conditions (8 h light / 16 h dark, 21 °C/ 18 °C; 170 μmol m⁻² s⁻¹). The first true leaves (the first grown leaves after the cotyledons) were cut off and placed on ½ MS solid media for dark adaptation and subsequent IMAGING-PAM measurements.

2.2.3.1. Germination and root growth experiments

The effects of salt treatment on the germination of seeds and root growth was performed according to Zhang et al. (2012a).

For the germination experimental setup, seeds were sterilized and stratified in fluid agarose media (Tab. 2.5.) in the dark at 4 °C for three days. Seeds were sown on ½ MS solid media containing either 50, 100 or 250, 400 mM NaCl or no supplements. The number of germinated seeds was counted on day: 0, 1, 2, 3, 4, 5, 6, 7, 8, 11, 14 using a stereo microscope.

The root growth experiment was performed using plants grown vertically for four days on ½ MS solid media before transferred on ½ MS solid media containing either 50, 100, 250, 400 mM NaCl or no supplements (0). After seven days, seedlings were documented, and root length measured using ImageJ software (Schindelin et al., 2012).

2.2.4. Analysis of membrane lipids

2.2.4.1. Extraction of total lipids

Plants were ground with mortar (2 cm diameter) and pestle in liquid N₂. After determination of the fresh weight, the powder was extracted in 4 ml of chloroform/methanol (1:2, v/v) and incubated on ice for 30 min. Then 1.5 ml chloroform and 1.5 ml 0.15 M NaCl were added, the suspension mixed, and the mixture centrifuged at 1000 x *g* and 4 °C for 2 min to separate phases. The same settings were used for all further centrifugation steps. The lower (organic) phase was transferred to a new glass tube. The remaining suspension was diluted by adding 1.3 ml chloroform and centrifuged again. The lower (organic) phase was united with the previously collected organic phase. The combined organic phase was evaporated in an Reacti-Therm triple-block heating module evaporator and the dried lipids dissolved in 500 µl chloroform. The lipid solution was stored at -20 °C or used directly for separation of lipid classes by solid phase extraction.

2.2.4.2. Solid phase extraction (SPE) of galactolipids and phospholipids

To analyze different lipid classes from the same sample, lipid classes were separated by using solid phase extraction as described in (Launhardt et al., 2021). SPE columns were placed in 8 ml glass tubes and equilibrated with 1 ml chloroform before loaded with the extracted total lipid solution. The neutral lipid fraction was removed by adding 2 ml chloroform to the column. In the next step 2 ml of acetone/methanol (9:1, v/v) were used for enrichment of galactolipids. For the final extraction of phospholipids, 2 ml of methanol/acetic acid (10:0.1, v/v) were added to the column. For efficient evaporation of the solution, lipids were extracted from the lower phase after addition of 2 ml chloroform and 2 ml of 0.15 M NaCl and centrifugation. To the remaining solution 1 ml chloroform was added, centrifuged at 1000 x *g* and 4 °C for 2 min and the lower phase united with the previously collected organic phase. Galactolipid and phospholipid fractions were evaporated and dissolved in 100 µl chloroform. Lipid fractions were directly used for analysis or stored at -20 °C.

2.2.4.3. Preparative thin layer chromatography (TLC)

To isolate MGDG and PC as the lipids of interest, TLC was performed to separate lipid classes by using suitable developing solvents. All steps were conducted in a fume hood. Developing solvents of acetone/toluene/water (90:30:7, v/v) or chloroform/methanol/acetic acid (65:25:8, v/v) were used to separate classes of galactolipids or phospholipids, respectively. Before chromatography, a sheet of Whatman paper (20 cm x 20 cm) was placed in the developing chambers to allow a solvent gas-atmosphere to form. Samples were applied in distinct spots 2 cm above the bottom edge of a silica-coated glass plate. For identification, 5 µg of MGDG or PC standards (Avanti/Merck, Darmstadt, Germany) for galactolipids and phospholipids, respectively, were also applied. After drying, TLC plates were placed vertically in the developing chambers with the silica side facing the Whatman sheet. Plates were removed when the front of the developing solvent reached a distance of 5 cm from the upper edge. Plates were dried in a fume hood and sprayed evenly with 0.02 % primuline solution (acetone/water, 80:20, v/v). The lipids were visualized with UV light at 260 nm, and according to the standard signal, MGDG and PC were isolated by scraping off the silica gel surface.

2.2.4.4. Transesterification of lipid-associated fatty acids

The lipids were chemically derivatized to detach the fatty acids from the glycerol backbones and transesterify the residues to methanol for analysis by gas chromatography (GC). To enable quantification of fatty acid methyl-esters (FAMES) afterwards, 10 µg of synthetic tripentadecanoin was added as an internal standard to the isolated lipids. For the transesterification reaction, 333 µl methanol/toluene (2:1, v/v) and 167 µl of 1 M sodium methoxide solution was added and mixed for 20 min. For efficient phase separation, 0.5 ml 5 M NaCl and 1.5 ml n-hexane were added, the solution was mixed and centrifuged at 1000 x g and 4 °C for 2 min. The upper (organic) phase was collected, evaporated under streaming air, and 100 µl acetonitrile was added to transfer the FAMES into the inserts of GC-vials. In the final step, acetonitrile sample was evaporated and 10 µl acetonitrile was added, which were used for GC-analysis.

2.2.4.5. Transesterification of total fatty acids by acidic methanolysis

For global fatty acid analysis, an alternative method was used for the transesterification of fatty acids, which forms FAMES from all cellular fatty acids, including lipid-associated and free fatty acids. Pools of ten seeds of each Arabidopsis line were treated with 2 ml FAME solution (2.75 % (v/v) H₂SO₄ in methanol, 2 % (v/v) 2,2-dimethoxypropane) and incubated at 80 °C in a water bath for 1 h. Samples were cooled and mixed with 200 µl of 5 M NaCl and 2 ml of n-hexane. The mixture was centrifuged for 2 min at 1000 x g and 4 °C and the upper (organic) phase was transferred to a new glass tube. Another 2 ml of n-hexane was added to the remaining mixture to centrifuge again and combine the upper phase with the previous one. Samples were evaporated under streaming air and dissolved in 100 µl of acetonitrile, which was transferred to the inserts of the GC-vials. In the final step, acetonitrile samples in GC-vials were evaporated and another 10 µl acetonitrile was added, which was then used for gas chromatography analysis.

2.2.4.6. Analysis of FAMES by gas chromatography

Samples containing transmethylated fatty acids were analyzed using a gas chromatograph (Shimadzu GC-2010 Plus). Samples were injected using an auto-injector AOC-20i. A volume of 1 µl was injected in split mode at a temperature of 250 °C and analytes were separated on a DB-23 column (30 m x 0.25 mm; solid phase: cyanopropyl polysiloxane; matrix thickness: 0.25 µm). Helium was used as a carrier gas at a flow rate of 1 ml/ min and a temperature gradient of 1 min at 150 °C, increasing to 250 °C at a rate of 25 °C/ min, and then held for 4 min. A flame ionization detector (FID) was used for detection, in which burnt fatty acids were thermally ionized, allowing the closure of an electric contact, and the electrical signal was measured. Using this method, fatty acids are separated according to their chain length and number of double bonds. To identify the fatty acids, fatty acids from menhaden fish oil were transmethylated and also measured in each run as an authentic standard to identify the analytes by their characteristic retention times.

Moreover, as described in 2.2.4.4. an internal standard of known concentration was present in every sample and was used to quantify the amount of fatty acids. The Shimadzu Postrun Analysis program was used to evaluate GC-FID-profiles.

2.2.5. Quantification of transcript abundance

2.2.5.1. RNA extraction

For experiments, where the abundance of transcripts in response to stress treatments was analyzed, vertically grown plants were frozen and homogenized in liquid N₂ with mortar and pestle. The ground powder was defrosted in 1 ml of trizol (Tab. 2.6.) and transferred to 2 ml reaction tubes. After 5 min of incubation at room temperature, samples were centrifuged at 18500 x *g* and 4 °C for 10 min and the supernatants transferred to new 1.5 ml reaction tubes. A volume of 200 µl chloroform was added, samples were mixed and incubated at room temperature for 2 min. Subsequent centrifugation at 18500 x *g* and 4 °C for 15 min resulted in phase separation. The upper phases were transferred to new tubes, half their volumes of isopropanol and 0.8 M high-salt precipitation buffer (Tab. 2.6.) were added and mixed by inverting. Samples were incubated for 10 min at room temperatures and centrifuged at 18500 x *g*, and 4 °C for 10 min. Supernatants were removed and the total RNA sediments washed twice by adding 900 µl of 75 % (v/v) ethanol, centrifugation at 9500 x *g* and 4°C for 5 min and removing the supernatant. After the last washing step, sediments were air dried for 15 min and dissolved in 20 µl bidist. water. Subsequently, 1 µl of each sample was used for determination of RNA concentration by nanodrop and for quality control with agarose gels and gel electrophoresis.

Table 2.6.: Solutions and buffers used for RNA extraction and proof of quality and quantity.

Buffer	Components
Trizol (according to volume of 10 ml)	3.8 ml Roti® Phenol (0.1 M citrate buffer; pH 4.3) 2 ml 4 M guanidinium thiocyanate 1 ml 4 M ammonium thiocyanate 334 µl 3 M sodium acetate, pH 5.0 500 µl glycerol 2.366 ml bidist. water
0.8 M High salt precipitation buffer	0.8 M sodium acetate 1.2 M sodium chloride
1 x Tris-acetate-EDTA (TAE)- buffer	40 mM tris(hydroxymethyl)aminomethane 20 mM acetic acid 1 mM ethylenediaminetetraacetic acid (EDTA)
5 x DNA loading buffer	60 % (v/v) glycerol 0.4 % (w/v) orange G 0.03 % (w/v) bromophenol blue 0.03 % (w/v) xylene cyanol PP

Determination of total RNA concentration

To determine the concentration of total RNA in the extracted samples, 1 µl of the extracted total RNA was used to measure the absorbance at 260 nm with a NanoDrop 2000 photometer. The RNA concentration in ng/ µl was calculated using the NanoDrop software using the following formula:

$$c_{\text{RNA}} = A_{260 \text{ nm}} \times 40 \mu\text{g}/\mu\text{l} \times \text{dilution factor} \quad (1)$$

Quality control of total RNA content by using gel electrophoresis

To test the integrity of the extracted RNA, 1 µl total RNA was mixed with 3 µl 5 x DNA loading buffer (Tab. 2.6.) and separated by electrophoresis on 1 % (w/v) agarose gels in 1 x TAE buffer (Tab. 2.6.). As a size standard, 1 kb GeneRuler™ DNA-Ladder (Thermo Fisher Scientific, Dreieich, Germany) was used. Prior to use, electrophoresis chambers were cleaned for 15 min with 1 % sodium lauryl sulfate (SDS) to reduce RNase contamination. For electrophoretic separation, a voltage of 130 V was applied and stopped before the marker bands of DNA loading buffer left the gel. After electrophoresis, gels were incubated for 20 min in an ethidium bromide bath (10 µl/ ml in water). RNA signals were documented by UV light in a gel detection system Quantum-ST4-3026.

2.2.5.2. Complementary DNA (cDNA) synthesis

Complementary DNA (cDNA) was synthesized from total RNA using the RevertAid H Minus First Strand cDNA Synthesis Kit (Thermo Fisher Scientific, Dreieich, Germany) according to manufacturer's instructions. In brief, samples were incubated with mix 1 (Tab. 2.7.), 8 µl of mix 2 (Tab. 2.7.; contained dNTPs purchased from NEB, Frankfurt am Main, Germany) was added to a sample volume of 20 µl and the mixture was briefly sedimented by centrifugation at 3500 x *g* and RT for 6s.

Table 2.7.: Components of cDNA synthesis.

Mix 1 - components	amount	Mix 2 - components	amount
Total RNA	5 µg	5 x RT-buffer	4 µl
Oligo-dT-primer	1 µl	10 mM dNTPs	2 µl
Bidist. water	~ ad 12 µl	RNase-Inhibitor	1 µl
		RT-Polymerase	1 µl

Reactions were incubated in a heating block at 42 °C for 1 h and terminated by heat-denaturation at 70 °C for 10 min. The samples were stored at -80 °C until further use.

2.2.5.3. Determination of transcript abundance by quantitative real time polymerase chain reaction (qPCR)

A quantitative reverse-transcriptase real-time polymerase chain reaction (qPCR) was performed to determine the transcript abundance of the genes listed in Table 2.9. The Luna® Universal qPCR Master Mix Kit (NEB, Frankfurt am Main, Germany) was used to set up reaction mix according to manufacturer's instructions as described in Table 2.8.

Table 2.8.: Reaction mix for qPCR.

qPCR Mix – Components	Amount
2x Luna Universal	10 µl
10 µM/ µl forward primer	0.5 µl
10 µM/ µl reverse primer	0.5 µl
cDNA	2 µl
Bidist. water	~ 20 µl

Table 2.9.: Used qPCR oligonucleotide (primer) combinations.

Gene	Oligonucleotides	sequence in 5'-3' – direction
<i>UBC10</i>	qUBC10-for	ACATCATGTAGCGCAGGTCC
	qUBC10-rev	CCGGAGGGAAATGGATGGTT
<i>DREB2A</i>	qDREB2A_1-for	TTCGTCCCCTATAGATTGTGTTGT
	qDREB2A_1-rev	CCACAGTAGTACCGTCACCT
<i>RD29B</i>	qRD29B_1-for	TCACCATCCAGAAGAAGAAGAGC
	qRD29B_1-rev	AGACTGTTCTTGATTTTCTTAGC
<i>FAD2</i>	qfad2-1-for	TTGCCATTCCCCATCTGACC
	qfad2-1-rev	CCTGCACCCATGTTTCTGGA
<i>FAD3</i>	qfad3-2-for	AGAGGCAAGGAATGGAGTTATC
	qfad3-2-rev	TGGCGTCGACCAAGTGATAG
<i>MGD1</i>	qmgd1-2-for	AGGAGGGATTGCCGTTGAAT
	qmgd1-2-rev	AGGGCGTATGATCTGTCCAC

S40-3	qAtS40-3.for	ACTTGAGTCGACACCGTAACA
	qAtS40-3.rev	TTCAAAGCTAAATCACATCCA
SAG13	qAtSAG13.for	AGTAACGATGTAAGGCCAAAGT
	qAtSAG13.rev	TTCTCCAACACGCCCCATT

The qPCR reactions were performed using a Rotor-Gene Q thermocycler equipped with a 72-Well rotor, based on the principle of conventional PCR with amplification steps listed in table 2.10. For the amplification of transcripts, corresponding oligonucleotides with a maximum length of 200 bp were designed using the online tool Primer-BLAST (National Center for Biotechnology Information, U.S. National Library of Medicine, Bethesda, MD, USA). The transcript abundance for the genes listed in table 2.9. was determined by using corresponding oligonucleotides and addition of fluorescence dye (SYBR Green), which intercalates in newly synthesized double stranded DNA. Fluorescence signals determined for each amplification cycle are proportional to the DNA amount generated. The transcript content of the *Ubiquitin-Conjugating Enzyme 10 (UBC10)* gene was used as a reference for normalization. The program Rotor-Gene Q was used for documentation of cycle-dependent fluorescence.

Table 2.10.: qPCR program for determination of transcript abundance.

Step	Temperature in °C	time in s
1. Initial Denaturation	94	300
2. Denaturation	94	10
3. Attachment	60	20
4. Elongation	72	30

The Rotor-Gene Q Series software was also used to convert the recorded data. Transcript abundancies were subsequently analyzed according to Pfaffl (2001), using the LinRegPCR program (Ruijter et al., 2009; Tuomi et al., 2010). NO values (Number of target copies in the reaction) were calculated including PCR efficiency, start of exponential phase and background fluorescence.

Based on the NO values, relative quantification (ΔCt) and relative transcript abundancies were determined:

$$\text{relative quantification} = \frac{\emptyset NO (\text{gene of interest})}{\emptyset NO \text{ UBC10}} \quad (2)$$

$$\text{relative transcript content} = \frac{\Delta Ct (\text{sample})}{\Delta Ct (\text{control sample})} \quad (3)$$

2.2.6. Quantification of chlorophyll and carotenoid contents.

For pigment analysis, at the end of the dark phase approximately 12 mg of shoot material of vertically grown plants were harvested into 2 ml reaction tubes containing six glass beads (size 3 mm) and 200 μ l bidist. water. Samples were kept in the dark and on ice. After determination of fresh weight, the plant material was homogenized at 4 °C for 40 s in a shaking mill at a frequency of 30 motions/s. Afterwards, 800 μ l cold acetone was added and the mixture incubated at 4 °C for 40 min rotating in an overhead shaker. Samples were centrifuged at 18500 x g and 4 °C for 5 min and 800 μ l of the supernatant transferred into a single-use cuvette. Using 80 % acetone as a blank, the absorbance at 663, 647 and 470 nm was measured in an Ultrospec 2100 pro photometer for chlorophyll a, chlorophyll b and carotenoids, respectively.

For evaluation of pigment amounts, the following formulas were used according to Lichtenthaler and Buschmann (2001) and ultimately divided by the respective fresh weights.

$$\text{Chl}_a = 12.25 \times A_{663 \text{ nm}} - 2.79 \times A_{647 \text{ nm}} \quad (4)$$

$$\text{Chl}_b = 21.5 \times A_{647 \text{ nm}} - 5.1 \times A_{663 \text{ nm}} \quad (5)$$

$$\text{Carotenoids} = \frac{(1000 \times A_{470 \text{ nm}} - 1.82 \times \text{Chl}_a - 85.02 \times \text{Chl}_b)}{198} \quad (6)$$

2.2.7. Analysis of photosynthetic parameters.

For the analysis of photosynthetic performance in different plant lines or upon stress treatments, the first true leaves of horizontally grown seedlings were collected and placed on ½ MS agar

plates. After dark adaption for at least five minutes, fluorescence parameters were detected by pulse-amplitude-modulated light excitation, using an IMAGING-PAM chlorophyll fluorometer, that consists of an IMAG-C control unit combined with an IMAG-L LED-Ring-Array and an IMAG-K CCD camera. The PAM excitation light (470 nm) was applied with an intensity of approx. $0.1 \mu\text{mol m}^{-2} \text{s}^{-1}$ and a modulation frequency of 1 Hz. A saturation pulse was used with a duration of 800 ms and an intensity of $2400 \mu\text{mol m}^{-2} \text{s}^{-1}$. Minimal fluorescence (F_0), maximal fluorescence (F_m) and variable fluorescence (F_v) parameters were determined for the dark-adapted leaves to obtain the maximum PSII quantum efficiency (max. PSII eff., [7]). A light-curve with 15 steps of photosynthetic active radiation (PAR, in $\mu\text{mol m}^{-2} \text{s}^{-1}$), increasing from 14 to $1200 \mu\text{mol m}^{-2} \text{s}^{-1}$ and duration intervals of 30 s was subsequently recorded. The steady state fluorescence directly before the saturation pulse (F') and plateau level fluorescence during the applied saturation pulse (F_m') were determined at the end of each light step and the effective PSII quantum yield (YII, [8]), non-photochemical quenching (NPQ, [9]) were calculated. Each individual leaf absorptivity (Abs., [10]) was estimated by values of red-light remission at 650 nm (R) and values of near infra-red-light remission at 780 nm (NIR) according to the IMAGING-PAM manufacturer's instructions. All measurements were recorded by ImagingWin software, which already automatically calculated the parameters mentioned.

$$\text{max. PSII eff.} = \frac{F_v}{F_m} \quad (7)$$

$$\text{YII} = \frac{F_q'}{F_m'} \quad (8)$$

$$\text{NPQ} = \left(\frac{F_m}{F_m'} \right) - 1 \quad (9)$$

$$\text{Abs.} = \frac{1-R}{\text{NIR}} \quad (10)$$

2.2.8. Determination of the de-epoxidation state of xanthophyll cycle (XC) pigments in Arabidopsis.

2.2.8.1. Thylakoid isolation

The analysis of the XC required the isolation of intact thylakoids. For thylakoid isolation from each plant line, green tissue was harvested from approximately 500 horizontally grown seedlings at the end of the dark phase. After incubation in iced water for 30 min, plants were homogenized in 5 ml of grinding buffer (Tab. 2.11.) by using mortar and pestle and filtered through two layers of cotton gauze. For maximum yield, the gauze was additionally washed with 10 ml of grinding buffer. Thylakoids and remaining intact chloroplasts were sedimented at $2600 \times g$ and $4 \text{ }^{\circ}\text{C}$ for 3 min, which were also the centrifugation settings for all further steps. Sediments were washed by careful resuspension in 3 ml resuspension buffer (Tab. 2.11.). The washing step was repeated one more time. To disrupt remaining intact chloroplasts, the sediment was first resuspended in 1 ml of hypotonic buffer (Tab. 2.11.) and the volume was then brought to 5 ml. After centrifugation, the sediment was resuspended in 1 ml of resuspension buffer and the thylakoid preparation stored on ice in the dark.

Table 2.11.: Buffer used for thylakoid extraction according to Casazza et al. (2001).

Buffer	Components
Grinding buffer	0.4 M sorbitol, 5 mM EDTA, 5 mM EGTA, MgCl_2 , 10 mM NaHCO_3 , 20 mM Tricine (NaOH; pH 8.4), 0.5 % (w/v) fatty acid free bovine serum albumin (BSA)
Resuspension buffer	0.3 M sorbitol, 2.5 mM EDTA, 5 mM MgCl_2 , 10 mM NaHCO_3 , 20 mM HEPES (NaOH; pH 7.6), 0.5 % (w/v) fatty acid free BSA
Hypotonic buffer	2.5 mM EDTA, 5 mM MgCl_2 , 10 mM NaHCO_3 , 20 mM HEPES (pH 7.6), 0.5 % (w/v) fatty acid free BSA

For all further experiments, the amounts of thylakoid preparation used was based on the calculated μg of total chlorophyll content. The total chlorophyll content of the thylakoid preparations was determined by dissolving 30 μl of thylakoid suspension in 5 ml of 80 % acetone.

After centrifugation at 4 °C at 2600 x *g* for 5 min, 1 ml of the supernatant was used for photometric determination of chlorophyll a and chlorophyll b absorbance at 663 nm and 647 nm, respectively. The thylakoid concentration of each sample was proportional to the total chlorophyll content, given by the sum of Chl a and Chl b concentrations (see 2.2.5.).

2.2.8.2. Analysis of the de-epoxidation state of XC pigments

The analysis of the de-epoxidation state of XC pigments under optimal conditions for violaxanthin de-epoxidase (VDE) as it was done with isolated thylakoids in the biochemical approach (see 2.2.8.2.1.) enabled to distinguish possible differences in maximal possible de-epoxidation of XC pigments between the different plant lines. Since in this way only the efficient functionality of the VDE can be investigated, but not the complexity of the XC mechanism within the functional organism of the plant lines can be analyzed, pigment amounts from light exposed leaves of the different plant lines were isolated and analyzed in the light-dependent approach (see 2.2.8.2.2.).

2.2.8.2.1. Preparation of the biochemical approach

To determine the maximal possible de-epoxidation of XC pigments in the isolated thylakoids, violaxanthin de-epoxidation was triggered biochemically by adding an excess of ascorbic acid. Isolated thylakoids corresponding to 20 µg total chlorophyll content/ ml based on final volume were pre-incubated for 5 min in 1 ml of reaction buffer (10 mM NaCl, 5 mM MgCl₂, 40 mM MES pH 5.0) in the dark at 30 °C. De-epoxidation was initiated by adding further 4 ml of 30 °C tempered reaction buffer containing 30 mM ascorbic acid, followed by immediate sampling of 750 µl at time 0 min. Reactions were performed in the dark over a period of 30 min and at 30 °C. To stop the reactions and extract the pigments, 750 µl of extracting solution (Tab. 2.12.) was added, the mixture centrifuged for 1 min at 21100 x *g* and 4 °C and 200 µl of the lower phases were transferred to new tubes. Solvents were evaporated under streaming N₂ and the residues kept at -20 °C for further analysis by high performance liquid chromatography (HPLC).

2.2.8.2.2. Preparation of the light-dependent approach

To assess the light-dependent, intrinsic degrees of violaxanthin de-epoxidation, an alternative experimental setup was used. For each line, five leaves of horizontally grown seedlings were collected and placed on ½ MS agar plates. Leaves were exposed to photosynthetic active radiation from an IMAGING-PAM chlorophyll fluorometer, using same settings as described in 2.2.7.1. Stepwise increases of radiation from 14 to 1200 $\mu\text{E m}^{-2} \text{s}^{-1}$ were used to expose leaves to 0, 170, 950, 1200 $\mu\text{E m}^{-2} \text{s}^{-1}$ of radiation. Leaves were collected in tubes containing glass beads (size 0.85-1.23 mm) and frozen in liquid N₂. For extraction of pigments, leaves were first ground for 1 min at -80 °C in a shaking mill at a frequency of 30 motions/ s and then for a second time after adding 750 μl of extracting solution (Tab. 2.12.). A volume of 750 μl of bidist. water was added and the samples centrifuged at 21100 x g and 4 °C for 1 min. The lower phase (200 μl) was transferred to a new tube, samples were evaporated with streaming N₂ and stored at -20 °C until pigments were analyzed by HPLC.

Table 2.12.: Media used for preparation and HPLC eluents for pigment separation according to Kraay et al. (1992).

Eluents/ media	Components
Extracting solution	chloroform:methanol:ammonia (1:2:0.004, v/v/v)
Injecting solution	Methanol - ammonium acetate mix / 0.2 M ammonium acetate (9:1, v/v) 10 % (v/v) ethyl acetate
A	Methanol/0.5 M ammonium acetate (85:15, v/v)
B	Acetonitrile/bidist. water (9:1, v/v)
C	100 % Ethyl acetate
D	100 % Methanol

2.2.8.3. Analysis of pigments by HPLC

For the analysis of pigments by HPLC, nitrogen-dried samples were resuspended in 200 μl injecting solution (Tab. 2.12.) and transferred into HPLC injection glass vials. Pigments were

separated and analyzed using a Dionex UltiMate 3000 HPLC system. For each measurement, 100 µl of sample were injected using a Dionex WPS-3000SL autosampler and directed on an ET 250/4 Nucleosil 120-5 C18 chromatography column. Pigments were separated in 30 min runs using an elution gradient according to Kraay et al. (1992) and a flow rate of 0.8 ml/ min (see Tables 2.12. and 2.13.). For an accurate mix of solvents, a Dionex LPG-3400A system was used, consisting of quaternary low-pressure pump with integrated vacuum degasser. The column thermostat TCC-3000 ensured a constant temperature of 20 °C for the duration of the chromatography. During the whole run the photodiode array detector PDA-3000 detected eluting pigments in a wavelength range between 350-750 nm and the patterns were recorded using Chromeleon software. For quantification of xanthophylls, values at 440 nm were used. Further absorption spectra were saved for post-processing. After every run, the column was washed with 100 % methanol, and this solution was also used for column storage.

Table 2.13.: Linear elution gradient for HPLC separation of thylakoid pigments according to Kraay et al. (1992).

Time [min]	Eluent A [%]	Eluent B [%]	Eluent C [%]
0	60	40	0
2	0	100	0
7	0	80	20
17	0	50	50
21	0	30	70
28.5	0	30	70
29.5	0	100	0
30.5	60	40	0

2.2.8.4. Quantification of xanthophyll pigments and de-epoxidation state

The pigment peaks from the HPLC analysis were the result of recorded absorption spectra at the respective retention times and were used to determine the integrals of the peak area (A_i) with

the Chromeleon software. The integrated peak areas together with the quantification wavelengths, the determined conversion factors (convert detector area in specific pigment amounts) of each peak area/ μg pigment (E) and the ideal molar mass (M) according to Lohr (2001) (Tab. 2.14.) were used to quantify the xanthophyll pigments and chlorophyll a according to the following formula:

$$n [\text{mmol}] = \frac{A_i}{E \times M} \quad (11)$$

Table 2.14.: Data used to calculate pigments according to Lohr (2001).

Pigment	Quantification	Conversion factor	Molar mass [g/ mol]
	wavelength λ_{quant} [nm]		
Violaxanthin	440	17741111	600.89
Antheraxanthin	480	14340454	584.89
Zeaxanthin	480	14295657	568.89
Chlorophyll a	430	7272969	893.52

The determined amounts of xanthophyll pigments were normalized against the amounts of chlorophyll a, because the amount of thylakoids used for the analysis was also based on the total chlorophyll concentration. The thus normalized amounts of xanthophyll cycle pigments were then used to determine the de-epoxidation state according to the following formula:

$$\text{DES} = \frac{(0.5 \times A_x) + Z_x}{(V_x + A_x + Z_x)} \quad (12)$$

2.2.9. Transmission electron microscopy

After the plant lines had grown vertically on plates, Dr. Gerd Hause (MLU Biozentrum, Halle) performed all further steps, which are described below. Leaves from plant lines were cut into segments and fixed for 3 h at room temperature with 3 % (w/v) glutaraldehyde in 0.1 M sodium

cacodylate buffer (SCB; pH 7.2). After fixation, the samples were rinsed in SCB and postfixed for 1 h at room temperature with 1 % (w/v) osmium tetroxide in SCB. Subsequently, the leaf segments were rinsed with water, dehydrated in a graded ethanol series (10 %, 30 %, 50 %, 70 % (containing 1 % (w/v) uranyl acetate), 70 %, 90 % and 2 × 100 % for 30 min each), infiltrated with epoxy resin according to Spurr (1969), and polymerized for 18 h at 70 °C. Ultrathin sections (70 nm) were prepared with an Ultracut R ultramicrotome. Sections were transferred to Formvar-coated copper grids, post-stained with uranyl acetate and lead citrate with an EMSTAIN (Leica, Wetzlar, Germany) and observed with an EM 900 transmission electron microscope at an acceleration voltage of 80 kV. Electron micrographs were recorded with a Variosped SSCCD camera SM-1k-120.

2.2.10. Statistics

Data were analyzed unbiased and tested for statistical relevance by two-sided Student's T-tests ($P < 0.05$). The T-tests and graphs were performed with Microsoft Excel (Microsoft Corporation, Redmond, WA, USA).

3. Results

3.1. Mild salt treatment of Arabidopsis plants changes membrane lipid composition.

The plasma membrane surrounding each cell is a lipid bilayer that represents the first barrier confronted with external stimuli and stresses, which require rapid and appropriate cellular responses. In previous studies, stresses experimentally applied to plants were often substantial in dosage, resulting in the recording of unphysiological responses, in cell damage, or (in our hands) even in the death of the treated plants (Fig. 6.2.). However, to study physiologically relevant recognition mechanisms and subsequent cellular responses, it is useful to treat plants with stress in a more subtle way to avoid inducing plant death. A suitable stress intensity may depend on the age of the plants studied or be related to the conditions or experimental setup used to grow the plants. In previous studies on dynamic lipid changes upon salt stress, plants were grown for ten weeks in hydroponic culture and then exposed to 400 mM NaCl (König et al., 2007). While substantial lipid changes were observed using this setup, the long-term hydroponic culture was detrimental to plant development, and the high concentration of salt used as an experimental trigger resulted in unphysiological responses and damage. Here, an attempt was made to address the salt-triggered dynamic of lipid changes at the plasma membrane by using a simpler cultivation system which was optimized for moderate salt stress without damaging the plant. By transferring two-week-old Arabidopsis seedlings grown on solid media containing $\frac{1}{2}$ MS to plates containing solid media with different concentrations of salt, it was determined that salt concentrations as low as 50 mM yielded reproducible effects on the plants, without affecting their survival or even the pattern of growth (Matzner, 2019). Using this setup, it was a main goal of this thesis to determine changes in membrane lipid biology during responses of Arabidopsis plants to mild salt conditions, within the range of physiological responsiveness of the plants.

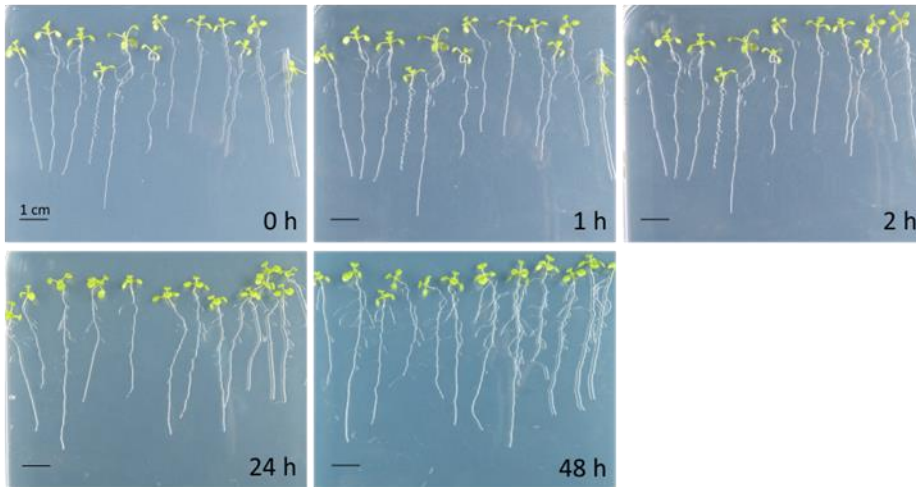
3.1.1. Perception of low salt concentrations without macroscopic effects on plant growth.

In order to get an impression of the extent to which a mild salt treatment with 50 mM NaCl macroscopically affected the plant growth, salt treated plants were observed under short-term

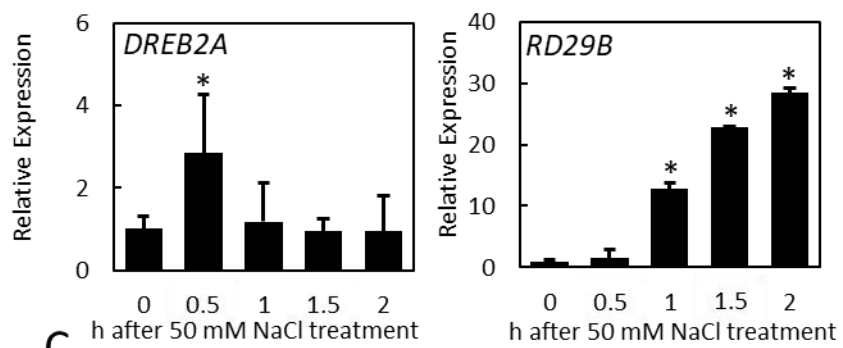
and long-term conditions. The plants analyzed were macroscopically not affected by the salt treatment after 1 h and 2 h and even after longer exposure to 50 mM NaCl for 24 or 48 h (Fig. 3.1. A). Since the plants looked vital and remained visually hydrated, it was concluded that the low salt concentrations used in subsequent experiments to study short term effects of salt on lipid abundance cause no harm for the plants (Fig. 3.1. A). The maintained vitality of the long-term treated plants could be an indication that eventual short-term salt-induced lipid dynamics were related to salt stress responses rather than to lipid degradation induced by plant death.

Furthermore, to test whether low salt concentrations were perceived by the plants, the expression of known salt stress marker genes was examined upon salt treatment by quantitative real-time PCR. The salt-inducible gene *Dehydration-responsive element-binding protein 2A (DREB2A)* encodes a transcription factor that initiates the expression of several other genes responding to drought and cold stress (Liu et al., 1998). One of the target genes of *DREB2A* is the downstream gene, *RESPONSIVE TO DESICCATION 29B (RD29B)*, which is discussed to be an element of abiotic stress signaling (Morimoto et al., 2013; Msanne et al., 2011). The abundance of transcripts for *DREB2A* and *RD29B* was analyzed to verify the perception of the low salt concentrations applied. During the salt treatment of the plants, the transcript levels of *DREB2A* and *RD29B* were monitored over a period of 2 h in intervals of 0.5 h (Fig. 3.1 B). The transcript abundance of *DREB2A* was significantly increased after 0.5 h and returned to basal level at 1, 1.5 and 2 h of treatment (Fig. 3.1. B).

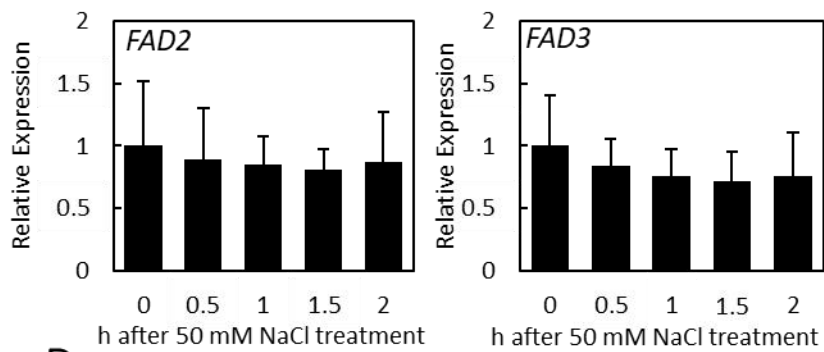
A



B



C



D

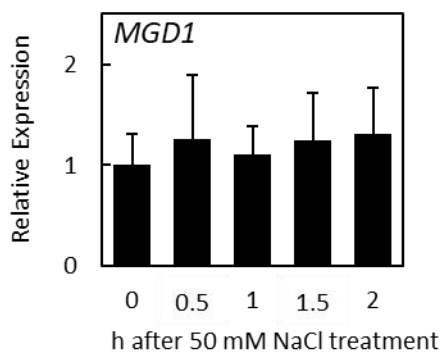


Figure 3.1.: Influence of low salt concentrations on growth of seedlings and transcript level of salt stress marker and genes involved in lipid biosynthesis.

A, Seedlings grown on solid media for two weeks were transferred on solid media containing 50 mM NaCl and were documented after 0, 1, 2, 24 and 48 h of the treatment. To avoid any contamination effects, set of seedlings showed in 0, 1 and 2 h images were kept the same while images of seedlings after 24 h and 48 h were a different set for each. B and C, Seedlings grown on solid media for two weeks were transferred on solid media containing 50 mM NaCl and harvested after 0, 0.5, 1, 1.5 and 2 h. RNA was extracted and used for cDNA synthesis to analyze expression of *DREB2A* and *RD29B* (B), *FAD2* and *FAD3* (C) and *MGD1* (D) by qPCR and normalized to *UBC10*. Data represent means \pm SD of four biological replicates from two independent experiments. Asterisks indicate significant changes compared to time point zero using Student's T-test ($*P<0.05$).

The transcript abundance of *RD29B* showed a significant increase after 1 h of 50 mM NaCl treatment and continued to rise until 2 h of treatment to reach a level approximately 30 times higher than the basal level. When treated with 100 mM NaCl, plants displayed a similar expression level of *DREB2A* and *RD29B*, differences appeared only in the dynamics of expression patterns over time (Fig. 3.2. A). Firstly, the increase in *DREB2A* transcript level after 0.5 h remained until 1.5 h of the salt treatment. Secondly, *RD29B* expression increased as soon as 0.5 h of salt treatment but decreased again after 2 h (Fig. 3.2. A). However, the changes of transcript abundance were not statistically evaluated due to the limited number of performed experiments.

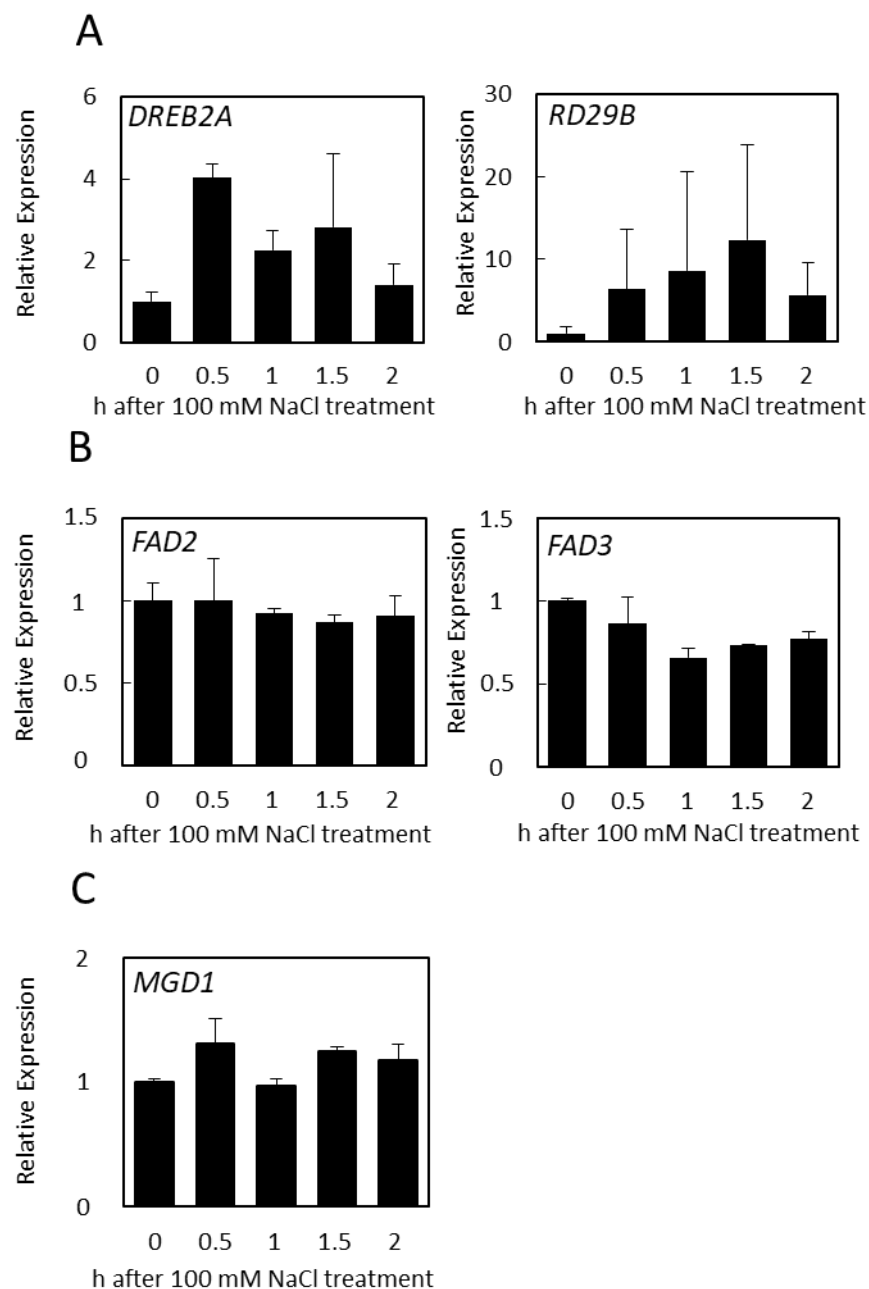


Figure 3.2.: Transcript abundance of salt stress marker genes and genes involved in lipid biosynthesis when treated with 100 mM NaCl.

Seedlings grown on solid media for two weeks were transferred on solid media containing 100 mM NaCl and harvested after 0, 0.5, 1, 1.5 and 2 h. A and B, RNA was extracted and used for cDNA synthesis to analyze expression of *DREB2A* and *RD29B* (A), *FAD2* and *FAD3* (B) and *MGD1* (C) by qPCR and normalized to *UBC10*. Data represent means \pm SD of two biological replicates from one experiment.

Besides the two known salt stress markers *DREB2A* and *RD29B*, the transcript levels of fatty acid desaturase genes *FAD2* and *FAD3* were also analyzed as constitutively expressed genes, to

compare with the salt-inducible genes and to test for changes in expression which might influence the abundance of lipids and fatty acids (Fig. 3.1. C). Compared to the salt stress markers, the transcript abundance of neither *FAD2* nor of *FAD3* changed over a period of 2 h in either of the salt treatments (Fig. 3.1. B, C; Fig. 3.2. A, B). Another gene tested, which proved relevant at a later stage of this study, was *MGD1* (Fig. 3.1. D; Fig. 3.2. C). The MGDG-synthase *MGD1* is the predominant enzyme mediating the *de novo* biosynthesis of MGDG in plastids. Kobayashi et al. (2009) demonstrated that *MGD1* is strongly expressed in Arabidopsis roots upon 6 h treatment with 150 mM NaCl. Since lower amounts of salt were used in this study and the response of plants were monitored during the first 2 h of salt stress, it was investigated whether this treatment resulted in a higher expression of *MGD1*. The qPCR analysis of salt treated plants did not show a significant change in *MGD1* transcript abundance during a 2 h treatment with 50 mM or 100 mM NaCl (Fig. 3.1. D; Fig. 3.2. C). The salt stress marker genes, thus, indicated the successful induction of short-term salt stress with low salt concentrations, and the changed transcript levels were not a consequence of an overall higher expression of genes (Fig. 3.1. C; Fig. 3.2. B). The maintenance of *FAD2*, *FAD3* and *MGD1* transcript levels during short-term treatment also suggests that eventual changes in lipid levels or fatty acid profile are not due to changes in the expression of these lipid biosynthesis/remodeling genes (Fig. 3.1. C, D; Fig. 3.2. B, C).

3.1.2. Extraplasmidial and plastidial lipids increase after short-term salt treatment.

Changes in membrane lipid composition, possibly reflecting lipid remodeling, are well known for various biotic and abiotic stresses and are an important physiological mechanism to maintain membrane integrity under changing environmental conditions (Barajas-Lopez et al., 2021; Gigon et al., 2004; Mosblech et al., 2008; Pical et al., 1999). Previous studies have shown that changes in lipid abundance can occur globally within the cells, but so far it is not well studied whether such adjustments are correlated between different cellular membranes. Two lipids which have previously been observed to change during salt stress are the phospholipid PC, which is the major lipid in the plasma membrane and most organelles, and the galactolipid MGDG, which is exclusive to the membranes of plastids (unless the plant experiences phosphate deprivation; Härtel et al.,

2000) and is overall the most abundant lipid in plant cells. When plants were treated with either 250 or 400 mM NaCl for longer time periods the amounts and degree of saturation in PC and MGDG might change but sooner or later led to the death of the plant (Fig. 6.1.; Fig. 6.2.). This might suggest that the shift in lipid abundance caused by high salt concentrations such as 250 or 400 mM NaCl are related to degradation processes rather than to acclimation of the plants to the stress.

Therefore, to investigate a potential link between the changes in PC and MGDG under stress, it was first analyzed whether changes in PC and MGDG were induced by mild salt concentration of 50 mM NaCl. Total lipids were extracted from salt treated plants after different times of treatment and the lipids were separated into galacto- and phospholipids by solid phase extraction chromatography. The individual lipid classes of galactolipid and phospholipids, respectively, were then separated by thin layer chromatography and visualized with 0.02 % primuline and UV illumination. Fluorescent bands of PC and MGDG were identified according to the migration of standards, the lipids isolated and their associated fatty acids transesterified to methanol. The resulting fatty acid methyl esters (FAMES) were then used to characterize fatty acid patterns and quantify the lipid amounts using gas chromatography (Fig. 3.3. A).

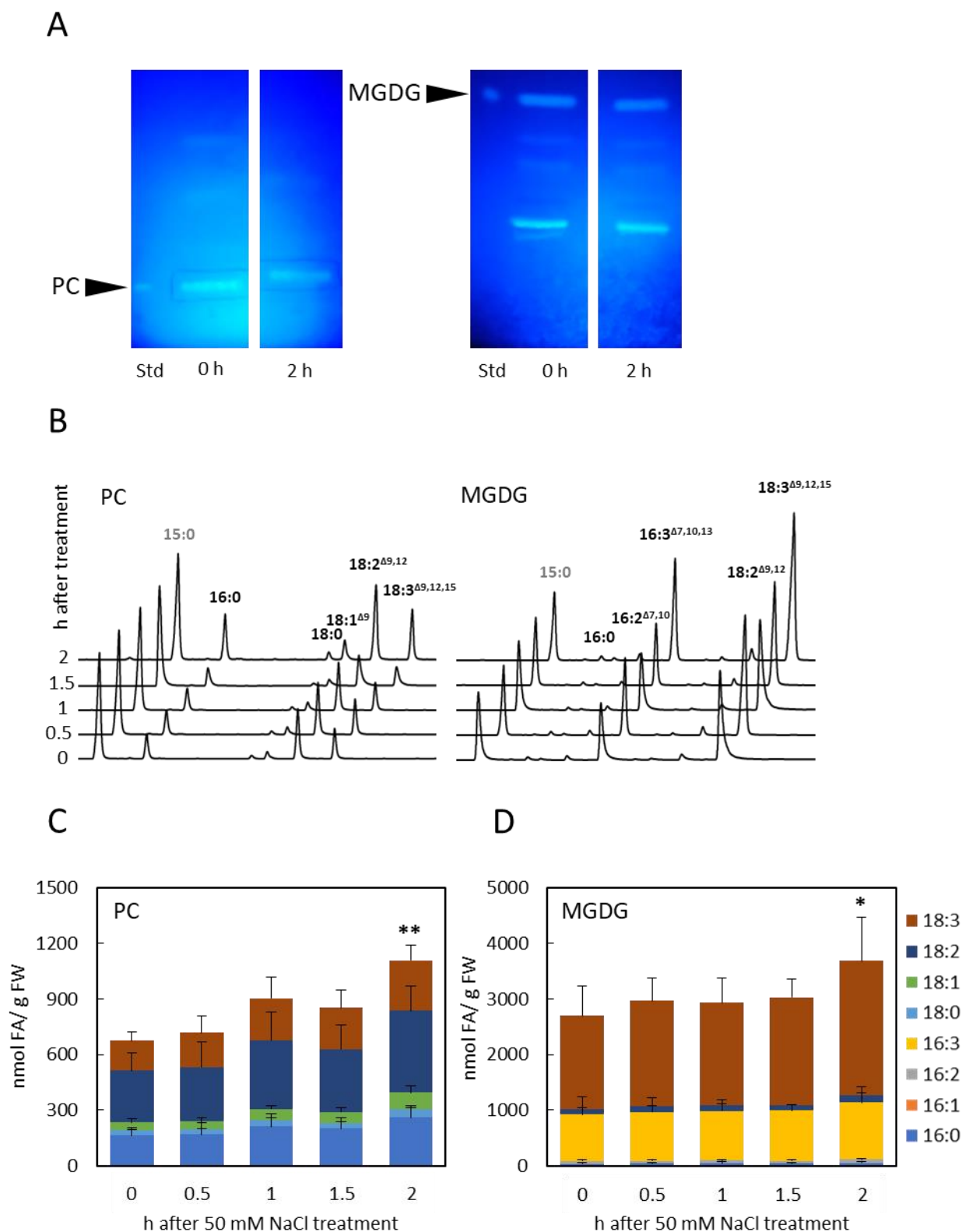


Figure 3.3.: Lipid analysis of extraplastidial and plastidial lipids in WT after treatment with low salt concentrations.

Seedlings were grown for two-weeks on $\frac{1}{2}$ MS solid media and then transferred on $\frac{1}{2}$ MS solid media containing 50 mM NaCl. Green tissue was harvested after 0, 0.5, 1, 1.5 and 2 h of treatment and prepared

for lipid extraction. Lipid extracts were separated in galacto- and phospholipid fraction by solid phase extraction. Galacto- and phospholipid fractions were separated into lipid classes on silica plates by thin-layer-chromatography using suitable developing solvents. A, Plates were visualized using 0.02% primuline (acetone/ water, 80:20, v/v) with UV at 260 nm and identified by respective standards (Std) to isolate phosphatidylcholine (PC) and monogalactosyldiacylglycerol (MGDG). Lipid-associated fatty acids were methyl transesterified and analyzed by gas chromatography. B, Time resolved 3D-illustration of signals derived from measured methyl transesterified fatty acids related to PC and MGDG samples, together with added internal standard tripentadecanoin (grey, 15:0; 10 µg) shown in peaks of a chromatograms obtained from Shimadzu Postrun Analysis program. C, After including the molar mass of each fatty acid (FA) and fresh weight (g FW), PC and MGDG are displayed in fatty acid profile, which shows the average and standard deviation of fatty acids of seven-ten biological replicates from three-four independent experiments. Asterisks indicate significant changes of lipid levels compared to time point zero using Student's T-test (* $P < 0.05$; ** $P < 0.01$). Identified fatty acids: blue, 16:0; orange, 16:1^{Δ7}; grey, 16:2^{Δ7,10}; yellow, 16:3^{Δ7,10,13}; light blue, 18:0; green, 18:1^{Δ9}; dark blue, 18:2^{Δ9,12}; brown, 18:3^{Δ9,12,15}.

The chromatograms of the gas chromatography show different fatty acids separated according to carbon chain length and the number of double bonds, and the intensity of the signals (i.e., the peak area) corresponds to their abundance. Chromatograms for fatty acids associated with PC or MGDG revealed characteristic fatty acid patterns for both lipids (Fig. 3.3. B). The main fatty acids esterified to PC were 16:0, 18:2 and 18:3, with smaller amounts of associated 18:0 and 18:1. In contrast, for MGDG the fatty acids 16:3 and 18:3 were predominantly associated and 16:0 and the precursors of the dominant fatty acids, 16:2 and 18:2 were present in traces. The overall sum abundance of fatty acids associated with each lipid, as quantified according to the internal standard 15:0, enables lipid quantification. Both PC and MGDG increased over a period of 2 h of salt treatment, and this increase appeared stronger for MGDG. Not only the internal standard 15:0 but also the fresh weight was considered as an alternative reference for quantification, and the respective calculations verified the observations based on the chromatograms. Figure 3.3. C shows the total fatty acid composition of PC and MGDG after 0, 0.5, 1, 1.5 and 2 hours of salt stress. The data shows that MGDG is already four times more abundant than PC before stress application. Moreover, the fatty acid composition in MGDG indicates a higher degree of unsaturation than in PC and these observations reflect known features of these lipids. While both lipids showed no difference in their amounts after one hour of salt treatment, they increased significantly after two hours, which was due mostly to a significant increase of associated 16:0, 18:2 and 18:3 for PC and of associated 18:3 for MGDG, respectively, and was also visualized in the 3D-illustration of the chromatogram resulted from the GC measurements (supplements Tab. 6.3.;

Fig. 3.3. B). The amount of PC almost doubled after the short salt treatment, but more surprising was the increase of MGDG, which is already a very abundant lipid and gained an average of 1000 nmol FA/ g FW, which corresponds to approximately the total amount of PC after two hours of salt treatment. When extending the duration of the 50 mM NaCl treatment up to 24 h and 48 h the amounts of PC and MGDG in WT plants remained increased (Fig. 3.4. A).

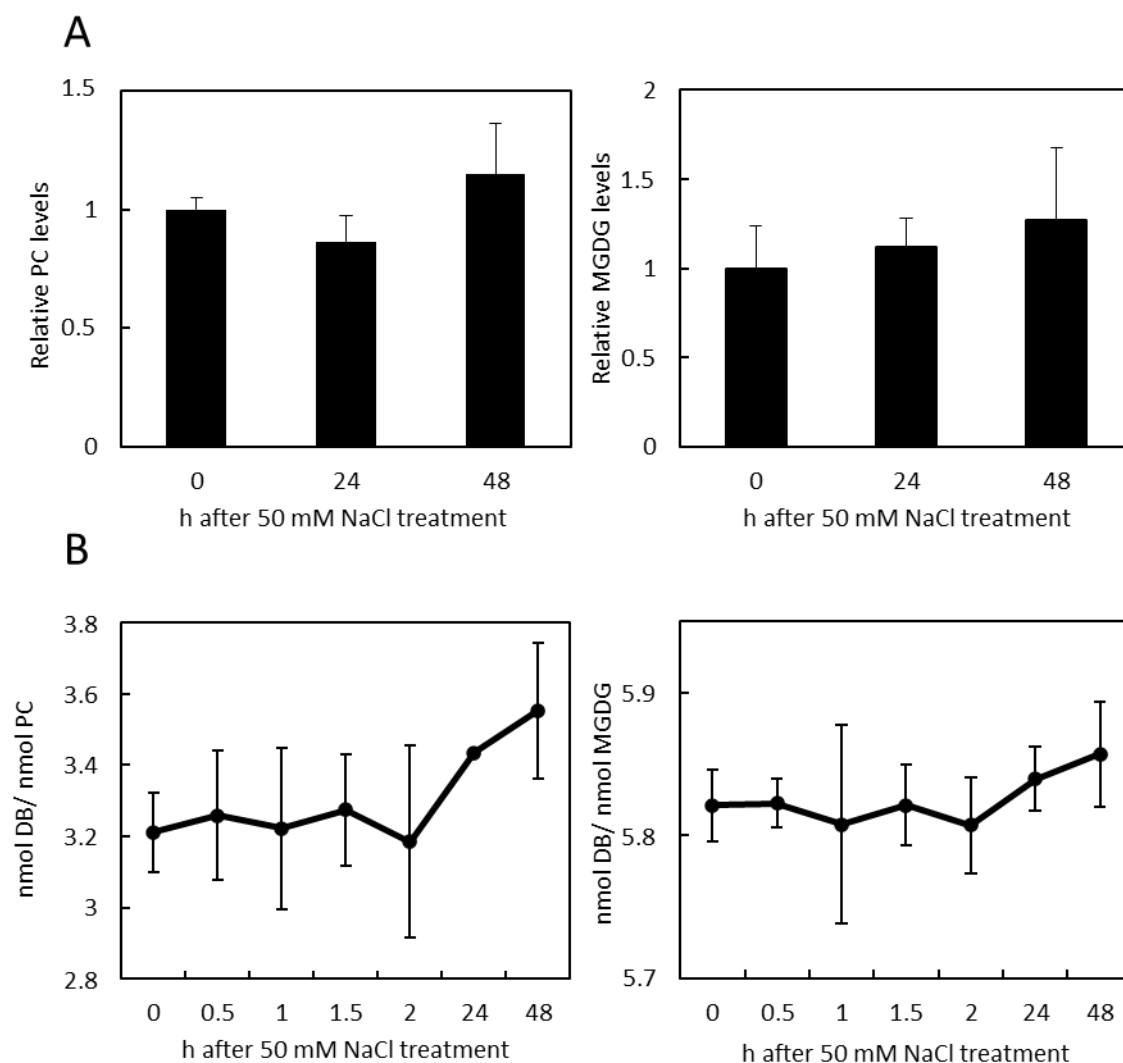


Figure 3.4.: Analysis of the degree of unsaturation of PC and MGDG in WT plants after long-term treatment with low salt concentrations.

Seedlings were grown for two-weeks on $\frac{1}{2}$ MS solid media and then transferred on $\frac{1}{2}$ MS solid media containing 50 mM NaCl. Green tissue was harvested after 0, 24 and 48 h of treatment and prepared for lipid extraction. Lipids were extracted, separated into galacto- and phospholipid fraction by solid phase chromatography. Thin layer chromatography was used for separation into lipid classes and isolation of phosphatidylcholine (PC) and monogalactosyldiacylglycerol (MGDG), and lipid-associated fatty acids were methyl transesterified before measured by gas chromatography. Fatty acid content per lipid was calculated using internal standard tripentadecanoin (15:0, 10 μ g), molar mass of fatty acids and fresh weight (g FW). A, The values were normalized to the amount of lipids at the time point 0 (=1) and displayed

in relative PC and MGDG levels. B, Based on the lipid amounts and fatty acid profiles of each time point displayed in Figure 3.3. Together with results of long-term salt treatment (24 and 48 h) the nmol double bonds (DB)/ nmol lipids for PC and MGDG were calculated. Data represent means \pm SD of two biological replicates from two individual experiments.

Based on the amounts and fatty profiles of PC and MGDG it was also possible to calculate the mean number of double bonds per lipid to determine whether the treatment led to changed unsaturation of the lipids. Figure 3.4. B sums up the double bonds per lipid for salt treatment up to 48 h to get a time-course-related overview of potential changes. But neither PC nor MGDG showed an alteration in the degree of saturation during the short-term salt treatment even though lipid levels of PC and MGDG were increased after 2 h (Fig 3.3. C, D). For MGDG it would have been unlikely to increase its unsaturation since with 5.8 double bonds per lipid under untreated conditions (0 h) it already reaches high level of unsaturation where any other measured associated fatty acids, besides 18:3 and 16:3, probably account for intermediate states. The increase of the lesser unsaturated PC, which is mainly associated to 18:3, 18:2 and 16:0, was based - as mentioned above - on the equal increase of exactly these fatty acids, resulting in the unchanged degree of approximately 3.2 double bonds per lipid (Fig. 3.4. B). Interestingly, longer exposure of plants to the salt treatment might result in a higher unsaturation of fatty acids associated to PC while MGDG did not change its amount of 5.8 double bonds per lipid at any time of the treatment (Fig. 3.4. B). However, possible changes of unsaturation in the long-term treatment could not be statistically evaluated due to the limited number of performed experiments.

Since the impact on biochemical and physiological processes often amplifies with the dosage of an applied stress, Arabidopsis plants were also treated with a higher salt concentration of 100 mM NaCl for a short period of time to investigate whether extraplastidial and plastidial lipid changes occur to a stronger extent. Interestingly, the amount of PC and MGDG changed when plants are exposed to 100 mM NaCl (Fig. 3.5. A). This was in line with an unchanged degree of saturation for both lipids during the entire duration of the treatment (Fig. 3.5. B).

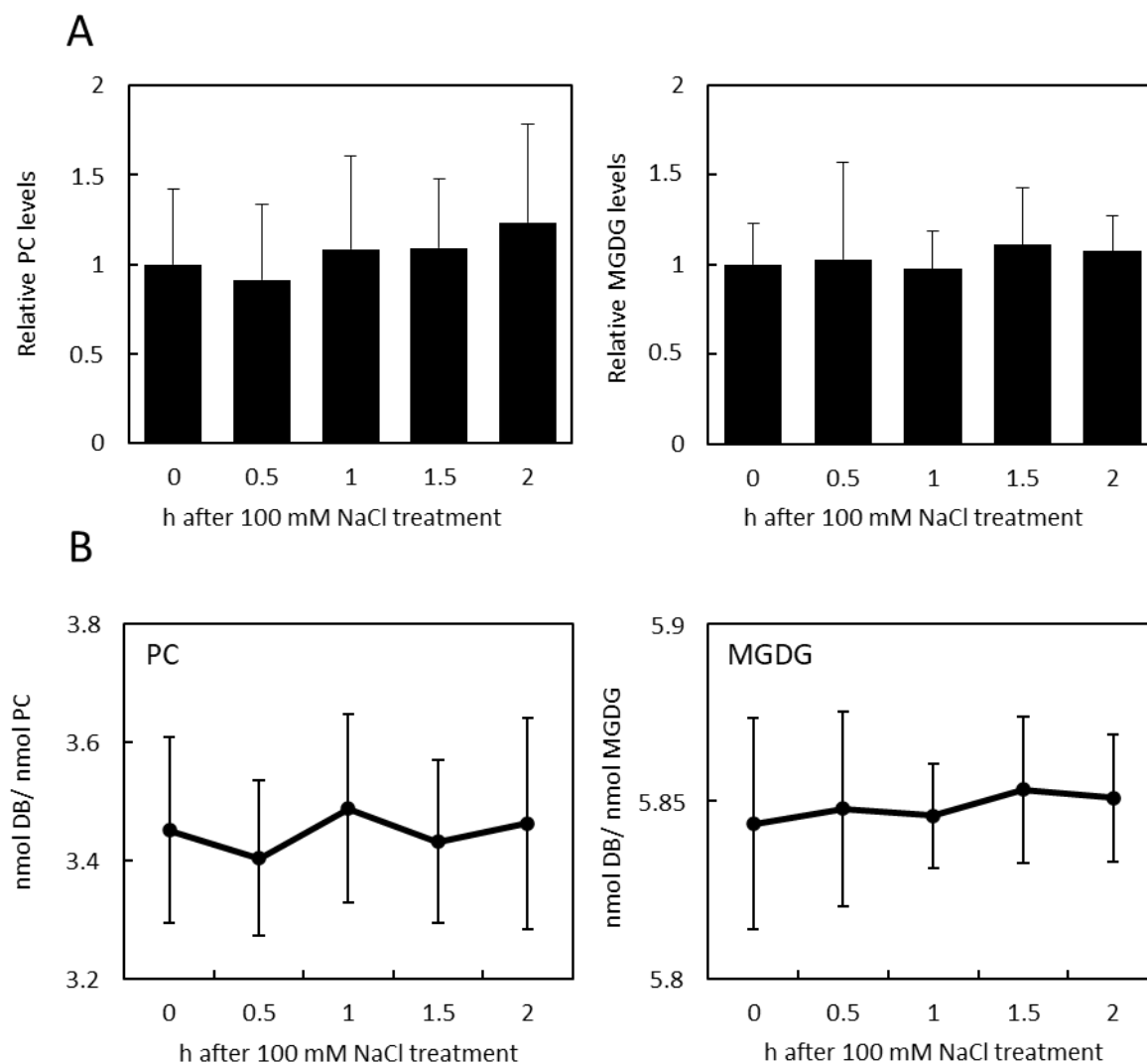


Figure 3.5.: Analysis of PC and MGDG levels of WT after short-term treatment with 100 mM NaCl.

Seedlings were grown for two-weeks on $\frac{1}{2}$ MS solid media and then transferred on $\frac{1}{2}$ MS solid media containing 100 mM NaCl. Green tissue was harvested after 0, 0.5, 1, 1.5 and 2 h of treatment and prepared for lipid extraction. Lipids were extracted, separated into galacto- and phospholipid fraction by solid phase chromatography. Thin layer chromatography was used for separation into lipid classes and isolation of phosphatidylcholine (PC) and monogalactosyldiacylglycerol (MGDG), and lipid-associated fatty acids were methyl transesterified before measured by gas chromatography. Fatty acid content per lipid was calculated using internal standard tripentadecanoin (15:0, 10 μ g), molar mass of fatty acids and fresh weight (g FW). A, The values were normalized to the amount of lipids at the time point 0 (=1) and displayed in relative PC and MGDG levels. B, Based on the lipid amounts and fatty acid profiles of each time point the nmol double bonds (DB)/ nmol lipids were calculated for PC and MGDG. Displayed are data for PC and MGDG after 0, 0.5, 1, 1.5 and 2 h of 100 mM NaCl treatment. Data represent means \pm SD of data of four to six biological replicates from three independent experiments.

These results show that mild NaCl treatment with 50 mM NaCl induces salt stress responses and that plants respond with short-term changes in lipid levels in both plastidial and in extraplastidial

membranes (Fig. 3.3. C, D). The extent to which changes in PC and MGDG amounts are related is not known at this point, but the temporal correlation suggests a possible link. As the molecular mechanisms of a postulated salt-triggered lipid exchange between plastidial and extraplastidial membranes are not well understood, subsequent experiments addressed whether known instances of such exchange would also be accompanied by a change in lipid levels in the respective membranes.

3.1.3. Bidirectional exchange of polyunsaturated fatty acids between ER and plastids.

The formation of trienoic fatty acids occurs independently both at the ER membrane and in the plastids, as different ω -3 fatty acid desaturases are localized in both compartments. While at the ER membrane FAD3 mainly converts PC-bound 18:2 to 18:3, in plastids the isoenzymes FAD7 and FAD8 introduce double bonds into 18:2 bound to any plastidial glycerolipid to form 18:3 (Browse et al., 1993; Iba et al., 1993). Additionally 16:2 esterified to MGDG is converted to 16:3 (Browse et al., 1993; Iba et al., 1993). Results in section 3.1.2. indicate an important role of the 18:3 ratio of PC and MGDG in early salt stress responses. Since the changes in PC and MGDG occur almost synchronously, it is possible that the changes reflect a rapid exchange of 18:3 or its precursors between ER and plastids. To test whether there is any exchange of polyunsaturated fatty acids at all, the levels of PC and MGDG were analyzed in different ω -3 fatty acid desaturase mutants of Arabidopsis. Since *FAD3* has previously been studied in the context of seed oil accumulation, fatty acids were first extracted from seeds of Arabidopsis WT plants, the *fad3-2* (*fad3*) mutant and a complemented *FAD3-4c* line ectopically expressing a fluorescence-tagged variant of FAD3 under the 35S promoter from the cauliflower mosaic virus in the *fad3-2* mutant background (The complemented line was provided by Dr. Larissa Launhardt, MLU Plant Biochemistry). The fatty acid patterns were determined by acidic methanolysis to analyze the total fatty acid composition. The predominant fatty acids in seeds of WT Arabidopsis were the monounsaturated fatty acids 18:1 and 20:1 (gondoic acid) characteristic for seeds, and the polyunsaturated fatty acids, 18:2 and 18:3. In the *fad3* mutant, the proportion of 18:2 was increased, whereas the seeds were almost devoid of 18:3, in line with the original description of the *fad3* mutant based on seed

analysis (James and Dooner, 1991) and highlighting the notion that plastidial fatty acid unsaturation does not contribute substantially to fatty acids in seed oil (Fig. 3.6. A).

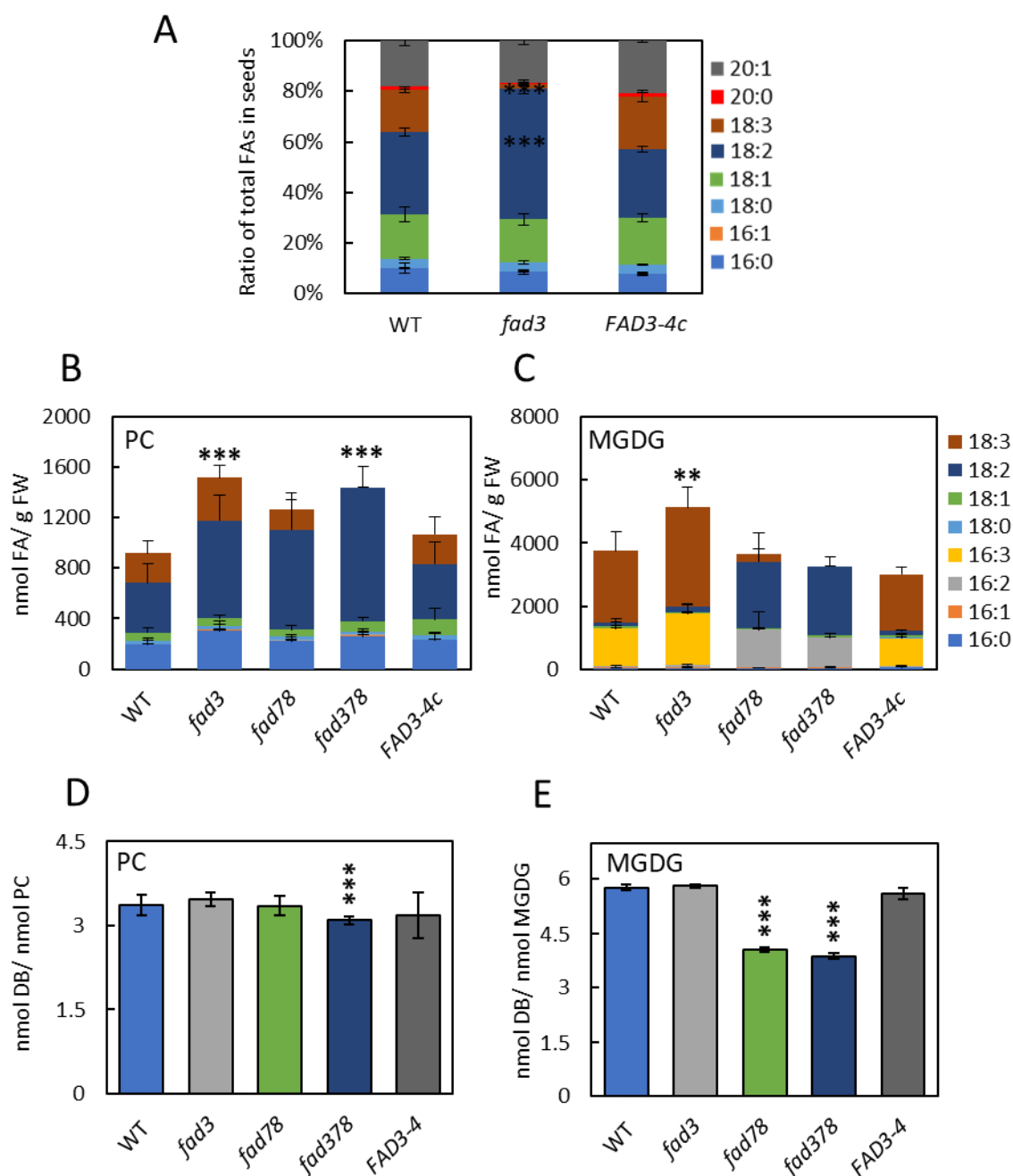


Figure 3.6.: Fatty acid profile in seeds and green tissue of *fad* mutants.

A, Total fatty acids from WT and *fad3* seeds were extracted using acidic methanolysis and were measured with gas chromatography. Data from complemented *FAD3-4c* line were obtained from Dr. Larissa Launhardt using lipid analysis of individual seeds. The proportion of fatty acids was expressed as a percentage and data represent means \pm SD of 6-23 biological replicates from one-four independent experiments. B and C, Total lipids from two-week-old seedlings of WT (blue), *fad78* (green), *fad378* (dark blue) and complemented *FAD3-4c* (dark grey) lines and from three-week-old seedlings of *fad3* (grey) lines

were extracted, separated into galacto- and phospholipid fraction by solid phase extraction. Thin layer chromatography was used for separation into lipid classes and isolation of phosphatidylcholine (PC) and monogalactosyldiacylglycerol (MGDG), and lipid-associated fatty acids were methyl transesterified before measured by gas chromatography. Fatty acid content per lipid was calculated using internal standard tripentadecanoin (15:0, 10 μ g), molar mass of fatty acids and fresh weight (g FW). Based on the lipid amounts and fatty acid profiles of each plant line nmol double bonds (DB)/ nmol PC (D) and nmol DB/ nmol MGDG (E) were calculated. Data represent means \pm SD of data of 6-12 biological replicates from three-five independent experiments. Asterisks indicate significant changes compared to WT results using Student's T-test (* P <0.05; ** P <0.01; *** P <0.001). Identified fatty acids: blue, 16:0; orange, 16:1 ^{Δ 7}/16:1 ^{Δ 9}; grey, 16:2 ^{Δ 7,10}; yellow, 16:3 ^{Δ 7,10,13}; light blue, 18:0; green, 18:1 ^{Δ 9}/ 18:1 ^{Δ 11}; dark blue, 18:2 ^{Δ 9,12}; brown, 18:3 ^{Δ 9,12,15}; red, 20:0; dark grey, 20:1 ^{Δ 11}.

By contrast, the complemented *FAD3-4c* line fully restored the 18:3 content in seeds to levels comparable to that of the WT controls with a functional FAD3 enzyme.

Germination of *Arabidopsis* plants and the first days of growth depend on external factors, such as water supply or temperature, but also on the storage compounds present in the seeds. Seedlings of the *fad3* line, which lacked 18:3, showed developmental deficits compared to WT, and the defects continued throughout shoot development, resulting in smaller rosettes and in shorter inflorescences (Fig. 6.3., 6.4., 6.5.). Such macroscopic differences were rescued in the complemented line, suggesting that the deficits were due to the *fad3* knock-out (Fig. 6.5.). As the *fad3* seedlings displayed developmental deficits, the basal PC and MGDG contents of green tissue were analyzed for *fad3* mutants after three weeks of growth to enable the comparison of plants at equivalent developmental stages with the state of other lines after two weeks of growth (Fig. 6.3.). Based on the analysis of associated fatty acids, the contents of PC and MGDG were both significantly higher in the *fad3* mutant compared to WT, resulting mostly from a higher 18:2 and 18:3 proportion in both lipids, though remaining its degree of unsaturation for both lipids (Fig. 3.6. B-E; Fig. 3.7. A, B).

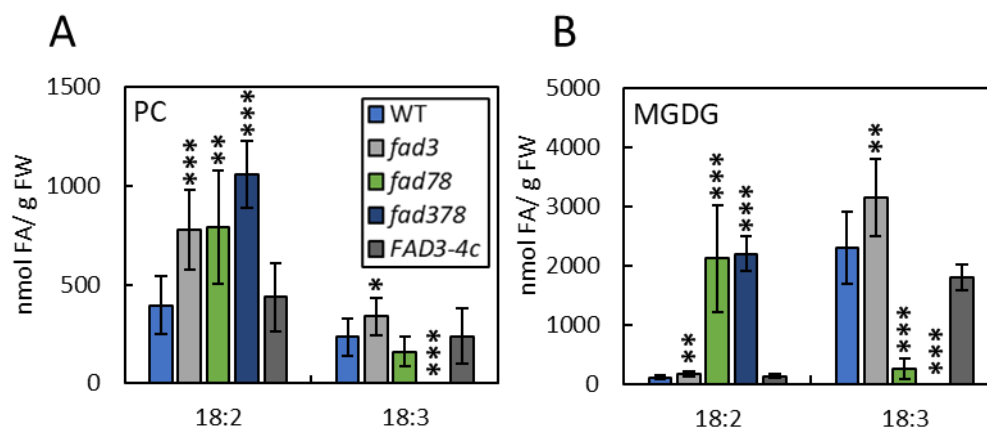


Figure 3.7.: Comparison of 18:2^{A9,12} and 18:3^{A9,12,15} fatty acid levels between WT and *fad* mutants.

Basal level proportion of 18:2 and 18:3 fatty acids associated to PC and MGDG from WT, *fad3*, *fad78*, *fad378* and complemented line *FAD3-4c*. Total lipids were extracted from two- or three-week-old seedlings and separated into galacto- or phospholipid fraction by solid phase extraction. Within the fractions, phosphatidylcholine (PC) and monogalactosyldiacylglycerol (MGDG) were isolated by thin layer chromatography and subsequently methyl transesterified. Fatty acids were measured by gas chromatography and the amounts calculated using internal standard tripentadecanoin (15:0; 10 µg), molar mass of fatty acids and fresh weight (g FW). Data represent means ± SD of 6-12 biological replicates from 3-5 independent experiments. Asterisks indicate significant changes compared to WT results using Student's T-test (* $P < 0.05$; ** $P < 0.01$; *** $P < 0.001$). Plant lines: blue, WT; grey, *fad3*; green, *fad78*; dark blue, *fad378*; dark grey, *FAD3-4c*.

A remarkable difference of the analysis of green tissue lipids as compared to the analysis of seed lipids is the presence of substantial amounts of 18:3 in PC (Fig. 3.6. B), an extraplastidial lipid. As in the *fad3* mutant this 18:3 cannot have been formed by FAD3 in the ER, it must therefore originate in the plastids and was moved out of the plastids to be associated with PC. Such exchange has previously been reported and it is known that in green tissues the lack of 18:3 production in plastids or the ER can be substituted by 18:3 formation in the respective other organelle (Browse et al., 1993). This substitution requires substantial movement of 18:3 across organellar borders, a process that is not well understood. The accumulation of 18:2 in PC (Fig. 3.6. B) additionally supports an origin of 18:3 in the plastid, as 18:3 is present in PC at the same time as its ER-precursor 18:2 accumulates. In light of the evident transport of 18:3 from the plastid to the ER seen in the *fad3* mutant, it is interesting to note that knocking out a FAD localized in the ER resulted in an increase in the plastidial lipid MGDG (Fig. 3.6 C). MGDG in the *fad3* mutant was not only higher in 18:3 but also in 16:3 levels, which may indicate a higher rate of lipid biosynthesis via the prokaryotic pathway (Fig. 3.6. C).

A reciprocal experiment with *Arabidopsis fad7-2 fad8* double mutants (*fad78*) in which plastidial *FAD7* and *FAD8* were knocked out showed no influence on plant growth besides a slightly altered leaf morphology (Fig. 6.3., 6.4., data not shown). The amounts of PC and MGDG in *fad78* were comparable to those of WT controls, however the fatty acid composition differed for both lipids (Fig. 3.6. B, C). Knockout of plastidial *FAD7* and *FAD8* did not influence the overall sum unsaturation of PC even though the fatty acid composition in PC was affected by significant increased amounts of 18:2 (Fig. 3.6. D; Fig. 3.7. A). On the other hand, MGDG in the *fad78* mutant contained enhanced proportions of 18:2 and 16:2, which were only found in trace amounts in WT controls resulting in a strong impact on unsaturation of MGDG by decreasing double bonds per lipid from 5.8 to 4.0 (Fig. 3.6. C, E). Interestingly, only small amounts of 18:3 were found associated with MGDG, and transport of 18:3 from the ER to the plastid did not appear to be as efficient as transport of 18:3 from the plastid to the ER, as shown in the *fad3* mutant line.

An interesting observation was made using an *Arabidopsis fad3 fad7 fad8* triple mutant (*fad378*), which combines the genetic lesions of the mutants described above. Even though *fad378* triple mutants are largely devoid of trienoic fatty acids, and a more severe phenotype might have been expected than that of the *fad3* single mutant, two-week-old *fad378* seedlings did not show any developmental deficit. In contrast to *fad3* and *fad78* mutants, the rosettes or inflorescences of *fad378* triple mutants were also not impaired and appeared even larger than those of WT controls (Fig. 6.3., 6.4., data not shown). The comparison of the mutant lines indicates that e.g., the developmental delay of the *fad3* mutant is, thus, not immediately related to the abundance of 18:3 in these plants. The macroscopic differences between the *fad378* plants and the other lines could be explained by the lack of jasmonic acid in the *fad378* mutant, which was evident in siliques that were not fully developed (Fig. 6.6.; McConn and Browse, 1996). Similarly, enhanced growth of the *fad378* mutant might be a consequence of the absence of a growth-inhibitory effect of JA. For a further analysis of a possible contribution of JA, please see section 3.3.2 below. The lipid analyses presented here show that the triple mutant combined lipid phenotypes of *fad3* and *fad78* although the formation of 18:3 was completely absent in this mutant. PC-species containing 18:2 account for a significantly increased PC content, which was also observed in the *fad3* line, but resulted here for the triple mutant in the decrease of PC unsaturation from 3.3 to 3.0 (Fig. 3.6. B, D). The fatty acid composition of MGDG in the *fad378* triple mutant resembled that of the

fad78 mutant and showed an accumulation of 16:2 and 18:2 and as well as a similar decrease in the unsaturation for MGDG (Fig. 3.6. C, E; Fig. 3.7. A, B).

The macroscopic growth and lipid levels were also determined for the complemented *fad3* mutant line *FAD3-4c* to test the possibility that other background mutations in *fad3* line may have resulted in the effects observed in the mutant. Neither development nor growth of the *FAD3-4c* line differed from that of WT controls (Fig. 6.3., 6.4., 6.5.). The contents of PC and MGDG, the composition of the associated fatty acids and degree of saturation were also not different from WT. These controls indicate that the changes observed in the *fad3* mutant were due to the knock-out of *FAD3* (Fig. 3.6. B-E).

The increased basal levels of PC and MGDG and the increased ratios of lipid-associated 18:3 in the *fad3* line (Fig. 3.6.) were similar to patterns observed in WT after 2 h of salt stress (Fig. 3.3. C, D). As the increased lipid levels in the *fad3* mutant are likely a reflection of membrane adjustments during the export of 18:3 from MGDG in the plastid to the ER and to other extraplastidial membranes, it is possible that the increased MGDG levels observed in WT upon salt treatment may also indicate such inter-organellar exchange. Reciprocally, if the changes in MGDG levels observed in WT reflect an adaptation response to salt, these might be related to altered salt tolerance of the *fad3* mutant compared to WT controls.

3.1.4. Salt treatment of ω -3 *fad* mutants.

Seed germination is a sensitive phase of plant growth implying that exposure to salt at this critical stage challenges the establishment of plants fundamentally. High salt concentrations impede water uptake, and the freshly germinated seedling is immediately surrounded by toxic ions that have a negative effect on shoot and root growth (Kumar et al., 2018). In previous studies which examined fatty acid desaturase mutants which were either impaired to form ω -6 fatty acids at ER (*fad2*) or in the plastids (*fad6*) showed decreased germination rates and root growth indicating a hypersensitivity towards salt based on a decreased unsaturation of lipids in those mutants (Zhang et al., 2009; Zhang et al., 2012a). Therefore, monitoring the germination rate and plant growth when exposed to salt could reveal whether any of the ω -3 *fad* knockout lines has changed their

ability to acclimatize to salt. The experimental set up described in Zhang et al. (2012a) was used as a template whereas the germination seeds of each plant line grown on solid media containing either 0, 50, 100 or 250 mM NaCl was monitored for a duration of 14 days (Fig. 3.8. A).

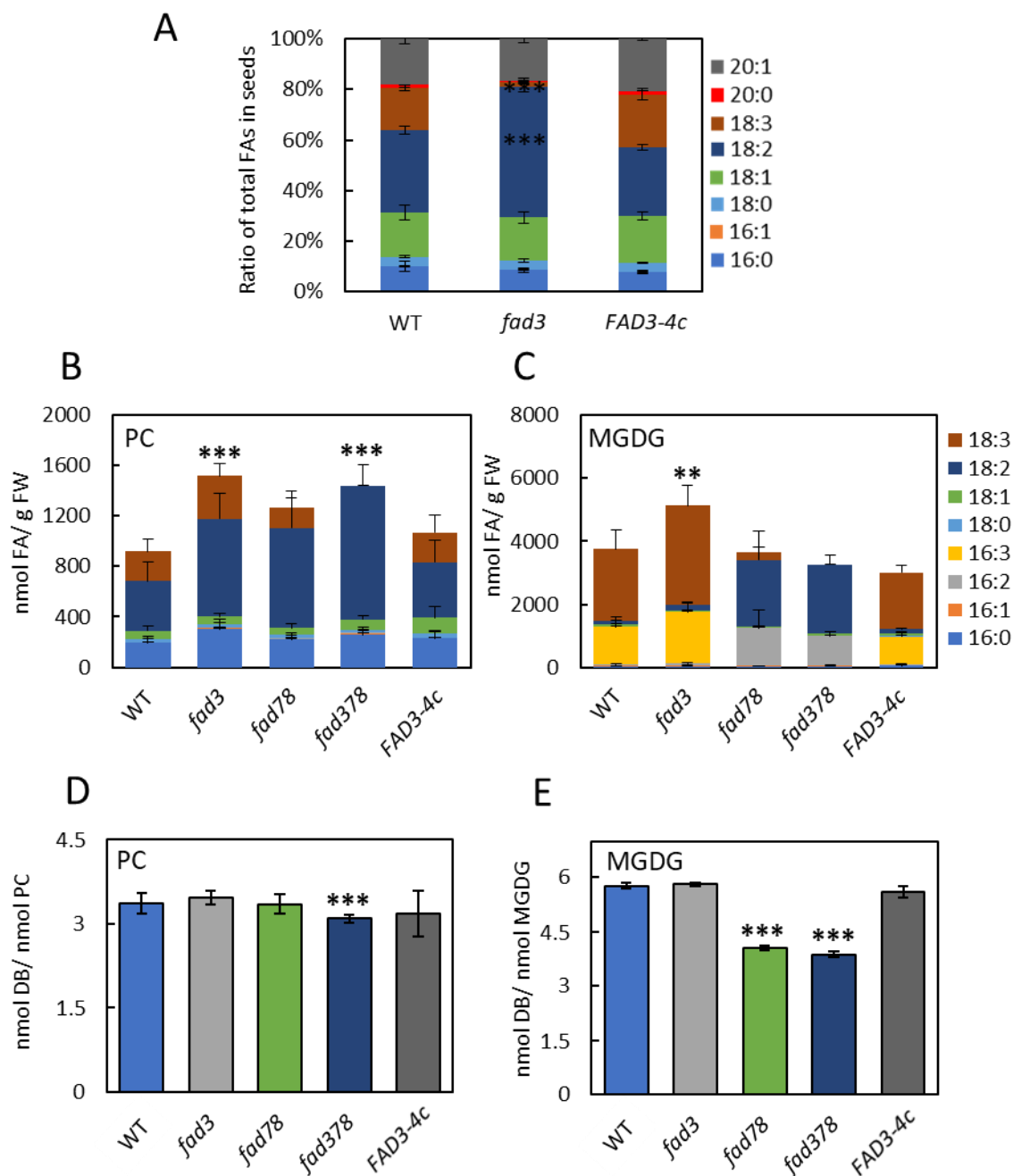


Figure 3.8.: Germination and root growth of WT, *fad3*, *fad78* and *fad378* seedlings under salt stress.

Experimental set up was performed according to Zhang et al. (2012a). A, Seeds of WT, *fad3* (grey), *fad78* (green) and *fad378* (dark blue) plant lines were stratified for three days and sown on $\frac{1}{2}$ MS solid media containing 0, 50, 100 and 250 mM NaCl. Germination was monitored for a duration of two weeks. Data represent means \pm SD from two independent experiments. For each experiment ≥ 35 seeds per plant line were sown. B, Seedlings of WT, *fad3*, *fad78* and *fad378* lines were grown for four days on $\frac{1}{2}$ MS solid media

before transferred on ½ MS solid media containing either 50 (black), 100 (grey), 250 (dark green), 400 (purple) mM NaCl or no supplements (white). After seven days, seedlings were documented, and root length measured using ImageJ software. For better comparison, values were normalized based on respective root length of each plant line grown on ½ MS media (=1) for seven days and expressed as relative root lengths. Data represent means ± SD of 12 biological replicates from two independent experiments. Asterisks show significant changes compared to root length of plants grown on media without salt using the Student's T-test (* $P < 0.05$; ** $P < 0.01$; *** $P < 0.001$).

Seeds germinated on solid media containing 0 or 50 mM NaCl displayed no remarkable difference between WT and the *fad* mutants with the majority of seeds germinating after three days (Fig. 3.8. A). When exposed to 100 mM NaCl, the seeds of all plant lines were still able to reach a germination rate of approximately 100 % by day five (Fig. 3.8. A). While the seeds from the *fad78* and *fad378* lines already reached this score after three days, WT and *fad3* mutant line showed a delay in seed germination by having a rate of only 90 % and 80 %, respectively, up to this point (Fig. 3.8. A). In contrast, none of the plant lines during the monitored time of the treatment with 250 mM NaCl maintained the germination rate, which was reached when treated with lower salt concentration. Seeds from *fad78* line displayed the highest germination rate with 86 % followed by WT and *fad3* line with an equal rate of 79 % and lowest rate of 63 % from the *fad378* mutant seeds (Fig. 3.8. A). Despite germinating fast under lower salt concentration, which could be reasoned with the fast development in the *fad378* plants in general, as mentioned above, the lack of ω -3 fatty acids in these plants could reduce the ability to tolerate high salt concentration during seed germination. The compensation of 18:3 formed either in the plastids or in the ER in the *fad3* and *fad78* lines is sufficient to compete with equal germination rate as the WT.

Since the effect of salt stress on plant growth can differ depending on the developmental stage of the plant also the root growth of seedlings from WT and the *fad* mutants was determined. Seedlings were grown for four days on ½ MS solid media before transferred on ½ MS solid media containing either 0, 50, 100, 250 or 400 mM NaCl and continued growing for seven days. The root lengths measured for each line were normalized to the root length reached on media without salt so that the changes in root lengths of the WT and the *fad* mutants were compared based on salt treatment and not confused by the normal phenotypes of the individual *fad* mutants. Surprisingly, WT and *fad3* mutant plants even significantly increased their root growth ability under mild stress of 50 mM NaCl whereas the knockout of plastidial *FAD7* and *FAD8* alone or in combination with

knock out of ER localized *FAD3* already tended to delay in root growth (Fig. 3.8. B). Elevated salt concentration of 100 mM NaCl led to a strong significant delay in root growth in all of the lines indicating a limit of tolerated NaCl concentration for Arabidopsis with or without knock-out of ω -3 FADs (Fig. 3.8. B). Moreover, stronger concentrations of 250 or 400 NaCl led shortly after transfer on respective media to the death of the plants and thereby a rapid stop of root growth (Fig. 3.8. B; Fig. 6.2.).

Together with the contrary effect of 50 mM NaCl on root growth between the *fad3* and *fad* mutants *fad78* and *fad378* (Fig. 3.8. B) and the effects of knocked out ω -3 fatty acid desaturases on lipid properties (Fig. 3.3. B, C), the question arose whether increased PC and MGDG might be required for the plant salt response. Therefore, the lipid levels of Arabidopsis *fad* mutant lines were determined upon salt treatment. Then results were normalized to lipid amounts measured at 0 h of salt treatment of each plant line to show the relative lipid levels for better comparison between the plant lines. Studies with various species of halophytes, which are highly adapted to conditions of high salt concentrations, show a tendency to increase PC content, and an overall higher proportion of polyunsaturated fatty acids with membrane lipids in these plants (Wu et al., 2005). Moreover, in halophytes, in particular changes in plastidial membrane lipids prevent chlorophyll degradation and protect against salt-induced photoinhibition (Sui and Han, 2014). Overexpression of rice MGDG synthase (*OsMGD*) in tobacco plants indicates a link between a high content of MGDG or DGDG and the maintenance of thylakoid structure in chloroplasts under salt stress conditions, and a high proportion of lipid-associated trienoic fatty acids also plays a role in salt tolerance (Wang et al., 2014). Overexpression of *FAD3* in tobacco plants or tobacco cell cultures also resulted in altered tolerance to drought and osmotic stress, respectively (Zhang et al., 2005). Since the *fad3* mutant displayed higher basal levels of PC and MGDG linked to higher proportions of polyunsaturated fatty acids associated with MGDG and PC and no delay in root growth when confronted with 50 mM NaCl (Fig. 3.8. B), it was next tested whether the lipid amounts or the fatty acids in *fad3* plants changed during salt stress treatment (Fig. 3.9.), beyond their already-changed basal levels (compare Fig. 3.6. B, C). The PC levels tended to decrease until 1.5 h of the salt treatment before increasing back to initial lipid levels after 2 h (Fig. 3.9. A). The degree of saturation of PC also decreased over the course of treatment, but similar to the levels of PC, none of the changes were significant (Fig. 3.9. B). The data indicate that during the 2 h salt

treatment the abundance of MGDG yet increases over the already elevated basal levels of the *fad3* mutant, but with no apparent change in the ratio of the associated fatty acids which was also mirrored in unchanged unsaturation of MGDG (Fig. 3.9. A, B).

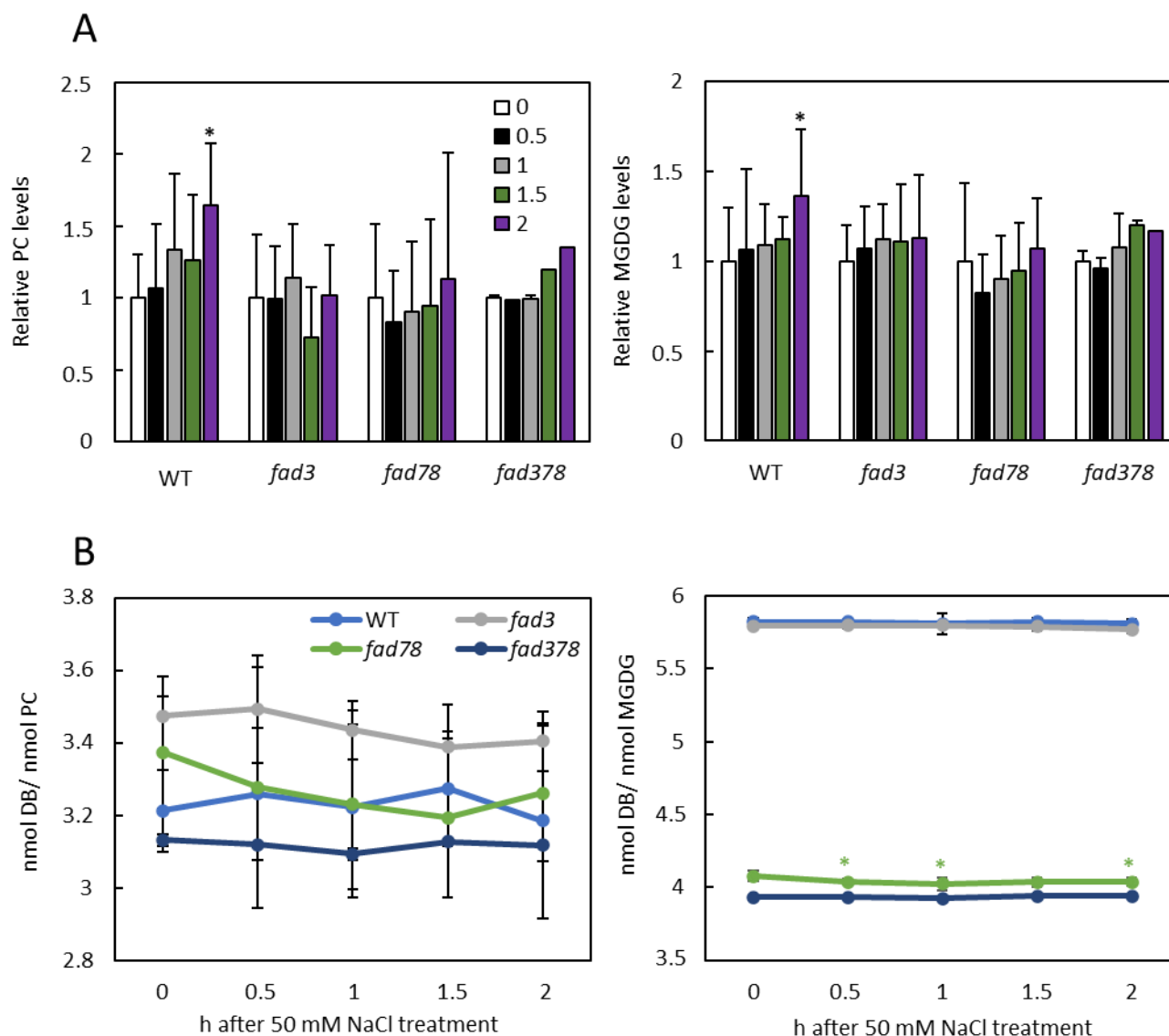


Figure 3.9.: Relative PC and MGDG levels of WT, *fad3*, *fad78* and *fad378* seedlings after short-term treatment with low salt concentrations.

Seedlings of WT (blue), *fad3* (grey), *fad78* (green) and *fad378* (dark blue) plants grown for two or three weeks, respectively, on $\frac{1}{2}$ MS solid media were transferred on $\frac{1}{2}$ MS solid media containing 50 mM NaCl. Total lipid content was extracted after 0 (white), 0.5 (black), 1 (grey), 1.5 (dark green) and 2 (purple) h of treatment and separated into galacto- and phospholipid fractions by solid phase extraction. For isolation of PC and MGDG, fractions were separated into lipid classes by thin layer chromatography. Lipid-associated fatty acids were methyl transesterified for gas chromatography. The amounts of measured fatty acids were calculated using internal standard tripentadecanoin (15:0; 10 μ g); molar mass of fatty acids and fresh weight (g FW). A, For better comparison between the plant lines, values were normalized based on respective lipid amounts of each plant line at time point 0 h (set as 1) and are displayed as relative PC and

relative MGDG levels. B, Based on the lipid amounts and fatty acid profiles of each plant line nmol double bonds (DB)/ nmol PC and nmol DB/ nmol MGDG were calculated. Data represent means \pm SD of one to six biological replicates from one-three independent experiments. Asterisks show significant changes compared to time point 0 of the respective plant line, according to a Student's T-test (* $P < 0.05$).

In the *fad78* double mutant, which showed lipid levels comparable to WT (Fig. 3.6. B, C) but displayed increased proportions of associated 18:2 (Fig. 3.6. B, C), the treatment with 50 mM NaCl resulted in a slight but not significant decrease of both lipids (Fig. 3.9. A). Even though significant changes in MGDG saturation degree were calculated after 0.5, 1 and 2 h of the treatment it is unlikely that these changes are biological relevant as these changes refer to the second decimal position and the double bonds of 4.0 per lipid did not differ (Fig. 3.9. B). The triple mutant *fad378* displaying higher PC levels and normal MGDG levels compared to WT but lacking the formation of ω -3 fatty acids did show an increase in levels of both lipids during the treatment of 2 h but remained in their unsaturation unchanged (Fig. 3.9. A, B). However, the changes did not appear to be as severe as in WT (Fig. 3.3. C, D; Fig. 3.9. A) and were not statistically evaluated due to the limited number of performed experiments.

Summarized, this observation may suggest a role for FAD7/ FAD8 in mediating lipid changes and membrane rearrangements during short-term responses to salt stress. The mutual substitution of plastidial or extraplastidial polyunsaturated fatty acids (Fig. 3.3. C, D) is an example for the trans-organelle exchange of biochemical compounds. In this context, the plastid may serve as a source for polyunsaturated fatty acids, and plants with no functional plastidial FAD7/FAD8 may lack the ability to adjust lipid content or the state of unsaturation also in extraplastidial membranes.

The lipid composition of thylakoids, which have particular requirements regarding membrane phase-order and flexibility to harbor the photosynthetic machinery is met by the richness in plastidial galactolipids and furthermore by the biophysical properties of polyunsaturated MGDG with degrees of unsaturation close to six double bonds per lipid (see Fig. 3.6. E; Hölzl and Dörmann, 2019). As in green tissues of the *fad3* mutant the amounts of MGDG changed in the plastids with perturbation of ER-located fatty acid unsaturation, it was a next goal to address the impact of membrane lipid unsaturation and trans-organelle lipid exchange on thylakoid function and the photosynthetic capacity.

3.2. Plastidial and extraplastidial FADs influence photosynthesis and photoprotection.

Membranes represent not only barriers defining cellular compartments, but they also form the environment for integral membrane proteins that may depend on a specific arrangement of lipids. For instance, membrane proteins may require a specific degree of membrane lipid unsaturation or carbon chain length (e.g. Na^+/H^+ -exchanger during salt stress; Zhang et al., 2012a) for their correct membrane integration and enzymatic functionality. Membranes are composed of different protein-to-lipid ratios, and these ratios can differ between membranes with values around 1 for the plasma membrane or higher values of 1.6 or 1.9 for highly crowded membranes like thylakoids or the inner mitochondrial membrane, respectively (Shishova and Yemelyanov, 2021; Quartacci et al., 1995; Chapman et al., 1983; Matos et al., 2007). Previous studies have shown that when MGD1 or the plastidial digalactosyldiacylglycerol synthases DGD1 were knocked out, decreases in MGDG or DGDG, respectively, negatively affected photosynthetic performance (Yu et al., 2020a; Fujii et al., 2014). The observation of altered levels of MGDG or its unsaturation in the Arabidopsis *fad3* or *fad378* mutants (see Fig. 3.6. C, E) might, thus, also have an impact on photosynthesis in consequence of cross-organellar exchange of lipids between plastids and the ER, and this has previously not been investigated in detail.

3.2.1. Altered chlorophyll and carotenoid amounts in *fad* mutants.

Chlorophylls and carotenoid pigments are the basis for photosynthesis and are mainly bound to photosystems and LHCs in thylakoid membranes. LHCI and LHCII are usually linked to PSI and PSII, respectively, whereas the LHCII trimers are mobile and important for switching between PS complexes within the membrane to allow more efficient photon absorption under low light conditions or down-regulated, controlled absorption under high light conditions (state transition; Wollman, 2001). It is possible that this movement and in consequence also photosynthetic efficiency might be inhibited if the amounts of plastidial lipids or the composition of their associated fatty acids change, physically affecting membrane fluidity. Therefore, total pigments were extracted from WT controls and from *fad3*, and complemented *FAD3-4c* line, *fad78* and the

triple mutant *fad378* and the contents of chlorophyll a (Chl a), chlorophyll b (Chl b) and carotenoids were photometrically determined (see 2.2.6.).

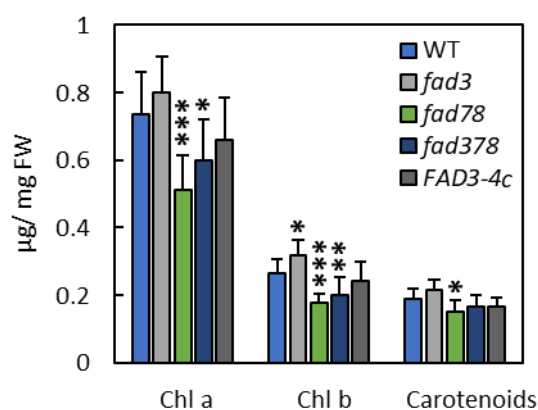


Figure 3.10.: Concentration of chlorophyll a, b and carotenoids in *fad* mutant lines of *Arabidopsis*.

Pigments were extracted from green tissues of seedlings grown for either two weeks (WT, *fad78*, *fad378*, *FAD3-4c*) or three weeks (*fad3*) using 80 % of acetone. Absorbance was measured photometrically at 663, 647 and 470 nm and amounts (μg) calculated according to (Lichtenthaler and Buschmann, 2001) based on fresh weight (mg FW). Data represent means \pm SD of six to ten biological replicates from two to four independent experiments. Asterisks show significant changes compared to WT results using the Student's T-test (* $P < 0.05$; ** $P < 0.01$; *** $P < 0.001$). Plant lines: blue, WT; grey, *fad3*; green, *fad78*; dark blue, *fad378*; dark grey, *FAD3-4c*.

Interestingly, the knockout of ER localized *FAD3* influenced thylakoid pigments by significantly increasing the amount of Chl b, which resembled WT levels in the complemented *FAD3-4c* line (Fig. 3.10.). This might indicate that the level of trienoic fatty acids within thylakoid membranes has an influence on LHC abundance or inhibits the ability to bind a certain number of pigments. Increased MGDG level in *fad3* mutant might decrease the Chl a/ Chl b ratio and influence thereby the photosynthetic performance in low light and highlight conditions (Fig. 6.7.). By contrast, the knockout of plastidial *FAD7* and *FAD8* led to a significant decrease in chlorophyll content (Fig. 3.10.). Interestingly, this effect was not as severe in the *fad378* triple mutant line (Fig. 3.10.). The *fad78* line also had a significantly lower carotenoid content, which was not observed in the *fad378* triple mutant (Fig. 3.10.). The patterns show that changes in plastidial membrane lipid composition are accompanied by altered levels of thylakoid pigments.

3.2.2. Photosynthetic performance is affected in *fad* mutants.

The efficient absorption of photons by pigments is only one fundamental aspect of photosynthesis. The electrons excited by the light energy are transported within the photosynthetic complexes, and the electron carriers plastoquinone and plastocyanin enable their movement from one complex to the next. The protein complexes of the entire photosynthetic machinery are embedded in thylakoid membranes, and this embedment depends on a defined lipid composition not only to maintain membrane fluidity for complex movement but also to ensure membrane integrity for the formation of a pH gradient in the thylakoid lumen. Therefore, thylakoid lipids are integral compounds in photosynthetic complexes and are essential for the functionality of the photosynthetic machinery (Kirchhoff et al., 2002; Kobayashi, 2016). It has in fact been proposed based on the x-ray crystal structure of photosystem II (Umena et al., 2011) and on modeling studies (van Eerden et al., 2017) that thylakoid lipids form specialized binding sites for protein subunits of PSII, are linked to the orientation of chlorophyll within the complex and contribute to an efficient exchange of electrons between PSII and plastoquinone (van Eerden et al., 2017).

The knockout of FADs localized to ER membranes or FADs in plastidial membranes affects the amounts and fatty acid composition in thylakoid lipids (Fig. 3.6. C, E). How these changes affect different aspects of photosynthesis was examined in these mutants using a chlorophyll fluorescence imaging system based on pulse amplitude modulation technique (Imaging-PAM) to detect changes in the photosynthetic apparatus (See 2.2.7.).

Figure 3.11. A shows the active quantum PSII efficiency (F_q'/F_m'), which represents the PSII operating efficiency when all primary plastoquinones of PSII were oxidized, plotted for different *fad* mutants in a light curve from 0 to 1400 $\mu\text{mol m}^{-2} \text{s}^{-1}$ (photosynthetic active radiation, PAR). For better comparison of the data for *fad3*, the complemented *FAD3-4c*, *fad78*, *fad378* and the WT controls, the panels 3.11. B, C and D are zoomed in on low light conditions (52 PAR), normal/growth light conditions (170 PAR), or high light conditions (580 PAR), respectively.

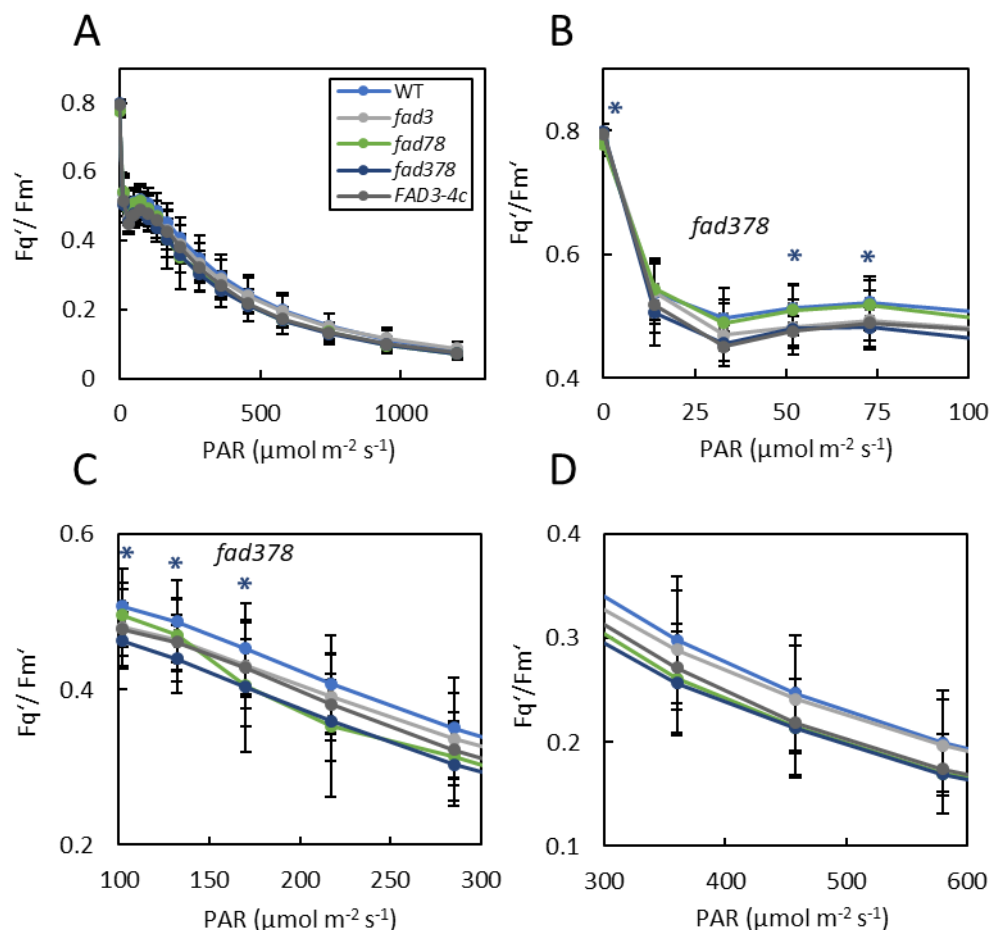


Figure 3.11.: The active quantum PSII efficiency of different Arabidopsis *fad* mutants.

A, First true leaves of seedlings, grown for two weeks (WT, *fad78*, *fad378*, *FAD3-4c*) or three weeks (*fad3*), were cut and placed on ½ MS agar plates. Leaves were dark-adapted for at least 5 min before starting with saturation pulse for 800 ms and an exposure of 2400 $\mu\text{mol m}^{-2} \text{s}^{-1}$. IMAGING PAM was used to measure a light curve with photosynthetically active radiation (PAR, in $\mu\text{mol m}^{-2} \text{s}^{-1}$) increasing from 14 to 1200 PAR in 15 steps and duration intervals of 30 s by. Parameters F_q' and F_m' were recorded to calculate active quantum PSII efficiency at each light intensity. Data represent means \pm SD of 4 to 15 biological replicates from two to eight independent experiments. At least five leaves were measured for each biological replicate. B, C and D show the light curve of NPQ in smaller ranges: 0-100, 100-300, 300-600 PAR. Plant lines: blue, WT; grey, *fad3*; green, *fad78*; dark blue, *fad378*; dark grey, *FAD3-4c*. Asterisks show significant changes compared to WT results using the Student's T-test (* $P < 0.05$).

The *fad3* mutant and the complemented *FAD3-4c* line both showed similar active PSII efficiency to WT at each light intensity (Fig. 3.11. B). By contrast, the knockout of plastidial *FAD7* and *FAD8* resulted in slightly lower active PSII efficiency under normal light conditions, however, these apparent differences were not significant (3.11. C; Tab. 6.8.). Only the triple mutant *fad378* showed significantly lower active PSII efficiency under low and normal light conditions (Fig. 3.11.

B, C), which may indicate that fully lacking trienoic fatty acids negatively influences the transfer of electrons at low and normal light intensities (Fig. 3.6. C; Fig. 3.11. B, C; Tab. 6.8.).

While the active quantum PSII efficiency shown in Figure 3.7 only shows light energy used for photochemistry by PSII absorbed energy that is not photochemically utilized by PSII may be quenched as heat, a process referred to as nonphotochemical quenching (NPQ; $(F_m/F_m')^{-1}$). This photoprotective process serves to quench excessive energy when the light intensity incurred exceeds the capacity of the plants to use the electrons (Holt et al., 2004). Regardless of increasing light intensities, WT, *fad78* and *fad378* maintained similar NPQ levels, although in the double and triple mutants, the energy was not used quite as efficiently for photochemistry in PSII as in WT (Fig. 3.12. A; Fig. 3.11. A).

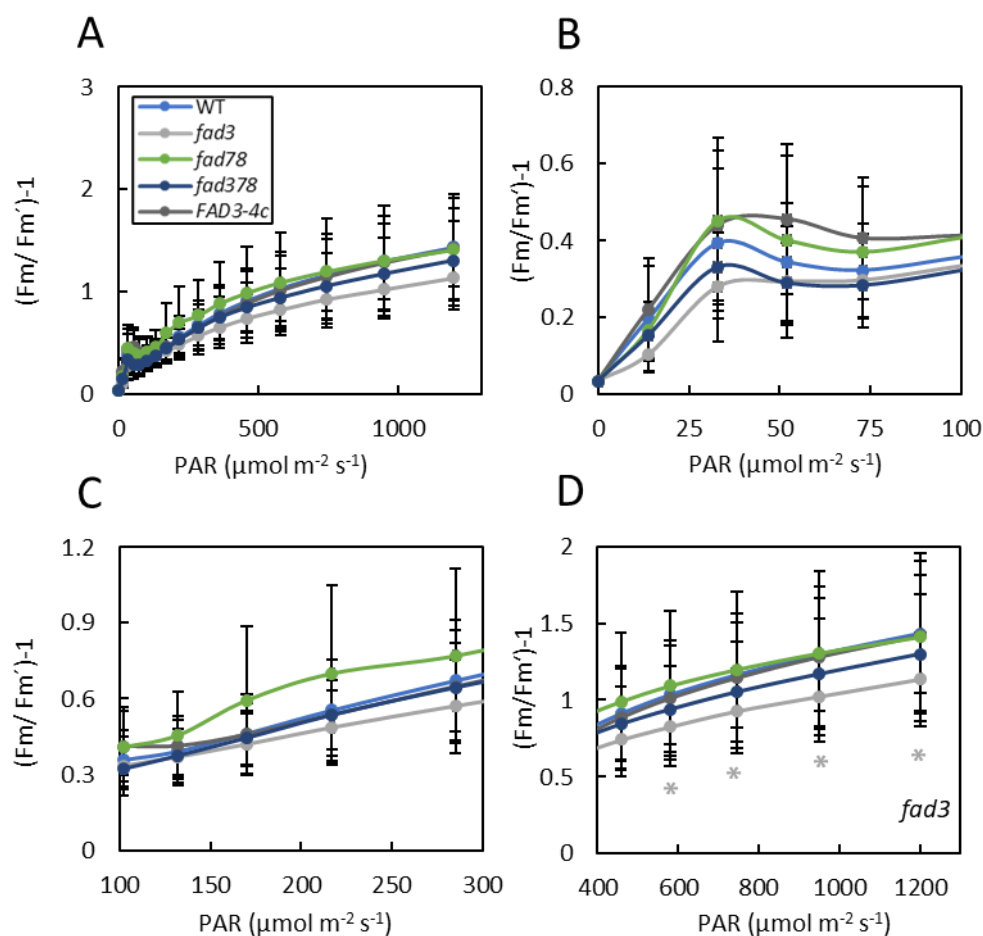


Figure 3.12.: The nonphotochemical quenching of different Arabidopsis *fad* mutants.

A, First true leaves of seedlings, grown for two weeks (WT, *fad78*, *fad378*, *FAD3-4c*) or three weeks (*fad3*), were cut and placed on ½ MS solid media. Leaves were dark-adapted for at least 5 min before starting with saturation pulse for 800 ms and an exposure of 2400 $\mu\text{mol m}^{-2} \text{s}^{-1}$. IMAGING PAM was used to measure a light curve with photosynthetically active radiation (PAR, in $\mu\text{mol m}^{-2} \text{s}^{-1}$), increasing from 14 to 1200 PAR in 15 steps and duration intervals of 30 s. Parameters F_m and F_m' were recorded to calculate non-

photochemical quenching (NPQ) at each light intensity. Data represent means \pm SD of 4 to 15 biological replicates from two to eight independent experiments. At least five leaves were measured for each biological replicate. B, C and D show the light curve of NPQ in smaller ranges: 0-100, 100-300, 400-1200 PAR. Plant lines: blue, WT; grey, *fad3*; green, *fad78*; dark blue, *fad378*; dark grey, *FAD3-4c*. Asterisks show significant changes compared to WT results using the Student's T-test ($*P < 0.05$).

Interestingly, the *fad3* mutant exhibited the lowest NPQ and differed significantly from WT dissipation values when exposed to high light (Fig. 3.12. A, D). By contrast, the complemented *FAD3-4c* line showed energy dissipation similar to the WT controls under all light conditions, indicating recovery of the mutant phenotype at the physiological level (Fig. 3.12. A, D). The most severe defects in photosynthetic performance were observed in the *fad378* triple mutant (Fig. 3.11. A). This observation could be related to a lower chlorophyll content and somehow due to the complete absence of trienoic fatty acids and, thus, a substantially lower degree of unsaturation in thylakoid lipids (Fig. 3.6. C, E; Fig. 3.11.). Overall, the analysis of photosynthetic performance for different *Arabidopsis fad* mutants indicates that a higher content of MGDG in the *fad3* mutant was accompanied by reduced photoprotection at high light conditions, whereas photosynthetic performance was not affected (Fig. 3.6. C; Fig. 3.12. D). As increases in MGDG levels as those seen in the *fad3* mutant were also associated with the plants' response to mild salt stress (Fig. 3.6. C; Fig. 3.3. C, D), it was next tested whether salt stress also exerted effects on thylakoid function, such as photosynthetic performance and/or photoprotection.

3.2.3. Salt application has a dose-dependent effect on photosynthesis.

Plants exposed to salt are affected in their growth and in some physiological processes, including long-term effects on photosynthesis. For instance, salt concentrations above 100-150 mM (depending on the age of the plant) already result in water loss, followed by osmotic stress within plant cells and the slow uptake and accumulation of Na⁺ and Cl⁻ ions (Munns, 2002; Munns and Tester, 2008). To limit water loss through evaporation, plants respond to salt stress by closing stomata, but this also inhibits gas exchange and limits carbon fixation. Limited carbon dioxide appears to reduce photosynthetic rate, however, the accumulation of salt ions combined with energy absorption also leads to PSII instability and loss of photosynthetic function of thylakoids

(Stepien and Johnson, 2009; Omoto et al., 2012). Based on the rapid increase in MGDG content observed in Arabidopsis seedlings after treatment with low salt concentrations (Fig. 3.3. D), it was hypothesized that photosynthesis might be perturbed already during early responses to mild salt stress. Therefore, photosynthetic parameters were determined by IMAGING-PAM using two-week-old Arabidopsis WT seedlings grown horizontally on $\frac{1}{2}$ MS solid media (mock) or on the same media with added 50 mM or 100 mM of NaCl (Fig. 3.13.). While the absorptivity values determined by the PAM-imaging of the leaves do not display the exact content of different chlorophyll species, the sum absorptivity can give an indication of the amount of chlorophyll present (Fig. 3.13. A). The mild salt treatment of the plants resulted in gradually decreasing absorptivity values with 50 mM or 100 mM NaCl, compared to mock treated controls (Fig. 3.13. A).

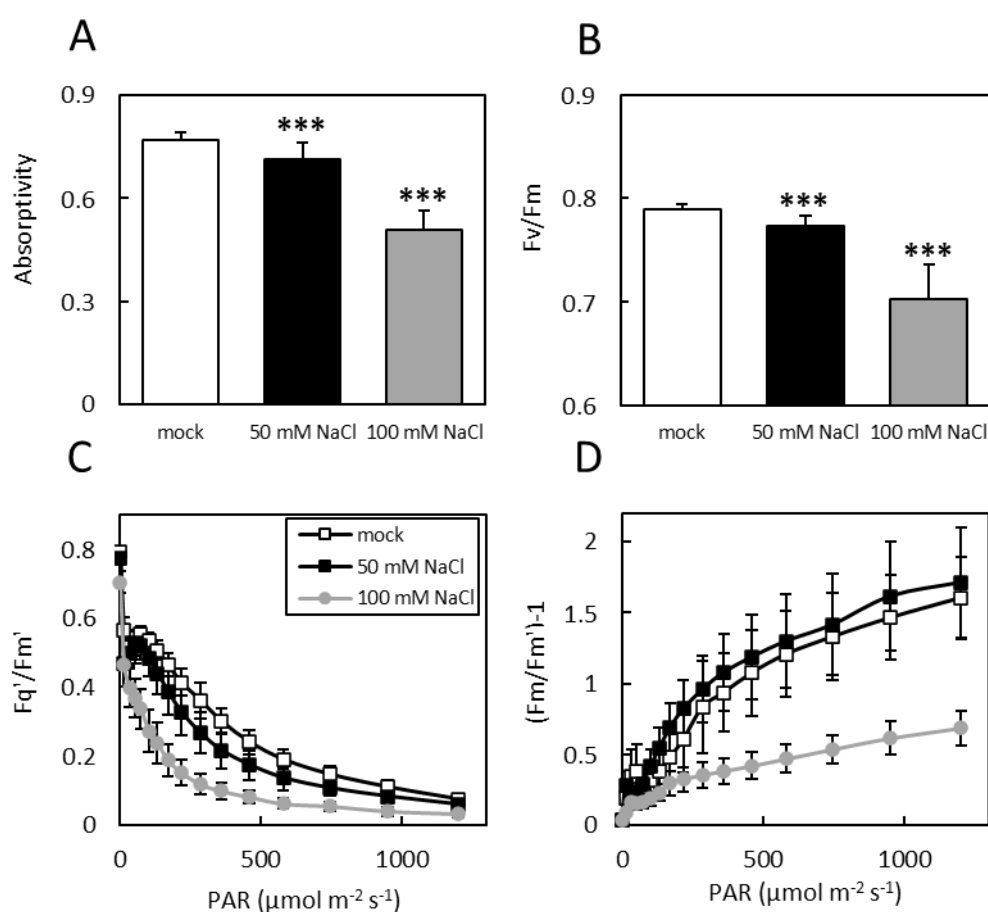


Figure 3.13.: Photosynthetic parameters of Arabidopsis WT seedlings treated with different salt concentrations.

First true leaves of two-week-old seedlings grown on $\frac{1}{2}$ MS solid media with 50 mM NaCl (black squares), 100 mM NaCl (grey circle) or without added salt (mock, white squares) were cut off and placed on $\frac{1}{2}$ MS

agar plates. Leaves were dark-adapted for at least 5 min before starting with saturation pulse of 800 ms and an exposure of $2400 \mu\text{mol m}^{-2} \text{s}^{-1}$. Parameters were measured to calculate A, absorptivity and B, maximum quantum PSII efficiency (Fv and Fm). IMAGING PAM was used to measure a light curve with photosynthetically active radiation (PAR, in $\mu\text{mol m}^{-2} \text{s}^{-1}$) increasing from 14 to 1200 PAR in 15 steps and duration intervals of 30 s. The recorded parameters Fm, Fm' and Fq' were used to calculate C, active quantum PSII efficiency; D, non-photochemical quenching (NPQ) at each light intensity. Data represent means \pm SD of four to five biological replicates from two independent experiments. At least five leaves were measured for each biological replicate. Asterisks show significant changes compared to WT results according to a Student's T-test (* $P < 0.05$; ** $P < 0.01$; *** $P < 0.001$).

Similar results were obtained for the maximum quantum PSII efficiency values (Fv/ Fm), and for both parameters treatment with 100 mM NaCl resulted in a more severe effect (Fig. 3.13. A, B). The active quantum PSII efficiency was also impaired by salt treatment, and plants treated with 50 mM salt displayed reduced active quantum PSII efficiency at normal and higher light intensities compared to mock treated plants (3.13. C), whereas plants treated with 100 mM NaCl exhibited significantly decreased active PSII efficiency at all light intensities (Fig. 3.13. C). This negative effect of the salt treatment was also reflected in a slow and limited increase in NPQ, which was significantly reduced at both low and high light conditions in salt-treated plants compared to mock controls (Fig. 3.13. D). By contrast, energy dissipation at low light intensities was significantly reduced upon treatment with 50 mM NaCl or with 100 mM compared to mock treatment, whereas dissipation was significantly increased at normal intensities and had the same level as in mock-treated plants at high light exposure (Fig. 3.13. D). In sum, the data indicate that plants exposed to 50 mM of NaCl displayed a decrease in photosynthetic functionality, but not to the same extent as when treated with 100 mM NaCl. Although PSII performance was reduced upon salt treatment compared to mock-treated plants, this effect did not result in a higher NPQ, but instead the NPQ appeared to increase more rapidly upon salt treatment at higher light intensities. These observations suggest that mild salt treatment, such as 50 mM NaCl, results in altered physiological processes to an extent that allows them to build a foundation for further growth and development (Fig. 6.8.). This could be due to the fact that reaction and acclimation processes, such as the observation of increased membrane lipid levels, are still highly effective at the low salt concentrations. By contrast, the plants treated with 100 mM NaCl hardly perform photosynthesis, while at the same time displaying low rates of NPQ at high light intensities,

resulting in an inability to quench excess energy and ensuing exposure to an increased abundance of harmful reactive oxygen species (ROS).

3.2.4. The xanthophyll cycle is inhibited in the *fad3* mutant.

To further address how a change in thylakoid lipid composition might influence photosynthetic energy dissipation, the xanthophyll cycle (XC) as one of the relevant components in the NPQ mechanism was analyzed in more detail again using the Arabidopsis *fad3* mutant as a model. The dissipation of excess light energy into heat depends on different photoprotective mechanisms within the thylakoid membrane. Acidification of the thylakoid lumen by accumulation of protons activates the enzyme violaxanthin de-epoxidase (VDE), which converts violaxanthin (Vx) to antheraxanthin (Ax) and then further to zeaxanthin (Zx) within the membrane, thereby buffering excess electrons ((Niyogi et al., 1998). Another relevant mechanism activated by a lower luminal pH is the protonation of the PSII complex subunit S (PsbS), which belongs to the LHC family of proteins and may play a role in the reorganization of PSII-LHCII super complexes during changing light conditions, promoting the transfer of excess electrons from chlorophyll of PSII complex to Zx (Li et al., 2000; Sacharz et al., 2017). Although these processes cannot be truly separated from one another, it has been suggested that the XC is involved in a quenching mechanism that requires a long induction time and displays also a long relaxation time (Nilkens et al., 2010; Quick and Stitt, 1989), in contrast to the faster quenching processes involving PsbS and Zx. Since all NPQ processes named above occur within the environment of the thylakoid membranes, thylakoid lipids might influence their physiological efficiency. It has been shown that the reorganization of LHCII under high light and the clustering of protein complexes mediating photochemical quenching within the membranes are associated with an accumulation of MGDG, which is required for the function of dimerized VDE to partially integrate into the membrane (Simidjiev et al., 1998; Vieler et al., 2008). This close link between function and lipid requirement led to the assumption that changes in fatty acid composition or the amount of MGDG, as is the case in some *fad* mutants, might affect photoprotection. Since the Arabidopsis *fad3* mutant displayed not only increased amounts of MGDG (Fig. 3.6. C) but also showed a significant decrease of NPQ under

high light conditions (Fig. 3.12. D), it was investigated whether the XC was perturbed in these plants. For this purpose, WT or *fad3* seedlings were exposed to different light intensities with the IMAGING-PAM and subsequently used for the extraction on XC-pigments and quantitative pigment analysis by HPLC (these experiments were performed in cooperation with Prof. Reimund Goss University of Leipzig). The analysis of the XC-pigment amounts showed slight differences in the content of neoxanthin (Nx) and lutein (L) (Fig. 3.14. A). The HPLC data furthermore confirmed that the *fad3* mutant contained more Chl b than the WT seedlings (Fig. 3.14. A).

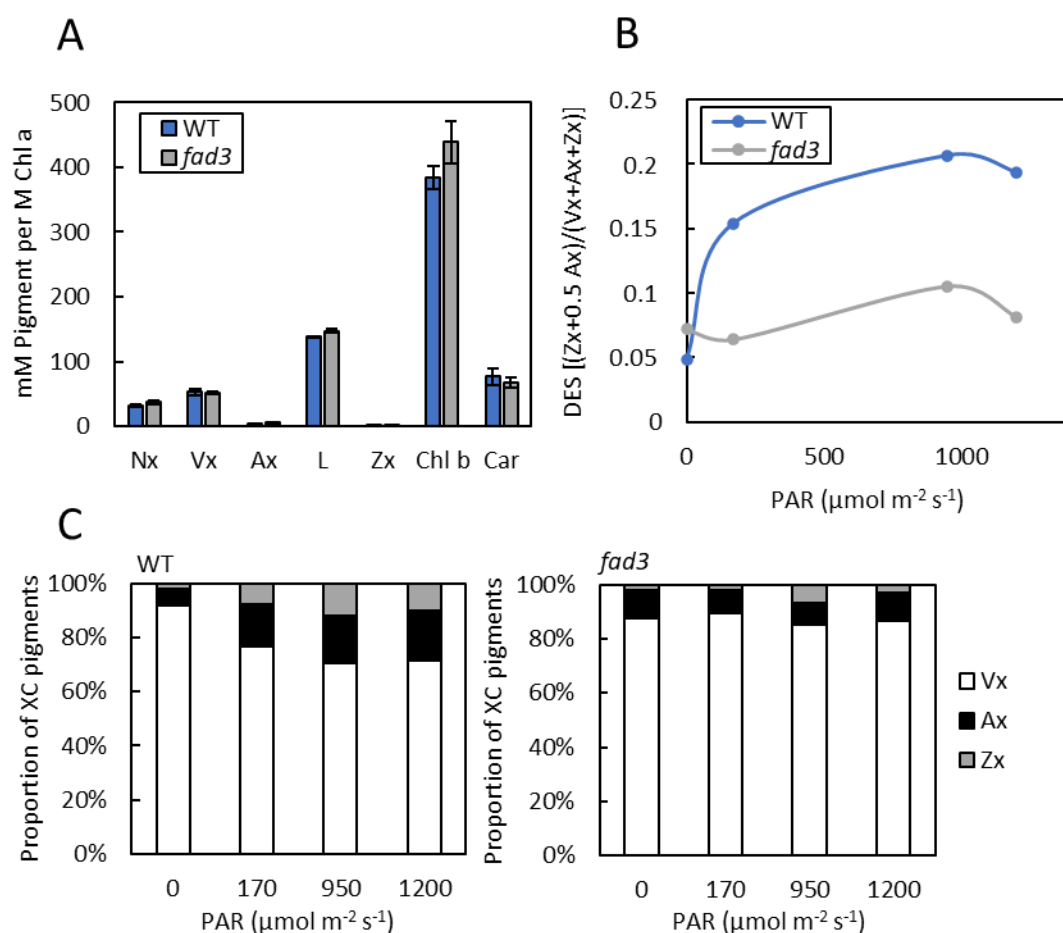


Figure 3.14.: De-epoxidation of XC-pigments in WT controls and the *fad3* mutant after exposure to different light intensities.

First true leaves of two-week-old WT (blue) and three-week-old *fad3* (grey) lines were cut and placed on $\frac{1}{2}$ MS solid media and dark-adapted for at least 5 min before starting with a saturation pulse for 800 ms and an exposure of $2400 \mu\text{mol m}^{-2} \text{s}^{-1}$. A light curve with photosynthetic active radiation (PAR, in $\mu\text{mol m}^{-2} \text{s}^{-1}$), increasing from 14 to 1200 PAR subsequently in 15 steps and duration intervals of 30 s by IMAGING PAM was used to expose seedlings with light intensities 0, 170, 950 and 1200 PAR. From exposed seedlings pigments were extracted for HPLC measurements. A, Amounts of the pigments neoxanthin (Nx), violaxanthin (Vx), antheraxanthin (Ax), lutein (L), zeaxanthin (Zx), chlorophyll b (Chl b) and beta-carotene (Car) in mM pigments per M of chlorophyll a (Chl a) measured at light intensity 0 PAR using HPLC in

cooperation with Prof. Reimund Goss, University of Leipzig. B, Amounts of xanthophyll cycle (XC) pigments were used to calculate de-epoxidation state (DES). C, Percentage of XC pigments Vx (white), Ax (black) and Zx (grey) at each exposed light intensity of WT and *fad3* leaves. Data represent means \pm SD of two to three biological replicates from one independent experiment.

The XC-pigment analyzed upon increased exposure from 0 to 1200 PAR served as a basis for the evaluation of the de-epoxidation state (DES) in WT and *fad3*, which serves as a measure for the sum conversion of Vx to Ax or Zx in the XC. While the pigment conversion indicated by the DES increased in WT plants already under normal light conditions (170 PAR), in *fad3* plants the DES decreased after dark-adaptation compared to the basal level (Fig. 3.14. B). Up to high light conditions at 950 PAR, the DES values for both lines increased, but were always about twice as high in WT as in *fad3*, even when the values decreased again beyond light intensities of 1200 PAR (Fig. 3.14. B). For better illustration, the ratios of XC pigments in WT and *fad3* are displayed in Figure 3.14. C. While the WT controls display an increase of Zx with exposure to increasing light intensities and at the same time a higher accumulation of Ax instead of complete conversion to Zx, the contents of Zx and Ax in *fad3* did not change, apart from a slight increase at 950 PAR (Fig. 3.14. C). These observations suggest a defect in XC function in the *fad3* mutant.

A defect in XC performance in the *fad3* mutant might be a consequence of reduced functionality of the key XC enzyme, VDE. To experimentally test whether VDE function is inhibited in the *fad3* mutant, thylakoids were isolated from WT and *fad3* mutants and used for de-epoxidation assays under optimal conditions for the VDE enzyme at pH 5.0 and a temperature of 30°C. Samples were analyzed before the start of the de-epoxidation reaction with ascorbic acid (0 min) and after 30 min of incubation by extracting the XC pigments and determining their conversion to the de-epoxidated states by HPLC (Fig. 3.15.; These experiments were performed in cooperation with Prof. Reimund Goss, University of Leipzig). According to this chemical-based in vitro analysis, both the WT controls and the *fad3* mutant displayed an increase in DES of more than fourfold after 30 min of de-epoxidation, compared to the basal values at 0 min (Fig. 3.15. A), indicating successful thylakoid preparation and pigment analysis.

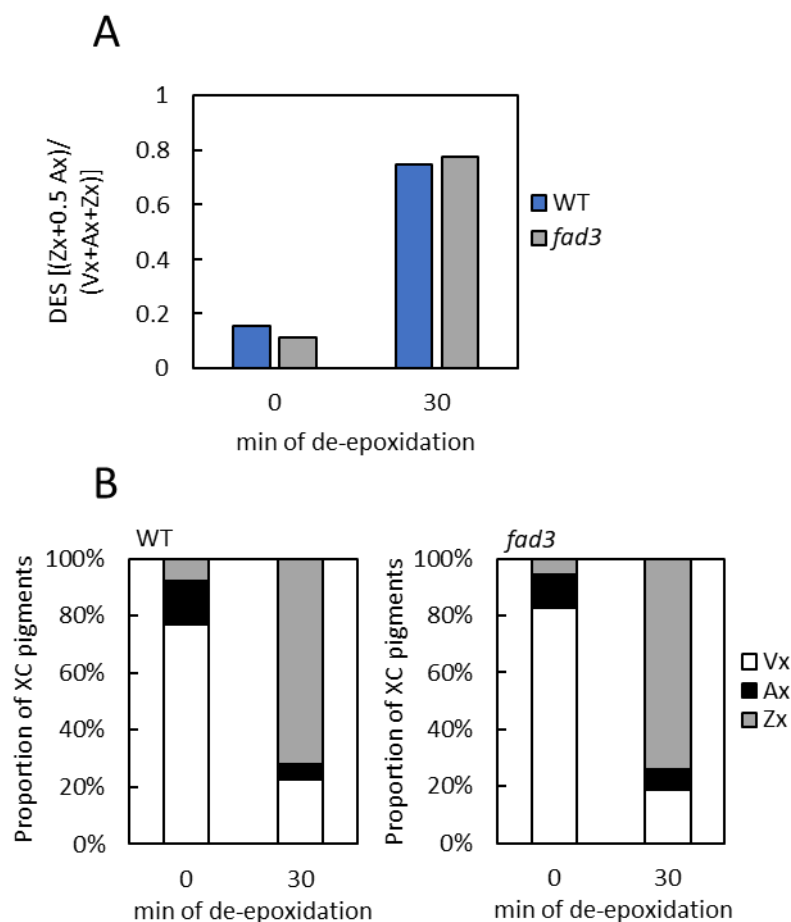


Figure 3.15.: De-epoxidation assay under optimal condition with isolated thylakoids from leaves of WT and *fad3* seedlings.

Seedlings of two-week-old WT (blue) and three-week-old *fad3* (grey) lines grown on ½ MS solid media were harvested, and the thylakoids isolated to perform de-epoxidation assays under optimal conditions at pH 5.0 and 30 °C and subsequent extraction of pigments. A, Shown is the de-epoxidation state (DES) calculated by the amount of xanthophyll cycle (XC) pigments measured by HPLC before and 30 min after start of the reaction with ascorbic acid added as co-factor. B, Proportion of XC pigments violaxanthin (Vx, white), antheraxanthin (Ax, black) and zeaxanthin (Zx, grey) in WT and *fad3* thylakoids before and 30 min after start of de-epoxidation. Data shown are representative for two independent experiments performed.

A similar pattern was observed for the ratios of XC pigments, with Vx forming the majority in both lines prior to the onset of de-epoxidation and Ax, as an intermediate, showing higher amounts than Zx (Fig. 3.15. B). This reversed after 30 minutes of reaction time, with Zx showing the highest proportion and Ax no longer accumulating (Fig. 3.15. B).

The *in organello* assay showed that VDE function in *fad3* was not different from that in WT controls, but also that the potential of XC pigment conversion in the assay did not reach its limit *in vivo* (Fig. 3.14. B; Fig 3.15. A). Light intensity-induced de-epoxidation showed a slight difference

between the WT and *fad3* lines, as in the NPQ results, but since this difference did not only occur at high light conditions, as seen in the NPQ measurements, it could be that other processes of photoprotection are also inhibited and play a role in the lower NPQ results and are more impaired at high light conditions (see also Fig. 3.12. D).

3.3. Reasons for and consequences of changes in membrane lipid levels.

As mentioned previously, the lipid composition as well as fatty acid distribution of organellar membranes has an optimal setup for certain membrane-associated processes, hence these parameters are maintained constant under standard physiological conditions. Stress-induced changes in the amount of lipid levels are often connected with signal transduction, stress adaptation or in the worst case, membrane damage. The consequences are often seen in altered plant hormone levels and phenotypic changes of cellular ultrastructure. Further experiments were performed to address some of the ensuing possibilities.

3.3.1. *fad* mutations do not result in massive changes in plastid ultrastructure.

To determine possible effects of altered thylakoid membrane lipid composition on plastid structure, the plastidial ultrastructure was evaluated by transmission electron microscopy (TEM). These experiments were performed in cooperation with Dr. Gerd Hause, core facility electron microscopy, MLU Biozentrum Halle (Saale). Under normal conditions, thylakoids in *Arabidopsis* chloroplasts are mostly organized in grana stacks, in which membranes appear in cluster-like stacked structures and only the upper, lower and lateral parts are exposed to the stroma. These stacked grana thylakoids appear in contrast to stromal thylakoid lamellae, which occur individually and are entirely surrounded by the stroma and form the connection between the grana stacks. These two thylakoid arrangements (grana thylakoids and stroma thylakoids) contain different elements of the photosynthetic machinery. While PSI and ATP synthases are mainly localized in stroma lamellae, PSII and LHCII are highly concentrated in grana stack complexes. The formation of grana stacks is a light-dependent process and requires the MGDG-mediated

transverse LHCII-LHCII interaction (Kirchhoff, 2014; Garab and Mustárdy, 2000; Simidjiev et al., 1998). All *fad* mutants studied for this work showed changes in MGDG amounts or the composition of MGDG-associated fatty acids, and thus a change in the state of MGDG saturation, which may influence processes that depend on structural properties of MGDG, such as stacking of thylakoid grana (Fig. 3.6. C). To investigate possible effects of the altered thylakoid lipid composition in these mutants, the first true leaves of WT, *fad3*, complemented *FAD3-4c* line, *fad78* and *fad378* were cut into ultrathin sections (70 nm) to analyze the ultrastructure of chloroplasts in mesophyll cells using an EM 900 transmission electron microscope (Fig. 3.16.).

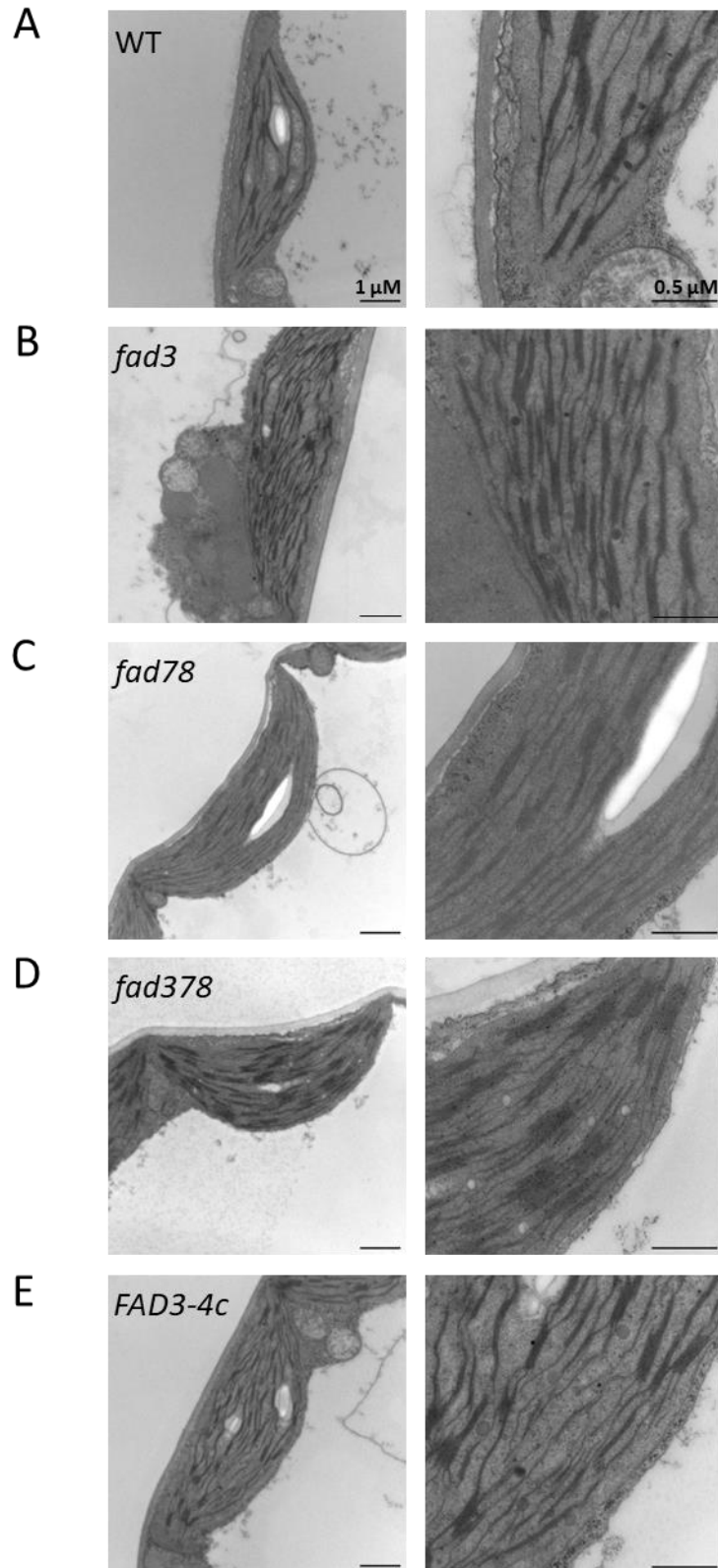


Figure 3.16.: Ultrastructure of chloroplasts from *Arabidopsis fad* mutants.

A-E, First true leaves of two-week-old WT, *fad78*, *fad378* and complemented *FAD3-4c* lines as well as three-week-old *fad3* line were cut and prepared for ultrastructural analyses using 900 EM transmission

electron microscope (Carl Zeiss Microscopy) in cooperation with Dr. Gerd Hause (Biozentrum Halle). Images were taken with a Variospeed SSCCD camera SM-1k-120. The image pairs on each level show the same chloroplasts, but images on the right are more magnified. Left images, scale bars = 1 μm ; right images, scale bars = 0.5 μm . Number of analyzed plants: 2-11.

The electron micrographs suggest that the *fad3* mutant contained more thylakoid membrane, which would correlate with higher MGDG levels (Fig. 3.16. B; compare Fig. 3.6. C). The *fad378* mutant line seemed to form larger grana stacks compared to WT, although no trienoic fatty acids were present (Fig. 3.16. D; Fig. 3.6. B, C). And furthermore, the osmium tetroxide-based EM staining technique might indicate a stronger contrast in case of WT, *fad3* and *FAD3-4c* containing more 16:3 and 18:3, possibly reflecting the level of trienoic fatty acids present, whereas the contrast was weaker in the case of *fad78* and *fad378* (Fig. 3.16. A-E; compare Fig. 3.6. C; White et al., 1976). However, the number of TEM images obtained was too low to be statistically evaluated, and the *fad* mutants did not display any massively aberrant ultrastructure compared to the WT controls or to the complemented *fad3* line, regardless of the amount of trienoic fatty acids bound to MGDG (Fig. 3.16. A-E). In consequence, the variation in photosynthetic parameters of *Arabidopsis fad* mutants does not result from obvious changes in the ultrastructure of chloroplasts (Fig. 3.11.; Fig. 3.12.).

Taken together, the data presented so far confirm that the defect in ER-based membrane lipid unsaturation present in the *fad3* mutant is compensated by the export of polyunsaturated fatty acids from the plastid (Fig. 3.6. B, C), as was previously demonstrated (Browse et al., 1993). The data presented here indicate that this export is accompanied by a substantial increase in the main thylakoid lipid, MGDG, and an equivalent increase was also observed upon mild salt treatment (Fig. 3.3.), for which export of polyunsaturated fatty acids from the plastids to extraplastidial membranes has also been proposed (König et al., 2007). The data presented here suggests that a pool of MGDG is formed in the plastid that may serve as a buffer to support the export of polyunsaturated fatty acids to the ER, possibly at the expense of the formation of thylakoids with photosynthetic capacity. While the plastidial ultrastructure of *fad3* mutants or other lines appeared largely unchanged, the analysis of the physiological consequences of the ER-based defect in fatty acid desaturation indicates changed thylakoid function, in form of a lower NPQ and

an altered photoprotective function of the XC *in vivo*. As the XC resides in the grana thylakoids, where MGDG contributes to the organization and dynamics of integral membrane protein complexes crowding the available thylakoid membrane area, it may be concluded that the complexity of grana functions is somehow impaired in consequence of the changes in lipid composition following the knock-out of the *FAD3* gene or similarly upon salt treatment.

3.3.2. Unaltered jasmonic acid levels and responses in the *fad3* mutant.

Besides serving as the main thylakoid lipid, an alternative physiological fate of MGDG is to provide a source of polyunsaturated fatty acids for the production of the phytohormone, JA. As the *fad3* mutant displayed delayed growth under the conditions used compared to WT controls or the complemented *FAD3-4c* line (Fig. 6.5., and normal growth was observed in the *fad378* triple mutant (data not shown), it was next addressed whether the increased MGDG abundance in the *fad3* mutant might have supported increased levels of JA. JA is an important plant hormone playing a crucial role in mediating plant defense responses at the expense of growth (Gomi, 2020). Studies on *dgd1* knockout plants showed that these plants exhibited inhibition of plant growth and elevated levels of JA, which may have influenced plant growth (Lin et al., 2016). In addition to an effect on MGDG levels, the *fad3* mutant line also showed an unusual growth phenotype, that disappeared in the JA-deficient *fad378* line, even though the triple mutant emerged from the *fad3* mutant line (Fig. 6.5.; McConn et al., 1997). To test whether a higher JA level in *fad3* can lead to a growth phenotype due to a higher substrate level for JA formation, the expression of the JA marker *JASMONATE ZIM-domain gene 10* (*JAZ10*) was first measured in roots and shoots of WT, *fad3* and complemented *FAD3-4c* under unwounded and 1 h past wounding conditions. These experiments were performed in cooperation with Dr. Debora Gasperini and Yunjing Ma from the IPB Halle. Although *JAZ10* expression level of *fad3* line showed high variability of expression in roots, the transcript abundance was not significantly different from that of the WT or *FAD3-4c* controls (Fig. 3.17. A).

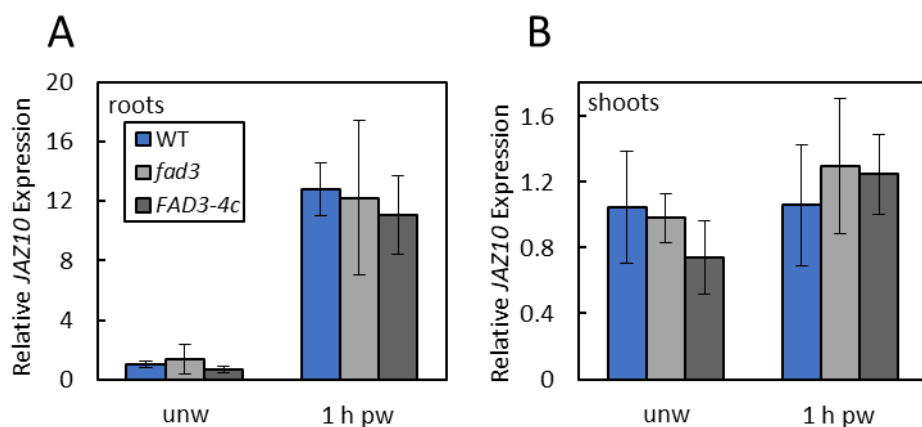


Figure 3.17.: Expression level of *JAZ10* in roots and shoots under unwounded and 1 h past wounding in *Arabidopsis* WT, *fad3* and complemented *FAD3-4c* line.

A and B, In cooperation with working group of Dr. Debora Gasperini (IPB Halle), the roots of six two-week-old seedlings of WT and complemented *FAD3-4c* lines and of six three-week-old seedlings of the *fad3* line were squeezed with tweezers to induce wounding and shoots and roots were harvested after 1 h (1 h pw). For comparison under unwounded (unw) conditions, the shoots and roots of six seedlings of each line were harvested. Each sample was prepared for RNA extraction to synthesize cDNA, which was used to analyze *JASMONATE ZIM-domain gene 10* (*JAZ10*) expression by qPCR. Expression levels were first normalized to UBQ21 expression level and additionally to of *JAZ10* level in unwounded roots and shoots of WT seedlings. Data represent means \pm SD of three biological replicates from one experiment.

After wounding, the abundance of *JAZ10* transcript increased and showed an approximately 12-fold higher abundance in all three *Arabidopsis* lines tested, but with no obvious differences between the lines (Fig. 3.17. B). In shoots, the basal transcript abundance and the expression levels after wounding also did not differ between WT, *fad3* or *FAD3-4c* (Fig. 3.17. B). Moreover, expression of *JAZ10* did not generally increase in shoots after wounding as it did in the roots. Since the expression of JA-dependent transcripts only indirectly indicates changes in JA content, and the expression of the JA-marker *JAZ10* investigated here did not show any changes in expression level in leaves after wounding, the levels of different oxylipin species were directly analyzed to determine directly whether an increased JA level in *fad3* mutants might play a role in the altered growth phenotype (Fig. 6.5.). These experiments were performed in cooperation with Dr. Cornelia Herrfurth (AG Feußner, University of Göttingen) using UPLC-NanoESI-MS/MS. The intermediates dinor-12-oxophytodienoic acid (dn-OPDA) and OPDA, which are processed from 16:3 and 18:3 fatty acids associated to MGDG, respectively, in the plastids, were measured, as well as JA, the product from OPDA after beta-oxidation steps in the peroxisomes, and jasmonoyl-isoleucine (JA-Ile), the bioactive conjugate formed in cytoplasm that directly regulates the

responses to jasmonate signaling (Sheard et al., 2010). While the analytes were all unambiguously identified in the lines tested, the data for the *fad3* mutant line displayed no significant changes in any of the measured oxylipin species compared to the levels measured in the WT or *FAD3-4c* controls (Fig. 3.18.).

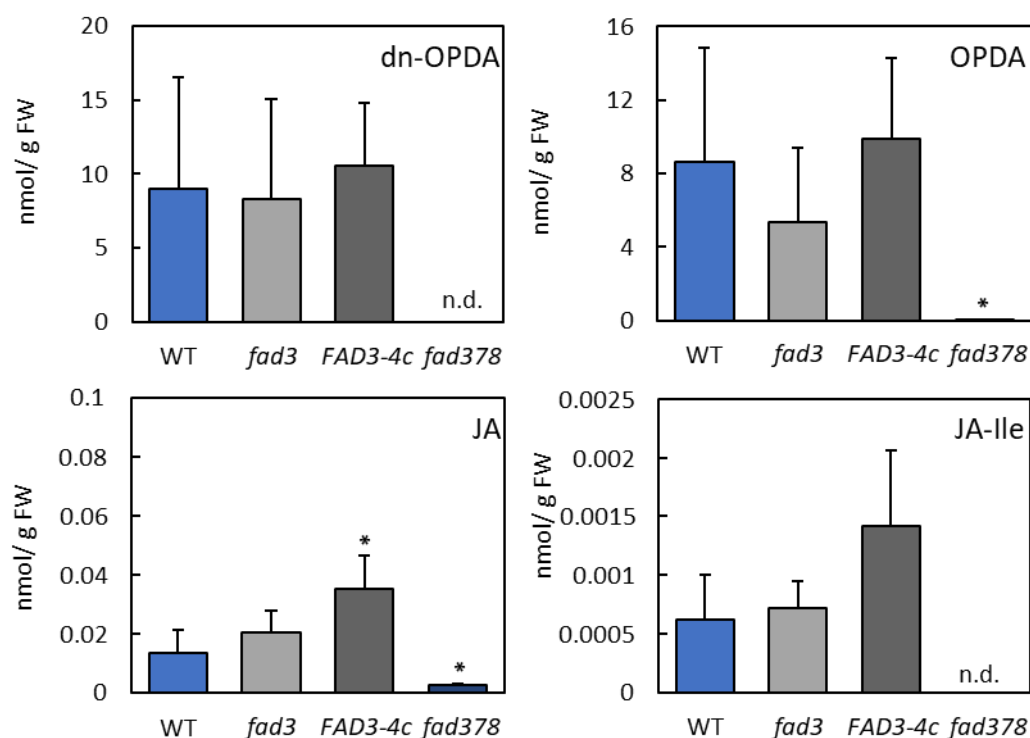


Figure 3.18.: Level of various oxylipin species in WT, *fad3*, *FAD3-4c* and JA-deficient mutant *fad378*.

Seedlings were grown on plates containing ½ MS solid media for two-weeks (WT, blue; *FAD3-4c*, dark grey; *fad378*, dark blue) or three-weeks (*fad3*, grey) and then harvested and ground. Further preparation and measurements of oxylipin levels using UPLC-NanoESI-MS/MS were done by Dr. Cornelia Herrfurth (Metabolomics Facility, AG Feußner, University Göttingen; Herrfurth and Feussner, 2020). Measured oxylipins are given in nmol/ g fresh weight (FW) and data represent means ± SD of four to five biological replicates from one experiment. dn-OPDA: dinor-12-oxophytodienoic acid, OPDA: 12-oxophytodienoic acid, JA: jasmonic acid, JA-Ile: jasmonoyl-isoleucine, n.d.: not detected. Shown asterisk were calculated using Student T-test (* $P < 0.05$).

Since the development and plant growth of the *fad3* mutant line is contrary to that of the triple mutant line *fad378*, the oxylipin content of the JA-deficient mutant, which cannot form ω 3-fatty acids in neither the plastids nor the ER, was also measured (Fig. 3.6. B, C; Fig. 3.18.). While dn-OPDA and JA-Ile were not detected, low concentrations of OPDA and JA were present, which could be related to 18:2 fatty acids used for OPDA and subsequent JA formation (Fig. 3.18.; Schaller et al., 2004). Overall, the analyses suggest that the JA concentration in the *fad3* mutant

does not change due to increased MGDG amounts and that the growth phenotype is a consequence of a different and yet unresolved process (Fig. 3.6. C; Fig. 3.18.; Fig. 6.5.).

3.3.3. Salt-induced lipid changes are linked to the induction of plant senescence.

To further investigate the possible basis for the growth delay of the *fad3* mutant, it was next tested whether the *fad3* mutant displayed altered expression patterns of senescence markers. Senescence can be triggered in plants in many ways, such as age, growth, hormones, and environmental stresses. Since senescence is a coordinated process in which biomolecules are degraded and remobilized for alternative processes, such as leaf growth or seed development, transcriptional remodeling is essential for all cell types and tissues involved. The large group of *SENESCENCE-ASSOCIATED GENES (SAG)* plays an important role in the control of plant senescence, and the expression of these genes is upregulated under light stress conditions, during darkness, and also under environmental stress conditions, including pathogen infection or in response to other stresses that induce the production of ROS (Dhar et al., 2020). Some genes of the *S40* family induce the expression of other *SAG* genes, and various *S40* genes from rice are induced under drought and salt stress conditions (Fischer-Kilbienski et al., 2010; Jehanzeb et al., 2017). Importantly, age-related senescence is associated with the turnover of glycerol membrane lipids and the formation of an increased amount of triacylglycerol (TAG), whereas genes of FA biosynthesis are simultaneously down-regulated (Koiwai et al., 1981; Troncoso-Ponce et al., 2013). It could therefore be that treatment with low salt concentrations might also induce senescence, thereby leading to a reallocation of FAs between cellular membranes. Therefore, the transcript abundance of the senescence markers *S40-3* and *SAG13* was determined in seedlings after short-term treatment with 50 mM NaCl. The expression of *S40-3* increased during short-term of salt stress after 1.5 h and reached even higher amounts after 2 h but none of the changes were significant (Fig. 3.19. A).

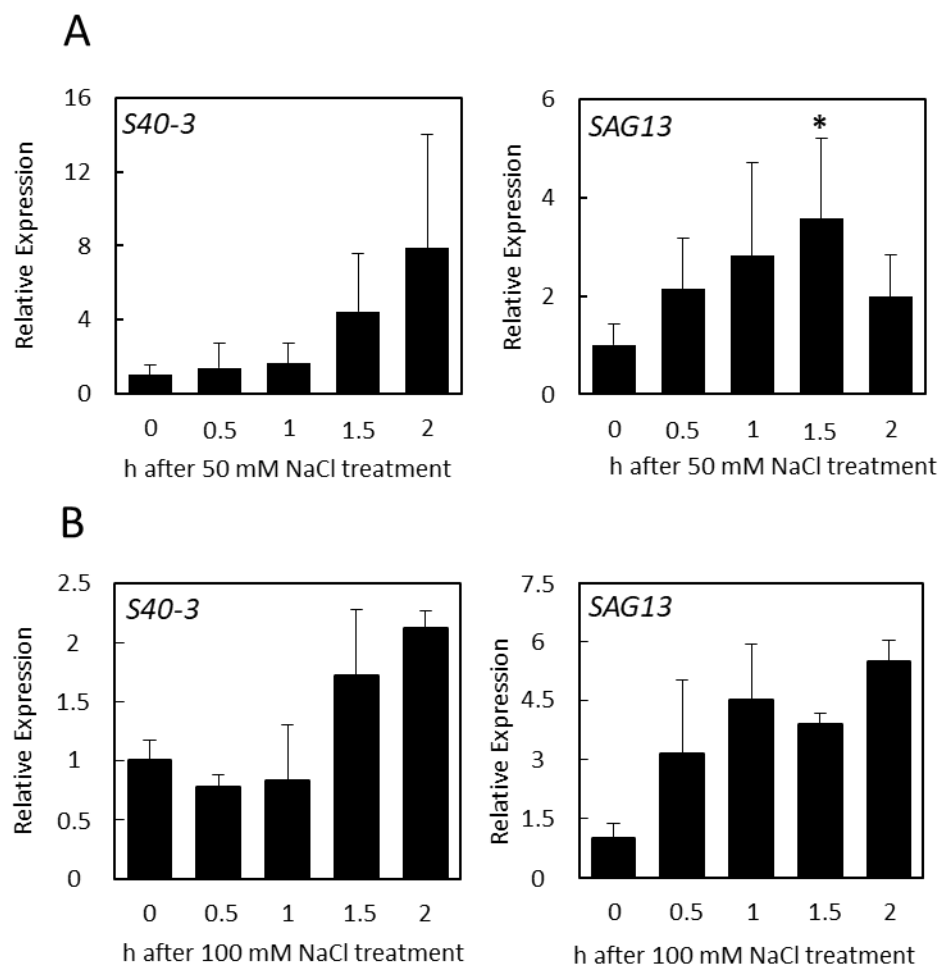


Figure 3.19.: Expression level of senescence marker *S40-3* and *SAG13* in Arabidopsis WT seedlings after short term treatment with low salt concentrations.

Two-week-old seedlings grown on ½ MS solid media were transferred on ½ MS solid media containing 50 mM NaCl (A) or 100 mM NaCl (B). Seedlings were harvested for RNA extraction after 0, 0.5, 1, 1.5 and 2 h of treatment and later used for cDNA synthesis to analyze expression level of *S40-3* and *SAG13* by qPCR. First, the data was normalized using *UBC10* level and the time series was additionally normalized to time point zero. Data represent means ± SD of four biological replicates from two independent experiments and (A) and of two biological replicates from one experiment (B). Shown asterisk were calculated using Student T-test (* $P < 0.05$).

The transcript abundance of *SAG13* showed a gradual increase during salt treatment, which was significant after 1.5 h (Fig. 3.19. A). A similar pattern in the transcript abundance of *S40-3* and *SAG13* were also displayed when treated with 100 mM NaCl with the only difference that here the transcript abundance of *SAG13* had a higher increase (Fig. 3.19. B). This shows that senescence is already induced in seedlings treated with low salt concentrations in a short-term

manner. It could also be considered that senescence is involved in the change of lipid levels of MGDG and/or PC after salt stress (Fig. 3.3. C, D).

Overall, the effects of mild salt treatment or the knock-out of FAD3 have similar effects on membrane lipid rearrangements between the ER and plastidial membranes, as described above. While the membrane rearrangements have profound impact on specific aspects of plastidial physiology, mainly in photoprotection, the reasons for the growth delay of the *Arabidopsis fad3* mutant remain unclear. The data indicate that the increased abundance of MGDG is not related to growth-limiting production of jasmonic acid, and it is possible that the membrane rearrangements observed in this thesis resemble processes occurring during the recycling of biological material as it occurs during plant senescence, including an induction of SAGs. However, this line of evidence remains largely unexplored and further analyses will be required to conclusively determine the basis of the growth defect.

4. Discussion

Dynamic changes in the composition of membrane lipids are important elements of plant responses to exogenous stress conditions, both to maintain the integrity of the membranes and to enable the function of integral membrane protein complexes. In experiments in this thesis, the treatment of Arabidopsis seedlings with mild salt conditions as 50 mM NaCl led to simultaneous increases of MGDG and PC abundance within 2 h. Expression analysis of various marker transcripts indicated that these changes might be connected to the perceived salt stress or might be part of an early stage of salt-induced senescence. The Arabidopsis mutant with defects in the production of 18:3 at the ER, the *fad3* mutant showed similarly increased lipid levels even before any salt treatment, and no further changes in the lipid composition were observed after exposure to salt. The finding that MGDG levels were altered in response to salt as well as in the *fad3* mutant, which has a defect in ER-associated fatty acid desaturation, suggested that the trans-organellar exchange of fatty acids known to occur in the *fad3* mutant exerts an influence on the composition and organization of plastidial membranes, including thylakoids (Browse et al., 1993). Based on the hypothesis that salt treatment results in the mobilization and export of lipid intermediates from the plastid to supply extraplastidial membranes with lipid precursors to maintain membrane integrity in the face of salt stress, stress-treated seedlings and seedlings of various Arabidopsis *fad* mutants were compared. Neither the *fad* double mutant *fad78* nor the triple mutant *fad378* showed notable changes when treated with the mild salt stress. In line with the effect of salt stress on plastid physiology, WT seedlings displayed a salt dose-dependent inhibition of photosynthesis when grown on salt media. By contrast, the changed lipid composition of Arabidopsis mutants with defects in different *fads* had largely no effect on photosynthesis performance, except for the *fad378* mutant, which displayed reduced photosynthetic performance under low and normal light intensities. Of note, the knockout of the ER localized FAD3 led to a change in plastidial photoprotection, characterized by a decreased NPQ under high light intensities, which may be connected to a defective xanthophyll cycle and related to membrane rearrangements due to trans-organellar lipid mobility.

4.1. Salt sensitivity of Arabidopsis.

In previous studies by König et al. (2007), changes in the abundance of different lipid classes were analyzed over a period of 2 h in ten-week-old Arabidopsis WT plants treated with 400 mM NaCl and, among other effects, changes in the amount of plastidial MGDG and extraplastidial PC were observed in close temporal coordination, suggesting a functional connection between these two most abundant structural membrane lipids (König et al., 2007). In preliminary studies in preparation for this thesis, ten-day-old WT seedlings were also treated with 400 mM NaCl, but despite the high expression of salt stress markers, no changes in PC or MGDG were observed, however, the seedlings were also no longer vital (Matzner, 2019). It appears likely that ten-week-old plants with fully grown rosettes, as it was the case in the studies by König et al. (2007), might resist longer against high osmotic potential of the surroundings than the much younger seedlings used here.

In contrast to some other well characterized plant species, such as rice (*Oryza sativa*) and wheat (*Triticum aestivum*), Arabidopsis belongs to the more salt sensitive plants (Munns and Tester, 2008) and is unable to complete its life cycle when continuously exposed to salt concentrations as low as 100 mM NaCl (Sickler et al., 2007). The low tolerance of Arabidopsis to salt could be particularly important at the seedling stage, as it is important to gain biomass quickly and efficiently at this stage, and salt stress reduces osmotic potential and thus leaf growth (Hasanuzzaman et al., 2019). To improve the experimental set up and enable the study of physiological responses, for experiments presented in this thesis the growth conditions were optimized (discussed in 4.5.) and salt stress experiments were performed using two-week-old seedlings and only mild concentrations of NaCl. Initially, the seedlings were exposed to 100 mM NaCl for 2 h, which induced the expression of salt stress markers and showed no visual phenotype in terms of viability, but apart from this, little changes in lipid content were detected (Fig. 3.2. A; Fig. 3.5.). In contrast to seedlings exposed to 100 mM NaCl, seedlings grown with 50 mM NaCl continued their root growth comparable to non-treated seedlings (Fig. 3.8.; Fig. 6.2.; Fig. 6.8.). Expression of salt stress markers confirmed that Arabidopsis seedlings recognized the short-term treatment with low salt concentrations, and photosynthetic parameters revealed that prolonged exposure to 50 mM NaCl already lead to a significant decrease in photosynthetic performance

(Fig. 3.1. A; Fig. 3.13.) under the conditions used. The consequences of salt stress were a decrease in active PSII efficiency and an increase in NPQ to dissipate the excessive electrons (Fig. 3.13.). By comparison, seedlings grown on 100 mM NaCl generally showed a greater reduction in the photosynthetic efficiency of PSII, probably due to stronger damage to the complex, as also indicated by a low maximum quantum efficiency of PSII (Fig. 3.13.; Maxwell and Johnson, 2000). The destructive effects of 100 mM NaCl even resulted in a strikingly low NPQ, although the electrons were not used efficiently for photochemistry. A possible explanation for this effect (and the apparent "loss of electrons") is that treatment with 100 mM salt caused disruption of the thylakoid membrane, and the subsequent unphysiological thylakoid leakage might have interfered with the proton gradient that controls the activation of the NPQ components of the PsbS protein for efficient qE and XC.

In previous long-term salt experiments, the abundance of membrane lipids was found to differ between *Arabidopsis* and its salt-tolerant relative, *Thellungiella halophila*, and it was proposed that membrane lipid composition is part of the mechanisms conferring salt tolerance to halophytes (Sui and Han, 2014). In *Thellungiella halophila*, the amount of 18:3-containing MGDG species increased at the expense of 16:0-containing MGDG species when treated with 100, 200 and 300 mM NaCl. While in *Arabidopsis* the degree of unsaturation of MGDG did not change when the plants were exposed to 100 mM NaCl, exposure to 200 mM NaCl resulted in a significant decrease in the degree of unsaturation, which was proposed to be the result of MGDG degradation due to induced senescence mechanisms (Sui and Han, 2014). Findings presented in this thesis are consistent with these earlier observations and suggest that salt-triggered changes in the abundance and the degree of unsaturation of MGDG might be part of the mobilization of unsaturated fatty acids from the plastid to extraplastidial membranes.

4.2. Salt-induced senescence of plants.

Senescence markers were found to be induced by the short-term mild salt treatment of seedlings (Fig. 3.19.), and therefore a contribution of senescence to the observed changes in membrane lipid composition must be considered. Leaf senescence occurs as a final stage of plant

development when biomolecules are recycled and reused for new emerging tissues, such as new leaves or inflorescences (Biswal et al., 2013). However, senescence is also induced by external stimuli, such as prolonged darkness, biotic stress or abiotic stress - such as salt (Sade et al., 2018). The controlled death and utilization of an older leaf is a useful tool for plants to survive salt exposure, as the toxic Na^+ and Cl^- ions that have entered the plant can accumulate excessively in the old tissue and be disposed of by leaf abscission. The nature of perceived salt stress can be distinguished into the effects especially of Na^+ toxicity, and the merely osmotic effects of the dissolved salt. Within two hours of salt treatment, plants are mostly stressed by altered water relations, caused by osmotic stress rather than the effects Na^+ toxicity, which in turn manifests when plants are exposed to salt for longer periods (Munns and Tester, 2008; Hasanuzzaman et al., 2019). Since senescence contributes to the degradation of macromolecular cellular assemblies, including membranes, and would not promote increased membrane lipid abundance, it appears unlikely that short-term increases of MGDG and PC (Fig. 3.3 C, D) are part of a senescence program. Instead, these changes will rather reflect an acclimation to the salt-induced osmotic stress. The significant increase in expression of the senescence-associated gene *SAG13*, a gene with a protective role in regulating ROS by activating antioxidant enzymes (Dhar et al., 2020), after 1.5 h salt treatment (Fig. 3.19. A) may be related to the production of abscisic acid (ABA) or induced by oxidative stress, as ROS are produced under acute osmotic changes and represent an important stress signal under salt stress conditions (Fig. 3.19.; Dhar et al., 2020; Zhao et al., 2016).

Following the temporal argument, the highest degree of osmotic stress will occur immediately after the plants are exposed to salt. Depending on the osmotic potential of the environment, plants now either adapt quickly and continue to develop new leaves, or their growth is inhibited in the longer term, if the stress does not lead to cell death (Munns and Tester, 2008; Hasanuzzaman et al., 2019). High osmotic stress can cause a reduction in MGDG in favor of the formation of TAG or jasmonate as a common response to oxidative stress and senescence, due to the activation of galactolipases and lipoxygenases (Guo et al., 2019). Additionally, it has been postulated that lipid transport proteins are upregulated during long-term salt stress and are involved in salt-induced senescence, but it is unlikely that these proteins are part of the short-term (less than 6 hours of salt stress) stress mechanism (Allu et al., 2014). In order to make a more

precise statement as to whether the indications of salt-induced senescence manifested in the seedlings treated with concentrations as low as 50 mM NaCl, the monitoring of senescence markers over a longer duration of these applied conditions would have been revealing. However, since increased levels of MGDG and PC were observed within few hours of treatment in this work, the corresponding effects on physiology should be reviewed as parts of the response to salt-induced osmotic stress and are likely to be a part of early acclimation processes (Fig. 3.3. C, D).

4.3. The role of dynamic changes in PC and MGDG upon stress.

The early effects of salt induce osmotic stress by increasing the osmotic potential of the immediate cellular environment, resulting in plant cell water loss and a decrease in turgor. The shrinkage of plant cell volume leaves an excess of plasma membrane that is internalized in the form of vesicles by membrane mechanisms, such as bulk flow endocytosis (Zwiewka et al., 2015; Leshem et al., 2007). While bulk-flow endocytosis has been described for the plasma membrane, the osmotic effects on endomembranes of plant cells are much less well explored. It is reasonable to assume that the plasma membrane will not display an isolated response, but that rather other cellular membranes will also change dynamically, either by serving as acceptors for membrane material internalized from the plasma membrane, or by providing membrane components required to stabilize and maintain plasma membrane integrity. Membrane rearrangements occurring during early responses to salt/osmotic stress, might, thus, change the lipid composition and fatty acid distribution to maintain the integrity of the plasma membrane and concurrently impact on other cellular membranes, as it was proposed in studies by König et al. (2007) when the amount of PC and associated 18:3 increased, whereas the amount and the degree of unsaturation of MGDG decreased. The changes in lipid composition vary between species displaying different degrees of salt tolerance, and range from a reduction in unsaturation of membrane lipids, to a constant degree of unsaturation, to an increase in unsaturation (Guo et al., 2019). It is a challenge to interpret dynamic changes in membrane lipid abundance or their degree of unsaturation upon stress, as reallocation of membrane lipids between cellular membranes might involve partial degradation of lipids, concurrent with enhanced resynthesis. For instance,

data reported by König et al. (2007) indicate a reduction of MGDG upon severe salt treatment, concurrent with an enhanced abundance of extraplastidial PC after a few hours of treatment. If MGDG is converted to an intermediate that is exported from plastids to supply an enhanced formation of polyunsaturated PC, the stress-induced additional demand on MGDG might result in resynthesis of MGDG. The data presented in this thesis on an increase of MGDG upon stimulation with a much milder treatment of only 50 mM NaCl are, therefore, not in contradiction to the earlier findings, as under the more physiological conditions the plastid might be able to increase MGDG production to meet the extraplastidial demand, explaining the increased abundance of MGDG observed upon salt treatment (Fig. 3.3. C, D). Such considerations also apply to data on plant species displaying different degrees of salt tolerance, and it is possible that even within one species, salt tolerance and the nature of lipid changes in response to salt stress may differ, depending on the tissue analyzed or the developmental stage of the plant. The apparent changes in lipid abundance upon stress may, thus, reflect a combination of how much lipid is required to be reallocated between membranes in response to a stress, and the capacity for lipid resynthesis of a plant in a given tissue or at a certain stage of development. This might be one of the reasons why in the studies of König et al. (2007), working with ten-week-old plants, the treatment with 400 mM NaCl induced changes in lipid content, whereas here two-week-old seedlings were not even vital after 2 h of an equivalent treatment, as mentioned in 4.1. It has not only been described that the life cycle of *Arabidopsis* cannot be finished when treated with 100 mM or more of NaCl, but also stress responses are already triggered in *Arabidopsis* at concentrations below 50 mM, as evident from observed leaf growth reduction (Munns and Tester, 2008). Evidently, the two-week-old *Arabidopsis* seedlings used here displayed a physiological response when confronted with 50 mM NaCl, and increased PC and MGDG levels were detected with no major reduction in vitality (Fig. 3.3. C, D; Fig. 3.1. B). A decrease in MGDG triggered by more severe salt treatment has previously been found to be associated with a reduction in chlorophyll content and photosynthetic capacity, and also a decrease in the abundance of PC is closely related to salt sensitivity, indicating a possible breakdown in membrane integrity and an increase in membrane permeability (Guo et al., 2019). Thus, maintaining the levels of PC and MGDG might be necessary to sustain physiological processes upon exposure to salt, and an increase of both lipids might enhance plant salt tolerance.

Overexpression of *OsMGD* in rice enhanced salt tolerance due to a higher DGDG to MGDG ratio which also have been linked in several studies to a higher protection of the photosynthetic apparatus and a stabilized thylakoid structure (Wang et al., 2014; Sui and Han, 2014; Guo et al., 2019). Three MGD-synthases are encoded in Arabidopsis, but only MGD1 is involved in the bulk synthesis of MGDG. While MGD1 has been reported to be induced by osmotic stress, this induction was not observed in the seedlings investigated in this thesis (Fig. 3.1.; Fig. 3.2. Kobayashi et al., 2009). It is assumed that an increased abundance of MGDG may not only serve as a precursor for DGDG but is also used for membrane repair or as a precursor for the production of oxylipins, including jasmonic acid. So far, however, the exact mode of action if altered MGDG levels in the Arabidopsis salt response is not clear.

4.4. Trans-organellar mobilization of membrane lipid intermediates.

It was one working hypothesis of this thesis that there is a physiological connection between increased levels of MGDG in the plastid and of extraplastidial PC in response to salt (Fig. 4.1. A; Fig. 3.3. C, D). If this connection were based on the observed higher production of MGDG, this MGDG might be converted to a transport intermediate to be exported from plastids to supply the demands of extraplastidial lipids for polyunsaturated PC. To supply a lipid intermediate for export from the plastid, MGDG might be degraded by acylated galactolipid-associated phospholipase 1 (AGAP1) to form lyso-MGDG. AGAP1 activity has been described to be triggered by various stresses (Fig. 4.1. B; Mueller et al., 2017; Arabidopsis eFPbrowser), and fatty acids might subsequently be detached from lyso-MGDG by a lipase to release 18:3-acyl groups which could be exported by fatty acid exporter 1 (FAX1). In the cytosol, the acyl groups might then be activated to CoA-esters by long chain acyl CoA synthetases (LACs) and be used to form PC at the ER membrane (Li et al., 2015). Alternatively, the galactosyl head group of MGDG may also be removed to form DAG, which could be converted to lyso-PC at the OEM of plastids, then exported and reacylated to PC at the ER (Fig. 4.1. B). This pathway is supported by the presence of PC molecular species containing combination of associated 18:3/18:2 in the *fad3* mutant (Fig. 6.11.), where the associated 18:3 must have originated in the plastid. The export of plastid-synthesized 18:3 fatty acids is likely favored over the import of 18:3 from the ER, as can be concluded from

comparing the greater amount of 18:3 associated with PC in the *fad3* mutant, compared to the smaller amount of 18:3 found in MGDG in *fad78* double mutants (Fig. 3.6. B, C). However, increased amounts of PC in salt-treated plants investigated here did not display a change in the degree of unsaturation in their membrane lipids, and the proportions of bound 18:3 and 16:0 increased equally (Fig. 3.3. B; Fig. 3.4. B; Tab. 6.1.; Tab. 6.2.). It has been reported that salt treatment led to the expression of phosphoethanolamine N-methyltransferase (PEAMT), which can convert PE into PC and thereby increases the amount of PC (Mou et al., 2002). In this way the ratio of PC to PE increases, which has previously been linked to improvement of salt tolerance (Mou et al., 2002). *De novo* biosynthesis of PC as early response to salt stress was also associated with upregulation of choline-kinase (Tasseva et al., 2004). An increased abundance of PC not only seems to be important to maintain membrane integrity of the plasma membrane upon salt exposure but may also serve as a precursor of signaling lipids, such as PA, which play important roles in activating signaling cascades for responses to salt stress (Pical et al., 1999). Therefore, the increase PC levels observed in salt treated plants (Fig. 3.3. C, D) are consistent with salt acclimation. An important role of PC in salt tolerance is further supported by PC acting as a source for the formation of glycolipids through the eukaryotic pathway of fatty acid modification and re-import of intermediates into the plastids, so a higher PC content might indirectly contribute to stabilizing plastidial membranes to maintain photosynthesis (Fig. 4.1. C).

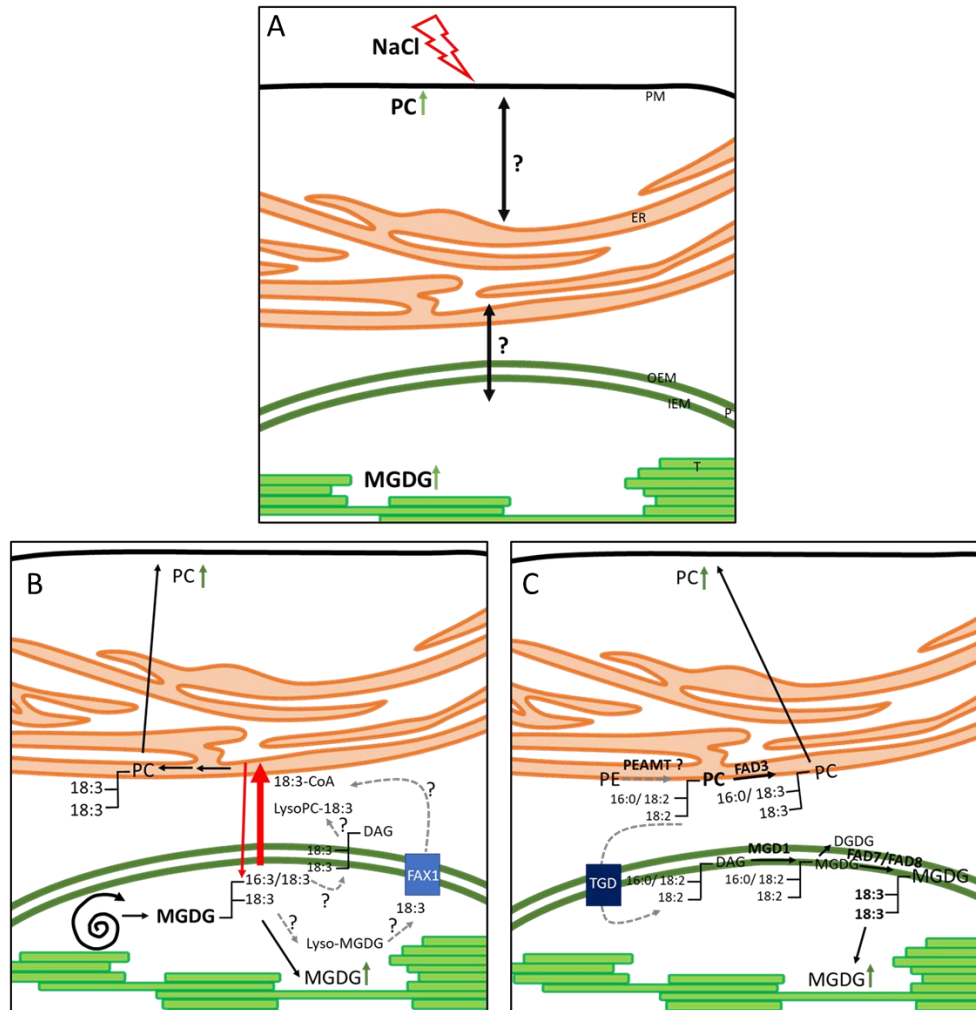


Figure 4.1.: Models of the possible interplay of PC and MGDG during the response to salt-induced osmotic stress.

A, Illustration of increased (green arrow) content of phosphatidylcholine (PC) at plasma membrane (PM, black) or extraplasmal membranes in general and increased amount of monogalactosyldiacylglycerol (MGDG) at plastidial membranes (P, green) as a result of salt stress exposure (red lightning). B, the source of the higher content in both lipids is MGDG as a result of higher biosynthesis mediated by MGD1. MGDG might be either converted to diacylglycerol (DAG), somehow transported to outer envelope membrane of plastids (OEM, outer dark green line), there converted to lyso-PC, carrying only one 18:3^{A9,12,15} (18:3) fatty acid, which is transported to endoplasmic reticulum membrane (ER, dark pink). Or degraded to lyso-MGDG and subsequently to free fatty acid species 18:3 by lipases, which might be exported by fatty acid exporter 1 (FAX1, blue), esterified to Coenzyme A (CoA) and transported to ER. Lyso-PC or 18:3-CoA can be used to form the lipid PC at ER, which is distributed within extraplasmal membranes such as PM. Red arrows indicated the possible flux of formed 18:3 between ER and plastids which has been emerged by analyzing *fatty acid desaturase (fad)* mutants, *fad3* and *fad78*. C, the source of the higher content in both lipids is PC by a conversion of phosphatidylethanolamine (PE) mediated by initial step of PE-N-methyltransferase (PEAMT). Since PC serves as precursor in eukaryotic pathway of plastidial lipid biosynthesis PC could be transported to OEM of plastids and PC itself or converted to lyso-PC/phosphatidic acid (PA)/DAG is imported by trigalactosyldiacylglycerol (TGD, dark blue) machinery. After several steps, formation of MGDG is mediated by MGD1 and bound fatty acids are unsaturated by FAD7/FAD8 to 18:3 and used for

thylakoid membrane (T) structure. Fatty acids bound to remaining PC at ER might be desaturated by FAD3 to 18:3 and distributed to extraplastidial membranes. Other explanations are possible.

Since the PEAMT is crucial for plant survival during salt stress conditions and PE contains a similar fatty acid composition as PC, PEAMT is one candidate enzyme for the rapid generation of increased levels of PC at the expense of PE (Mou et al., 2002). The resulting PC itself or lyso-PC, PA or DAG as PC-derivatives could be transported to plastids and imported by trigalactosyldiacylglycerol (TGD) machinery and used by MGD1 to form MGDG and further on probably DGDG by DGD1 (LaBrant et al., 2018). The esterified fatty acids, mostly 18:2, might then be desaturated by FAD7/FAD8 to form 18:3, thereby accounting for the observed increase in polyunsaturated MGDG in the plastids (Fig. 3.3. C, D). The lipid analysis presented here (Fig. 3.3. D; Tab. 6.1.) also showed that the proportion of 18:2 and 18:3 fatty acids increased significantly in MGDG, whereas the proportion of 16:3 was not affected, an observation consistent with an involvement of the eukaryotic (i.e. ER-based) pathway for fatty acid modification. In addition, PC still localized at the ER membrane would be desaturated by FAD3 to increase the proportion of associated 18:3, accumulating in extraplastidial membranes. In this way, the action of FAD3 would be required to increase the unsaturation of fatty acids bound to PC in the ER, whereas FAD7/FAD8 act in plastids to generate polyunsaturated fatty acids bound to MGDG (Fig. 4.1.C). It has previously been shown that overexpression of either *FAD3* or *FAD8* in tobacco BY-2 cell cultures increased the tolerance of the cells under osmotic stress conditions (Zhang et al., 2005). In addition, it could be shown that the inhibition of FAD7 protein biosynthesis in transgenic tobacco lines by the antisense expression of *FAD7* increased susceptibility to salt (Im et al., 2002). Salt treatment of seedlings of *fad3*, *fad78* or *fad378* mutants did not induce a change in PC or MGDG content beyond the already increased basal levels of these lipids in the mutants (Fig. 3.9.; Fig. 3.6. A, B). Although the *fad3* mutant had a higher basal content in both PC and MGDG, and both lipids also had a significantly higher proportion of associated 18:3 compared to the *fad78* mutant, these particular lipid patterns were not correlated with an increased or decreased salt tolerance (Fig. 3.6. B, C; Fig. 3.9.). Interestingly, the Arabidopsis mutants deficient in either of the ER or plastid localized ω -6 fatty acid desaturases FAD2 and FAD6, respectively, which are responsible for the desaturation of 18:1/16:1 to 18:2/16:2, display reduced salt tolerance (Zhang et al., 2009; Zhang

et al., 2012a). A more detailed study of the salt tolerance of seedlings exposed to lower or higher salt concentrations would have been insightful but was not performed as part of this thesis. Moreover, it would be interesting to study the abundance of transcripts for AGAP1 or PEAMT, which in combination with more comprehensive lipidomics data on the abundance of PE, DGDG and other membrane lipids might indicate the pathway used for membrane lipid rearrangement that is the most likely of the alternatives displayed in Figure 4.1.

A main finding of this thesis, then, is the observation of increased levels of MGDG and PC in physiological situations where an exchange of lipid intermediates between plastids and ER is warranted (Fig. 3.3., Fig. 3.6.). As the increased levels of MGDG in plastids, observed upon salt treatment and in different *fad* mutants, coincide with defects in photosynthetic performance, it appears likely that the MGDG formed is not available to support the function of photosynthetic thylakoids. Instead, it may be proposed that the increased MGDG represents a pool of lipids serving as a buffer to supply the export of lipid intermediates to extraplastidial membranes, according to cellular requirements. These requirements might be the support of ER-membrane unsaturation in the *fad3* mutant, or an increased demand for polyunsaturated fatty acids in the ER and/or at the plasma membrane during short-term responses to salt treatment. This hypothesis is in line with the notion that depending on the intensity of a perceived stress, the membrane lipid buffer may be continuously replenished or fully drained, manifesting in increased or decreased lipid levels upon stress treatment, respectively, as previously observed. There are many examples of substances accumulating in plastids before being exported, including the accumulation of transitory starch during the day (Weise et al., 2006). Evidently, MGDG accumulating for export from the plastids might best be located in the IEM at the plastidial periphery, rather than being incorporated into the protein-rich membrane stacks of thylakoids from where it would be difficult to mobilize. However, the analysis of plastidial ultrastructure revealed no obvious changes in the morphology of plastids of WT controls compared to the *fad* mutants analyzed, so there is currently insufficient data to prove or disprove the buffer hypothesis (Fig. 3.16.).

4.5. Differences of lipid amounts and fatty acid profiles due to plant culture conditions.

Conditions of high or low temperature were frequently used to test the growth limitation or physiological advantages or disadvantages caused by the knockout of different fatty acid desaturases and the ensuing changes in fatty acid biosynthesis (Wallis and Browse, 2002). Biophysical membrane properties, such as membrane fluidity, must be maintained roughly constant even when faced with a changing environment, and thus membranes can acclimate towards environmental changes. Membrane composition is adjusted not only upon temperature changes but also with different light conditions used for plant cultivation. Obviously, the lipid composition of plants depends on the growing conditions, as shown recently when the lipid content and fatty acid profiles of *Camelina sativa* plants grown in soil and in liquid media were compared (Klińska et al., 2021). When *Arabidopsis fad* mutant lines *fad3*, *fad78* or *fad378* were established around 30 years ago, lipids were mostly analyzed from plants grown on soil under continuous light at 130-150 $\mu\text{mol m}^{-2} \text{s}^{-1}$ (Browse et al., 1993; McConn and Browse, 1996, 1998). The use of such conditions might explain differences in lipid content and fatty acid profiles even between studies investigating the same plant lines. It also demonstrates how sensitive plants respond to their environment by acclimating their membrane lipid composition. When (Sui and Han, 2014) analyzed *Arabidopsis* plants for plastidial lipids and their fatty acid profiles while exposing them to different salt concentrations, untreated WT plants contained MGDG species with a high proportion of associated 16:0 fatty acids, whereas in analyses performed in this thesis, MGDG species containing 16:0 were barely detectible in untreated WT plants (Fig. 3.3.D). This difference could be due to the growth conditions with a photoperiod of 12 hours per day, a light intensity of 600 $\mu\text{mol m}^{-2} \text{s}^{-1}$ and high temperatures of 28 °C during the day and 23 °C at night (Sui and Han, 2014), considering that the detection of MGDG-species containing saturated fatty acids was not a consequence of oxidative degradation of the samples. If different cultivation systems lead to large variations in lipid content and fatty acid profiles in the same plant line, then this could also lead to different starting conditions when the plants are exposed to a stress treatment, potentially leading to a variation in stress responses in terms of timing and mechanisms. The degree of uncertainty represented by differences in growth conditions poses a challenge when

interpreting results obtained by using different experimental setups or when comparing literature data.

4.6. Global changes in *fad* mutants, which might also influence photosynthetic parameters.

Changes of membrane lipids and their associated fatty acid profiles in *fad* mutants might not have direct effects on photosynthesis parameters and may also globally influence cellular membrane biology and lead to general changes in morphology and biochemical processes. Already five decades ago, cotton plants grown in the field and in the phyto-chamber were compared and it was found that photosynthetic performance depends on the thickness of the leaves (Patterson et al., 1977). Since *fad3* and *fad378* display an altered growth phenotype compared to WT plants, it is possible that these mutants also display different cell sizes in leaves, possibly resulting in changed leaf thickness (Fig. 6.3.; Fig. 6.5.). Increased leaf thickness by itself might reduce the number of photons received at the thylakoids and decrease the efficiency of photosynthesis or lead to a delay of NPQ component activation. However, leaf cross sections of *fad* mutants showed no difference in leaf thickness, or the shape of leaf cells compared to WT and this explanation could therefore be excluded (Fig. 6.10).

The pigment analysis of various *fad* mutants revealed changes in chlorophyll and carotenoid content, and depending on their increased or decreased amounts these effects on pigment contents might result in a changed functionality of light harvesting complexes, thereby indirectly influencing photosynthetic capacity (Fig. 3.10.). The *fad78* mutant plants displayed a reduced carotenoid content and might thus have a limited pool of XC pigments during salt stress for XC based NPQ. Moreover, the formation of ABA is based on xanthophylls as precursors (Fig. 3.10.), and ABA plays an important role in early salt stress responses by controlling the conductance of stomata and regulating the activation of acclimation processes (Kumar et al., 2018; Munns and Tester, 2008). The polyunsaturated fatty acid 18:3 serves as a precursor for the formation of JA, and it has been shown that the activity of antioxidants during salt stress conditions is dependent on JA (Abouelsaad and Renault, 2018). Therefore, plants with JA deficiency are susceptible to salt-induced oxidative stress. It is possible that one of the effects of short-term salt treatment on the *fad378* mutant line, which completely lacks trienoic fatty acids, is that salt-induced ROS

production damages the membrane lipids at an early stage of a perceived salt treatment (Fig. 3.6. B, C).

4.7. Adjustments for Imaging-PAM measurements and light-exposure experiments.

The use of Imaging-PAM to determine light-dependent effects on photosynthetic parameters provided a helpful impression of the diversity of effects on PSII efficiency in response to increasing light exposure under the influence of different salt concentrations or with different 18:3 proportions in $\omega 3$ -*fad* knockout mutants (Fig. 3.11.; 3.12.; 3.13.). It has previously been described that healthy and non-stressed *Arabidopsis* leaves will have a maximum quantum yield of PSII photochemistry (F_v/F_m) value of around 0.8 (Barbagallo et al., 2003; Hogewoning et al., 2012), a value not reached with WT plants used in this thesis. This disparity might indicate that the dark adaptation of 5 min used here, which was supposed to ensure that the primary quinone acceptor of PSII was maximally oxidized, has not been sufficient (section 2.2.7.). However, since F_v/F_m of the *fad378* mutant was significantly higher than the value of the WT mutant, it also appears possible that the wounding stress induced by cutting the leaves from the seedling, intended to increase the leaf area used and enhance the quality of the measurements, had a negative effect on PSII photobiochemistry that was not induced in the *fad378* mutant, which cannot produce JA or mount an effective wound response (Fig. 3.6. C; Fig. 3.12.; Fig. 6.7.). It could be also considered that a decrease in lipid unsaturation as severe as in plastids of *fad378* mutant and subsequent decrease in fluidity could reduce the efficient movement of electron carriers plastoquinone and plastocyanin between protein complexes of electron transport chain. The result would be an accumulation of electrons at the primary acceptor quinone of the PSII and a decrease of electron flow within the PSII. So far, however, no influence on plastoquinone diffusion by changes in the degree of saturation of the plastidial lipids could be detected. In previous studies, increasing the viscosity of pea (*Pisum sativum*) thylakoid membranes by saturating the lipids did not change the efficiency of cytochrome f reduction (Gombos et al., 1988). However, in the diatom *Phaeodactylum tricornutum* even the opposite was shown, and the redox state of plastoquinones can influence the degree of saturation of plastidial lipids by retrograde signaling (Cheong et al.,

2022). Evidently, there remain many open questions regarding the influence and control of membrane lipid unsaturation and thylakoid function.

Since salt stressed plants were grown for two-weeks on media containing salt, the exposure to $170 \mu\text{mol m}^{-2} \text{s}^{-1}$ of light during an 8 h photoperiod, might induce photoinhibition by damaging the PSII D1 protein, which decreases F_v/F_m and active PSII efficiency. This effect might falsify the PSII measurements, possibly resulting in elevated apparent NPQ values due to pre-injured D1 proteins during overlapping stresses (Fig. 3.13.; Baker, 2008). To ensure the recovery of D1, it has been proposed to keep plants for a longer period of one or two days in the dark (Baker, 2008). However, the use of such long dark adaptation periods to prepare for optimal capacity measurements of PSII photochemistry might in turn induce senescence and enhance jasmonate production (Keech et al., 2007; Seltmann et al., 2010), thereby abolishing any positive effect.

The settings used here for the light treatments were chosen to allow to analyze the performance of PSII photochemistry from 0-1200 PAR, and when utilization of electrons for photochemistry reached its limit then measurements of NPQ values gave insights into the heat dissipation of excess electrons (Fig. 3.12.; Fig. 3.13.). For each light intensity analyzed, plants were exposed for only 30 s, which is sufficient to analyze photosynthetic performance, but the resulting NPQ values gave only a glimpse into the dimension of consequences which salt or altered proportion of 18:3 can have on photoprotective energy dissipation (Fig. 3.12.; Fig. 3.13.; section 2.2.7.). The photoprotective mechanisms to dissipate excessive electrons are induced at different time scales, but the NPQ as determined by the PAM represents an overlap of these instances, depending on the duration plants are exposed to high light intensities. Since in this work the plant leaves were exposed for only 30 s at each light intensity, it is more likely that the NPQ values mainly indicate q_E , whose main contribution resulted from the activation of PsbS by lowering the pH in the thylakoid lumen (section 2.2.7.). PsbS mediates reorganization of PSII-LHCII supercomplex by binding to the light harvesting complex binding proteins (Lhcb) 1 and 3, and this is responsible for the initial dissipation of energy within 1 min or less of exposure (Sylak-Glassman et al., 2014). It is assumed that the conversion of V_x to Z_x is necessary for q_E to reach its maximum, and that an increased Z_x content in antenna proteins mediates the PsbS connection and thus causes further rearrangements of the protein complexes. When plants are exposed to high light intensities for long periods of time, Z_x accumulates and operates as an independent NPQ component, termed

qZ (Nilkens et al., 2010). The NPQ values shown in Figure 3.12. are more likely to be caused by qE, which would indicate that compared to WT, this mechanism is also inhibited in *fad3* mutants. The Vx content in the *fad3* mutant remained almost unchanged compared to WT after exposure to 1200 PAR, but the experiments with isolated thylakoids proved that VDE is functional in *fad3*, showing similar DES to WT (Fig. 3.14.). This observation implies that either the mechanism of Vx conversion is impaired in *fad3* mutants, or VDE activity has not yet been fully activated (Fig. 3.14., Fig. 3.15.). The comparison of the de-epoxidation state in WT leaves and in isolated thylakoids showed that only a small fraction of Vx was converted when exposed to 1200 PAR, clearly indicating that a 30 s exposure is not sufficient to exhaustively analyze NPQ and its components (Fig. 3.14., Fig. 3.15.). Reliable information on the proportion of NPQ components in the *fad* mutants would be possible by analyzing the NPQ component-specific relaxation times after exposing the leaves to high light conditions for a longer period, possibly as long as 30 minutes. Future experiments will be geared towards elucidating the effects of the *fad3* mutation, which affects an ER-resident protein, on photoprotection and NPQ in thylakoids in more detail. Regardless of the particular effects on NPQ, the key observation remains that altered membrane lipid unsaturation in the ER is accompanied by an increased abundance in plastidial MGDG and by a functional effect on photoprotection in thylakoids. As polyunsaturated MGDG is required for the function of the photosynthetic machinery and for protein complexes involved in photoprotection by forming inverted hexagonal lipid phases that are essential for the function of thylakoids, the postulated mobilization of MGDG to supply polyunsaturated fatty acids to extraplastidial membranes upon salt treatment might well have an impact on thylakoid function.

4.8. Phenotypes of stacked *fad* mutants suggests an influence of trans-organelar lipid exchange on plant performance.

The comparison of different *fad* mutants in this thesis provides potentially interesting insights into the global effects of how lipid intermediates are exchanged between the plastid and the ER. The notion of mutual substitution of defects in plastidial or ER-based 18:3 formation is not new, and it is well known that *fad3* mutants contain 18:3 in extraplastidial membrane lipids that has

been formed in the plastids (Browse et al., 1993). Reciprocally, to a lesser extent, *fad78* mutants contain 18:3 in plastidial lipids that was imported from the ER (McConn et al., 1994), highlighting the importance of trans-organellar mobility of lipid intermediates. The importance of these exchange processes becomes obvious even at the level of macroscopic phenotypes. Surprisingly, neither the NASC (Nottingham Arabidopsis Stock Centre) website nor the authors of the original report (James and Dooner, 1991; Browse et al., 1993) have described an obvious growth phenotype for the *fad3* mutant. While the cultivation conditions may influence the manifestation of a growth defect, as discussed in section 4.5., in experiments performed in this thesis, the *fad3* mutant displayed strongly delayed development, shorter roots and short bushy inflorescences when grown on soil under short-day conditions (Fig 6.5.; Fig. 6.1.; Fig 6.8.). The *fad78* double mutant displays normal inflorescence growth but shows an altered leaf morphology (Fig. 6.4.; Data not shown). Interestingly, the *fad378* triple mutant, generated by crossing the *fad3* and *fad78* lines, does not display any growth retardation and is in fact faster in development, has longer roots and similar inflorescence growth to WT (Fig. 6.5.; Data not shown). This enhanced growth of the *fad378* plants can be explained by their inability to form JA, a phytohormone inhibiting growth, due to the absence of ω -3 fatty acids (Fig. 3.18.; Fig. 6.3.). The growth phenotype of the *fad* triple mutant resembles that of other lines with JA deficiency, such as the line of *allene oxide synthase* (*aos*) mutant or line of *13-lipoxygenase 3/4* double mutant, which are defective in early steps of JA production in the plastid (Park et al., 2002; Caldelari et al., 2011). With regard to the growth retardation of the *fad3* mutant, it was hypothesized that the increased abundance of polyunsaturated MGDG in these plants might have supported enhanced biosynthesis of JA, thus accounting for the growth inhibition. In a study analyzing the Arabidopsis *dgd1* mutant, which results in reduced biosynthesis of DGDG and subsequent accumulation of MGDG (Lin et al., 2016), the severe growth phenotype of *dgd1* mutant may be amplified by a combination of reduced DGDG, which decreases photosynthesis performance, and an oversupply of MGDG causing higher production of JA. The expression of phospholipase A (PLA-I γ 3) might additionally be enhanced, which has a high affinity to MGDG and might be required for generating a basal level of JA in nonwounded conditions. Based on the similar increase of MGDG level in *dgd1* and *fad3* and the similar growth phenotypes of these mutants, it was hypothesized that JA is possibly also overproduced in *fad3*. However, both the levels of JA or various precursors and the

induction of JA-dependent transcripts was unchanged in *fad3* mutants compared to WT controls (Fig. 3.17.C; Fig. 3.18.; Tab. 6.12.; Tab. 6.13.), indicating that no enhanced production of JA occurred. It has been reported that the *JAZ10* expression 1 h of wounding in leaves is lower compared to other JAZ genes, such as *JAZ1*, *JAZ2* and *JAZ9*, which was in line with the levels measured for this work (Fig. 3.17. B; Chung et al., 2008). In contrast after 1 h of wounding, *JAZ10* transcript levels were similar in roots of WT controls, the *fad3* mutant and the complemented line *FAD3-4c*. This pattern indicates that wounding at the root was successful (Fig. 3.17. A). If the *fad3* mutant overproduces JA, it would be expected that JA-responsive genes would also be upregulated under normal/ unwounded conditions, however, the MGDG levels in roots of the *fad3* mutant was not measured, and as MGDG is not strongly produced in roots it remains uncertain whether the roots also have a higher MGDG level. To clarify directly whether enhanced MGDG content in *fad3* mutants resulted in higher JA level various oxylipin levels were measured and the oxylipin levels in the *fad3* mutant did not differ from those in WT controls (Fig. 3.6. C; Fig. 3.18.).

Overall, while the effects of the *fad3* mutation on plastidial MGDG levels are clear, the physiological consequences of the increased MGDG levels remain unclear. When studying the *dgd1* mutant, Lin et al. (2016) discussed that the overproduction of JA caused by an increased content of MGDG might be connected with the MGDG/DGDG ratio, as overexpression of rice *OsMGD* in tobacco plants was not detrimental to growth result due to a higher JA level (Wang et al., 2014), as might have been expected. In contrast to the *dgd1* mutant, where the MGDG/DGDG ratio increased due to blocked DGDG production, the MGDG/DGDG ratio remained the same in tobacco plants with overexpressed *OsMGD*, which could also be true for the *fad3* mutant line. However, this question remains unanswered, as the DGDG level in the *fad3* mutant was not measured in this work. It is possible that MGDG might be differentially available for certain physiological functions, such as its structural role in protein-dense thylakoid membranes or as a precursor for jasmonic acid production. Such differential availability might be related to its sub-organellar location, for instance in the grana stacks or in the envelope membranes. However, there is currently no technical approach to visualize such different populations of MGDG. In the context of MGDG increases occurring in the plastid to support the formation of lipid intermediates

for export to the ER, as it might occur upon salt treatment or in the *fad3* mutant, it remains to be seen whether this MGDG represents a dedicated pool of lipids with this particular function.

5. References

- Abouelsaad, I., and Renault, S.** (2018). Enhanced oxidative stress in the jasmonic acid-deficient tomato mutant *def-1* exposed to NaCl stress. *Journal of plant physiology* **226**: 136–144.
- Allakhverdiev, S.I., Kinoshita, M., Inaba, M., Suzuki, I., and Murata, N.** (2001). Unsaturated fatty acids in membrane lipids protect the photosynthetic machinery against salt-induced damage in *Synechococcus*. *Plant physiology* **125** (4): 1842–1853.
- Allu, A.D., Soja, A.M., Wu, A., Szymanski, J., and Balazadeh, S.** (2014). Salt stress and senescence: identification of cross-talk regulatory components. *Journal of experimental botany* **65** (14): 3993–4008.
- Andersson, M.X., Goksör, M., and Sandelius, A.S.** (2007). Optical manipulation reveals strong attracting forces at membrane contact sites between endoplasmic reticulum and chloroplasts. *The Journal of biological chemistry* **282** (2): 1170–1174.
- Athenstaedt, K., and Daum, G.** (1999). Phosphatidic acid, a key intermediate in lipid metabolism. *European journal of biochemistry* **266** (1): 1–16.
- Baker, N.R.** (2008). Chlorophyll fluorescence: a probe of photosynthesis in vivo. *Annual review of plant biology* **59**: 89–113.
- Barajas-Lopez, J.d.D., Tiwari, A., Zarza, X., Shaw, M.W., Pascual, J.S., Punkkinen, M., Bakowska, J.C., Munnik, T., and Fujii, H.** (2021). EARLY RESPONSE TO DEHYDRATION 7 Remodels Cell Membrane Lipid Composition during Cold Stress in *Arabidopsis*. *Plant & cell physiology* **62** (1): 80–91.
- Barbagallo, R.P., Oxborough, K., Pallett, K.E., and Baker, N.R.** (2003). Rapid, noninvasive screening for perturbations of metabolism and plant growth using chlorophyll fluorescence imaging. *Plant physiology* **132** (2): 485–493.
- Barelli, H., and Antony, B.** (2016). Lipid unsaturation and organelle dynamics. *Current opinion in cell biology* **41**: 25–32.
- Basu Ball, W., Neff, J.K., and Gohil, V.M.** (2018). The role of nonbilayer phospholipids in mitochondrial structure and function. *FEBS letters* **592** (8): 1273–1290.
- Bates, P.D., Ohlrogge, J.B., and Pollard, M.** (2007). Incorporation of newly synthesized fatty acids into cytosolic glycerolipids in pea leaves occurs via acyl editing. *The Journal of biological chemistry* **282** (43): 31206–31216.
- Bauwe, H., Hagemann, M., and Fernie, A.R.** (2010). Photorespiration: players, partners and origin. *Trends in plant science* **15** (6): 330–336.
- Biswal, B., Krupinska, K., and Biswal, U.C.** (2013). *Plastid Development in Leaves during Growth and Senescence* (Dordrecht: Springer Netherlands).

- Bobik, K., and Burch-Smith, T.M.** (2015). Chloroplast signaling within, between and beyond cells. *Frontiers in plant science* **6**: 781.
- Botella, C., Sautron, E., Boudiere, L., Michaud, M., Dubots, E., Yamaryo-Botté, Y., Albrieux, C., Marechal, E., Block, M.A., and Jouhet, J.** (2016). ALA10, a Phospholipid Flippase, Controls FAD2/FAD3 Desaturation of Phosphatidylcholine in the ER and Affects Chloroplast Lipid Composition in *Arabidopsis thaliana*. *Plant physiology* **170** (3): 1300–1314.
- Browse, J., Kunst, L., Anderson, S., Hugly, S., and Somerville, C.** (1989). A mutant of *Arabidopsis* deficient in the chloroplast 16:1/18:1 desaturase. *Plant physiology* **90** (2): 522–529.
- Browse, J., McConn, M., James, D., and Miquel, M.** (1993). Mutants of *Arabidopsis* deficient in the synthesis of alpha-linolenate. Biochemical and genetic characterization of the endoplasmic reticulum linoleoyl desaturase. *The Journal of biological chemistry* **268** (22): 16345–16351.
- Browse, J., and Somerville, C.** (1991). Glycerolipid Synthesis: Biochemistry and Regulation. *Annu. Rev. Plant. Physiol. Plant. Mol. Biol.* **42** (1): 467–506.
- Caldelari, D., Wang, G., Farmer, E.E., and Dong, X.** (2011). *Arabidopsis* lox3 lox4 double mutants are male sterile and defective in global proliferative arrest. *Plant molecular biology* **75** (1-2): 25–33.
- Caplan, J.L., Kumar, A.S., Park, E., Padmanabhan, M.S., Hoban, K., Modla, S., Czymmek, K., and Dinesh-Kumar, S.P.** (2015). Chloroplast Stromules Function during Innate Immunity. *Developmental cell* **34** (1): 45–57.
- Casazza, A.P., Tarantino, D., and Soave, C.** (2001). Preparation and functional characterization of thylakoids from *Arabidopsis thaliana*. *Photosynthesis research* **68** (2): 175–180.
- Chapman, D.J., De-Felice, J., and Barber, J.** (1983). Growth temperature effects on thylakoid membrane lipid and protein content of pea chloroplasts. *Plant physiology* **72** (1): 225–228.
- Cheong, K.Y., Jouhet, J., Maréchal, E., and Falkowski, P.G.** (2022). The redox state of the plastoquinone (PQ) pool is connected to thylakoid lipid saturation in a marine diatom. *Photosynthesis research* **153** (1-2): 71–82.
- Chung, H.S., Koo, A.J.K., Gao, X., Jayanty, S., Thines, B., Jones, A.D., and Howe, G.A.** (2008). Regulation and function of *Arabidopsis* JASMONATE ZIM-domain genes in response to wounding and herbivory. *Plant physiology* **146** (3): 952–964.
- Dar, A.A., Choudhury, A.R., Kancharla, P.K., and Arumugam, N.** (2017). The FAD2 Gene in Plants: Occurrence, Regulation, and Role. *Frontiers in plant science* **8**: 1789.
- Dhar, N., Caruana, J., Erdem, I., Subbarao, K.V., Klosterman, S.J., and Raina, R.** (2020). The *Arabidopsis* SENESCENCE-ASSOCIATED GENE 13 Regulates Dark-Induced Senescence and Plays Contrasting Roles in Defense Against Bacterial and Fungal Pathogens. *Molecular plant-microbe interactions MPMI* **33** (5): 754–766.

- Dutilleul, C., Driscoll, S., Cornic, G., Paepe, R. de, Foyer, C.H., and Noctor, G.** (2003). Functional mitochondrial complex I is required by tobacco leaves for optimal photosynthetic performance in photorespiratory conditions and during transients. *Plant physiology* **131** (1): 264–275.
- Fischer-Kilbienski, I., Miao, Y., Roitsch, T., Zschiesche, W., Humbeck, K., and Krupinska, K.** (2010). Nuclear targeted AtS40 modulates senescence associated gene expression in *Arabidopsis thaliana* during natural development and in darkness. *Plant molecular biology* **73** (4-5): 379–390.
- Fujii, S., Kobayashi, K., Nakamura, Y., and Wada, H.** (2014). Inducible Knockdown of MONOGALACTOSYLDIACYLGLYCEROL SYNTHASE1 Reveals Roles of Galactolipids in Organelle Differentiation in *Arabidopsis* Cotyledons. *Plant physiology* **166** (3): 1436–1449.
- Garab, G., and Mustárdy, L.** (2000). Role of LHCII-containing macrodomains in the structure, function and dynamics of grana. *Functional Plant Biol.* **27** (7): 723.
- Garab, G., Ughy, B., and Goss, R.** (2016). Role of MGDG and Non-bilayer Lipid Phases in the Structure and Dynamics of Chloroplast Thylakoid Membranes. *Sub-cellular biochemistry* **86**: 127–157.
- Gerth, K., Lin, F., Menzel, W., Krishnamoorthy, P., Stenzel, I., Heilmann, M., and Heilmann, I.** (2017). Guilt by Association: A Phenotype-Based View of the Plant Phosphoinositide Network. *Annual review of plant biology* **68**: 349–374.
- Gigon, A., Matos, A.-R., Laffray, D., Zuily-Fodil, Y., and Pham-Thi, A.-T.** (2004). Effect of drought stress on lipid metabolism in the leaves of *Arabidopsis thaliana* (ecotype Columbia). *Annals of botany* **94** (3): 345–351.
- Gombos, Z., Barabás, K., Joó, F., and Vigh, L.** (1988). Lipid Saturation Induced Microviscosity Increase Has No Effect on the Reducibility of Flash-Oxidized Cytochrome f in Pea Thylakoids. *Plant physiology* **86** (2): 335–337.
- Gomi, K.** (2020). Jasmonic Acid: An Essential Plant Hormone. *International journal of molecular sciences* **21** (4).
- Goss, R.** (2003). Substrate specificity of the violaxanthin de-epoxidase of the primitive green alga *Mantoniella squamata* (Prasinophyceae). *Planta* **217** (5): 801–812.
- Greer, M.S., Cai, Y., Gidda, S.K., Esnay, N., Kretzschmar, F.K., Seay, D., McClinchie, E., Ischebeck, T., Mullen, R.T., Dyer, J.M., and Chapman, K.D.** (2020). SEIPIN Isoforms Interact with the Membrane-Tethering Protein VAP27-1 for Lipid Droplet Formation. *The Plant cell* **32** (9): 2932–2950.
- Gui, J., Zheng, S., Liu, C., Shen, J., Li, J., and Li, L.** (2016). OsREM4.1 Interacts with OsSERK1 to Coordinate the Interlinking between Abscisic Acid and Brassinosteroid Signaling in Rice. *Developmental cell* **38** (2): 201–213.

- Guo, Q., Liu, L., and Barkla, B.J.** (2019). Membrane Lipid Remodeling in Response to Salinity. *International journal of molecular sciences* **20** (17).
- Hallin, E.I., Hasan, M., Guo, K., and Åkerlund, H.-E.** (2016). Molecular studies on structural changes and oligomerisation of violaxanthin de-epoxidase associated with the pH-dependent activation. *Photosynthesis research* **129** (1): 29–41.
- Hanada, K., Kumagai, K., Yasuda, S., Miura, Y., Kawano, M., Fukasawa, M., and Nishijima, M.** (2003). Molecular machinery for non-vesicular trafficking of ceramide. *Nature* **426** (6968): 803–809.
- Harayama, T., and Riezman, H.** (2018). Understanding the diversity of membrane lipid composition. *Nature reviews. Molecular cell biology* **19** (5): 281–296.
- Härtel, H., Dormann, P., and Benning, C.** (2000). DGD1-independent biosynthesis of extraplastidic galactolipids after phosphate deprivation in Arabidopsis. *Proceedings of the National Academy of Sciences of the United States of America* **97** (19): 10649–10654.
- Hasanuzzaman, M., Nahar, K., Fujita, M., Oku, H., and Islam, T.M., eds** (2019). Approaches for enhancing abiotic stress tolerance in plants (Boca Raton, London, New York: CRC Press).
- He, M., and Ding, N.-Z.** (2020). Plant Unsaturated Fatty Acids: Multiple Roles in Stress Response. *Frontiers in plant science* **11**: 562785.
- Heldt, H.W., and Piechulla, B.** (2015). *Pflanzenbiochemie* (Berlin, Heidelberg: Springer Berlin Heidelberg).
- Herrfurth, C., and Feussner, I.** (2020). Quantitative Jasmonate Profiling Using a High-Throughput UPLC-NanoESI-MS/MS Method. *Methods in molecular biology* (Clifton, N.J.) **2085**: 169–187.
- Herrfurth, C., Liu, Y.-T., and Feussner, I.** (2021). Targeted Analysis of the Plant Lipidome by UPLC-NanoESI-MS/MS. *Methods in molecular biology* (Clifton, N.J.) **2295**: 135–155.
- Hogewoning, S.W., Wientjes, E., Douwstra, P., Trouwborst, G., van Ieperen, W., Croce, R., and Harbinson, J.** (2012). Photosynthetic quantum yield dynamics: from photosystems to leaves. *The Plant cell* **24** (5): 1921–1935.
- Holt, N.E., Fleming, G.R., and Niyogi, K.K.** (2004). Toward an understanding of the mechanism of nonphotochemical quenching in green plants. *Biochemistry* **43** (26): 8281–8289.
- Hölzl, G., and Dörmann, P.** (2019). Chloroplast Lipids and Their Biosynthesis. *Annual review of plant biology* **70**: 51–81.
- Hu, J., Baker, A., Bartel, B., Linka, N., Mullen, R.T., Reumann, S., and Zolman, B.K.** (2012). Plant peroxisomes: biogenesis and function. *The Plant cell* **24** (6): 2279–2303.
- Hurlock, A.K., Roston, R.L., Wang, K., and Benning, C.** (2014). Lipid trafficking in plant cells. *Traffic* (Copenhagen, Denmark) **15** (9): 915–932.
- Iba, K., Gibson, S., Nishiuchi, T., Fuse, T., Nishimura, M., Arondel, V., Hugly, S., and Somerville, C.** (1993). A gene encoding a chloroplast omega-3 fatty acid desaturase complements

alterations in fatty acid desaturation and chloroplast copy number of the *fad7* mutant of *Arabidopsis thaliana*. *The Journal of biological chemistry* **268** (32): 24099–24105.

Ikon, N., and Ryan, R.O. (2017). Cardiolipin and mitochondrial cristae organization. *Biochimica et Biophysica Acta (BBA) - Biomembranes* **1859** (6): 1156–1163.

Im, Y.J., Han, O., Chung, G.C., and Cho, B.H. (2002). Antisense expression of an *Arabidopsis* omega-3 fatty acid desaturase gene reduces salt/drought tolerance in transgenic tobacco plants. *Molecules and cells* **13** (2): 264–271.

Isayenkov, S.V., and Maathuis, F.J.M. (2019). Plant Salinity Stress: Many Unanswered Questions Remain. *Frontiers in plant science* **10**: 80.

Ischebeck, T., Werner, S., Krishnamoorthy, P., Lerche, J., Meijón, M., Stenzel, I., Löffke, C., Wiessner, T., Im, Y.J., Perera, I.Y., Iven, T., Feussner, I., Busch, W., Boss, W.F., Teichmann, T., Hause, B., Persson, S., and Heilmann, I. (2013). Phosphatidylinositol 4,5-bisphosphate influences PIN polarization by controlling clathrin-mediated membrane trafficking in *Arabidopsis*. *The Plant cell* **25** (12): 4894–4911.

Jaillais, Y., and Ott, T. (2020). The Nanoscale Organization of the Plasma Membrane and Its Importance in Signaling: A Proteolipid Perspective. *Plant physiology* **182** (4): 1682–1696.

James, D.W., and Dooner, H.K. (1990). Isolation of EMS-induced mutants in *Arabidopsis* altered in seed fatty acid composition. *TAG. Theoretical and applied genetics. Theoretische und angewandte Genetik* **80** (2): 241–245.

James, D.W., and Dooner, H.K. (1991). Novel seed lipid phenotypes in combinations of mutants altered in fatty acid biosynthesis in *Arabidopsis*. *TAG. Theoretical and applied genetics. Theoretische und angewandte Genetik* **82** (4): 409–412.

Jarvis, P., and López-Juez, E. (2013). Biogenesis and homeostasis of chloroplasts and other plastids. *Nature reviews. Molecular cell biology* **14** (12): 787–802.

Jehanzeb, M., Zheng, X., and Miao, Y. (2017). The Role of the S40 Gene Family in Leaf Senescence. *International journal of molecular sciences* **18** (10).

Kaiser, E., Correa Galvis, V., and Armbruster, U. (2019). Efficient photosynthesis in dynamic light environments: a chloroplast's perspective. *The Biochemical journal* **476** (19): 2725–2741.

Kalisch, B., Dörmann, P., and Hölzl, G. (2016). DGDG and Glycolipids in Plants and Algae. *Sub-cellular biochemistry* **86**: 51–83.

Kay, J.G., and Grinstein, S. (2013). Phosphatidylserine-mediated cellular signaling. *Advances in experimental medicine and biology* **991**: 177–193.

Keech, O., Pesquet, E., Ahad, A., Askne, A., Nordvall, D., Vodnala, S.M., Tuominen, H., Hurry, V., Dizengremel, P., and Gardeström, P. (2007). The different fates of mitochondria and chloroplasts during dark-induced senescence in *Arabidopsis* leaves. *Plant, cell & environment* **30** (12): 1523–1534.

- Kirchhoff, H.** (2014). Structural changes of the thylakoid membrane network induced by high light stress in plant chloroplasts. *Philosophical transactions of the Royal Society of London. Series B, Biological sciences* **369** (1640): 20130225.
- Kirchhoff, H., Mukherjee, U., and Galla, H.-J.** (2002). Molecular architecture of the thylakoid membrane: lipid diffusion space for plastoquinone. *Biochemistry* **41** (15): 4872–4882.
- Klimecka, M., and Muszyńska, G.** (2007). Structure and functions of plant calcium-dependent protein kinases. *Acta biochimica Polonica* **54** (2): 219–233.
- Klińska, S., Kędzierska, S., Jasieniecka-Gazarkiewicz, K., and Banaś, A.** (2021). In Vitro Growth Conditions Boost Plant Lipid Remodelling and Influence Their Composition. *Cells* **10** (9).
- Kobayashi, K.** (2016). Role of membrane glycerolipids in photosynthesis, thylakoid biogenesis and chloroplast development. *Journal of plant research* **129** (4): 565–580.
- Kobayashi, K., Nakamura, Y., and Ohta, H.** (2009). Type A and type B monogalactosyldiacylglycerol synthases are spatially and functionally separated in the plastids of higher plants. *Plant physiology and biochemistry PPB* **47** (6): 518–525.
- Koiwai, A., Matsuzaki, T., Suzuki, F., and Kawashima, N.** (1981). Changes in Total and Polar Lipids and Their Fatty Acid Composition in Tobacco Leaves during Growth and Senescence. *Plant and Cell Physiology*.
- König, S., Ischebeck, T., Lerche, J., Stenzel, I., and Heilmann, I.** (2008). Salt-stress-induced association of phosphatidylinositol 4,5-bisphosphate with clathrin-coated vesicles in plants. *The Biochemical journal* **415** (3): 387–399.
- König, S., Mosblech, A., and Heilmann, I.** (2007). Stress-inducible and constitutive phosphoinositide pools have distinctive fatty acid patterns in *Arabidopsis thaliana*. *FASEB journal official publication of the Federation of American Societies for Experimental Biology* **21** (9): 1958–1967.
- Kraay, G.W., Zapata, M., and Veldhuis, M.J.W.** (1992). SEPARATION OF CHLOROPHYLLS c1c2, AND c3 OF MARINE PHYTOPLANKTON BY REVERSED-PHASE-C18-HIGH-PERFORMANCE LIQUID CHROMATOGRAPHY1. *J Phycol* **28** (5): 708–712.
- Kumar, V., Wani, S.H., Suprasanna, P., and Tran, L.-S.P.** (2018). *Salinity Responses and Tolerance in Plants*, Volume 1 (Cham: Springer International Publishing).
- Kunst, L., Browse, J., and Somerville, C.** (1988). Altered regulation of lipid biosynthesis in a mutant of *Arabidopsis* deficient in chloroplast glycerol-3-phosphate acyltransferase activity. *Proceedings of the National Academy of Sciences of the United States of America* **85** (12): 4143–4147.
- Kunst, L., Browse, J., and Somerville, C.** (1989). A mutant of *Arabidopsis* deficient in desaturation of palmitic Acid in leaf lipids. *Plant physiology* **90** (3): 943–947.

- LaBrant, E., Barnes, A.C., and Roston, R.L.** (2018). Lipid transport required to make lipids of photosynthetic membranes. *Photosynthesis research* **138** (3): 345–360.
- Launhardt, L., Matzner, M., Heilmann, M., and Heilmann, I.** (2021). Analysis of Phosphoinositides from Complex Plant Samples by Solid-Phase Adsorption Chromatography and Subsequent Quantification via Thin-Layer and Gas Chromatography. *Methods in molecular biology* (Clifton, N.J.) **2295**: 379–389.
- Lee, E., Vanneste, S., Pérez-Sancho, J., Benitez-Fuente, F., Strelau, M., Macho, A.P., Botella, M.A., Friml, J., and Rosado, A.** (2019). Ionic stress enhances ER-PM connectivity via phosphoinositide-associated SYT1 contact site expansion in Arabidopsis. *Proceedings of the National Academy of Sciences of the United States of America* **116** (4): 1420–1429.
- Leshem, Y., Seri, L., and Levine, A.** (2007). Induction of phosphatidylinositol 3-kinase-mediated endocytosis by salt stress leads to intracellular production of reactive oxygen species and salt tolerance. *The Plant journal for cell and molecular biology* **51** (2): 185–197.
- Li, N., Gügel, I.L., Giavalisco, P., Zeisler, V., Schreiber, L., Soll, J., and Philippar, K.** (2015). FAX1, a novel membrane protein mediating plastid fatty acid export. *PLoS biology* **13** (2): e1002053.
- Li, T., Zhang, Y., Liu, H., Wu, Y., Li, W., and Zhang, H.** (2010). Stable expression of Arabidopsis vacuolar Na⁺/H⁺ antiporter gene AtNHX1, and salt tolerance in transgenic soybean for over six generations. *Chin. Sci. Bull.* **55** (12): 1127–1134.
- Li, X.P., Björkman, O., Shih, C., Grossman, A.R., Rosenquist, M., Jansson, S., and Niyogi, K.K.** (2000). A pigment-binding protein essential for regulation of photosynthetic light harvesting. *Nature* **403** (6768): 391–395.
- Li-Beisson, Y., Shorrosh, B., Beisson, F., Andersson, M.X., Arondel, V., Bates, P.D., Baud, S., Bird, D., Debono, A., Durrett, T.P., Franke, R.B., Graham, I.A., Katayama, K., Kelly, A.A., Larson, T., Markham, J.E., Miquel, M., Molina, I., Nishida, I., Rowland, O., Samuels, L., Schmid, K.M., Wada, H., Welti, R., Xu, C., Zallot, R., and Ohlrogge, J.** (2010). Acyl-lipid metabolism. *The arabidopsis book* **8**: e0133.
- Lichtenthaler, H.K., and Buschmann, C.** (2001). Chlorophylls and Carotenoids: Measurement and Characterization by UV-VIS Spectroscopy. *Current Protocols in Food Analytical Chemistry* **1** (1): F4.3.1-F4.3.8.
- Lin, Y.-T., Chen, L.-J., Herrfurth, C., Feussner, I., and Li, H.-M.** (2016). Reduced Biosynthesis of Digalactosyldiacylglycerol, a Major Chloroplast Membrane Lipid, Leads to Oxylipin Overproduction and Phloem Cap Lignification in Arabidopsis. *The Plant cell* **28** (1): 219–232.
- Liu, L., and Li, J.** (2019). Communications Between the Endoplasmic Reticulum and Other Organelles During Abiotic Stress Response in Plants. *Frontiers in plant science* **10**: 749.
- Liu, Q., Kasuga, M., Sakuma, Y., Abe, H., Miura, S., Yamaguchi-Shinozaki, K., and Shinozaki, K.** (1998). Two transcription factors, DREB1 and DREB2, with an EREBP/AP2 DNA binding domain

- separate two cellular signal transduction pathways in drought- and low-temperature-responsive gene expression, respectively, in *Arabidopsis*. *The Plant cell* **10** (8): 1391–1406.
- Lohr, M.** (2001). Beziehungen zwischen den Xanthophyllzyklen und der Biosynthese von Lichtsammelxanthophyllen in Chlorophyll a/c-haltigen Algen.
- Marty, F.** (1999). Plant vacuoles. *The Plant cell* **11** (4): 587–600.
- Matos, A.R., Hourton-Cabassa, C., Çiçek, D., Rezé, N., Arrabaça, J.D., Zachowski, A., and Moreau, F.** (2007). Alternative oxidase involvement in cold stress response of *Arabidopsis thaliana* fad2 and FAD3+ cell suspensions altered in membrane lipid composition. *Plant & cell physiology* **48** (6): 856–865.
- Matzner, M.** (2019). Ein Testsystem für Salz-induzierte Membranprozesse bei *Arabidopsis thaliana* unter Verwendung Agar-haltiger Festmedien. Master thesis (Halle).
- Maxwell, K., and Johnson, G.N.** (2000). Chlorophyll fluorescence--a practical guide. *Journal of experimental botany* **51** (345): 659–668.
- McConn, M., and Browse, J.** (1996). The Critical Requirement for Linolenic Acid Is Pollen Development, Not Photosynthesis, in an *Arabidopsis* Mutant. *The Plant cell* **8** (3): 403–416.
- McConn, M., and Browse, J.** (1998). Polyunsaturated membranes are required for photosynthetic competence in a mutant of *Arabidopsis*. *The Plant journal for cell and molecular biology* **15** (4): 521–530.
- McConn, M., Creelman, R.A., Bell, E., Mullet, J.E., and Browse, J.** (1997). Jasmonate is essential for insect defense in *Arabidopsis*. *Proceedings of the National Academy of Sciences of the United States of America* **94** (10): 5473–5477.
- McConn, M., Hugly, S., Browse, J., and Somerville, C.** (1994). A Mutation at the fad8 Locus of *Arabidopsis* Identifies a Second Chloroplast omega-3 Desaturase. *Plant physiology* **106** (4): 1609–1614.
- McCourt, P., Kunst, L., Browse, J., and Somerville, C.R.** (1987). The effects of reduced amounts of lipid unsaturation on chloroplast ultrastructure and photosynthesis in a mutant of *Arabidopsis*. *Plant physiology* **84** (2): 353–360.
- McDonald, C., Jovanovic, G., Wallace, B.A., Ces, O., and Buck, M.** (2017). Structure and function of PspA and Vipp1 N-terminal peptides: Insights into the membrane stress sensing and mitigation. *Biochimica et Biophysica Acta (BBA) - Biomembranes* **1859** (1): 28–39.
- Meng, X., Zhou, J., and Sui, N.** (2018). Mechanisms of Salt Tolerance in Halophytes: Current Understanding and Recent Advances. *Open life sciences* **13**: 149–154.
- Michaud, M., and Jouhet, J.** (2019). Lipid Trafficking at Membrane Contact Sites During Plant Development and Stress Response. *Frontiers in plant science* **10**: 2.

- Miquel, M., and Browse, J.** (1992). Arabidopsis mutants deficient in polyunsaturated fatty acid synthesis. Biochemical and genetic characterization of a plant oleoyl-phosphatidylcholine desaturase. *The Journal of biological chemistry* **267** (3): 1502–1509.
- Miquel, M., James, D., Dooner, H., and Browse, J.** (1993). Arabidopsis requires polyunsaturated lipids for low-temperature survival. *Proceedings of the National Academy of Sciences of the United States of America* **90** (13): 6208–6212.
- Mongrand, S., Cassagne, C., and Bessoule, J.J.** (2000). Import of lyso-phosphatidylcholine into chloroplasts likely at the origin of eukaryotic plastidial lipids. *Plant physiology* **122** (3): 845–852.
- Morimoto, K., Mizoi, J., Qin, F., Kim, J.-S., Sato, H., Osakabe, Y., Shinozaki, K., and Yamaguchi-Shinozaki, K.** (2013). Stabilization of Arabidopsis DREB2A is required but not sufficient for the induction of target genes under conditions of stress. *PloS one* **8** (12): e80457.
- Mosblech, A., König, S., Stenzel, I., Grzeganeck, P., Feussner, I., and Heilmann, I.** (2008). Phosphoinositide and inositolpolyphosphate signalling in defense responses of Arabidopsis thaliana challenged by mechanical wounding. *Molecular plant* **1** (2): 249–261.
- Mou, Z., Wang, X., Fu, Z., Dai, Y., Han, C., Ouyang, J., Bao, F., Hu, Y., and Li, J.** (2002). Silencing of phosphoethanolamine N-methyltransferase results in temperature-sensitive male sterility and salt hypersensitivity in Arabidopsis. *The Plant cell* **14** (9): 2031–2043.
- Msanne, J., Lin, J., Stone, J.M., and Awada, T.** (2011). Characterization of abiotic stress-responsive Arabidopsis thaliana RD29A and RD29B genes and evaluation of transgenes. *Planta* **234** (1): 97–107.
- Mueller, S.P., Unger, M., Guender, L., Fekete, A., and Mueller, M.J.** (2017). Phospholipid:Diacylglycerol Acyltransferase-Mediated Triacylglycerol Synthesis Augments Basal Thermotolerance. *Plant physiology* **175** (1): 486–497.
- Munns, R.** (2002). Comparative physiology of salt and water stress. *Plant, cell & environment* **25** (2): 239–250.
- Munns, R., and Tester, M.** (2008). Mechanisms of salinity tolerance. *Annual review of plant biology* **59**: 651–681.
- Nilkens, M., Kress, E., Lambrev, P., Miloslavina, Y., Müller, M., Holzwarth, A.R., and Jahns, P.** (2010). Identification of a slowly inducible zeaxanthin-dependent component of non-photochemical quenching of chlorophyll fluorescence generated under steady-state conditions in Arabidopsis. *Biochimica et biophysica acta* **1797** (4): 466–475.
- Niyogi, K.K., Grossman, A.R., and Björkman, O.** (1998). Arabidopsis mutants define a central role for the xanthophyll cycle in the regulation of photosynthetic energy conversion. *The Plant cell* **10** (7): 1121–1134.
- Omoto, E., Taniguchi, M., and Miyake, H.** (2012). Adaptation responses in C4 photosynthesis of maize under salinity. *Journal of plant physiology* **169** (5): 469–477.

- Park, J.-H., Halitschke, R., Kim, H.B., Baldwin, I.T., Feldmann, K.A., and Feyereisen, R.** (2002). A knock-out mutation in allene oxide synthase results in male sterility and defective wound signal transduction in *Arabidopsis* due to a block in jasmonic acid biosynthesis. *The Plant journal for cell and molecular biology* **31** (1): 1–12.
- Pastor-Cantizano, N., Bernat-Silvestre, C., Marcote, M.J., and Aniento, F.** (2018). Loss of *Arabidopsis* p24 function affects ERD2 trafficking and Golgi structure, and activates the unfolded protein response. *Journal of cell science* **131** (2).
- Patterson, D.T., Bunce, J.A., Alberte, R.S., and van Volkenburgh, E.** (1977). Photosynthesis in relation to leaf characteristics of cotton from controlled and field environments. *Plant Physiol.* **59** (3): 384–387.
- Perico, C., and Sparkes, I.** (2018). Plant organelle dynamics: cytoskeletal control and membrane contact sites. *The New phytologist* **220** (2): 381–394.
- Pfaffl, M.W.** (2001). A new mathematical model for relative quantification in real-time RT-PCR. *Nucleic acids research* **29** (9): e45.
- Pical, C., Westergren, T., Dove, S.K., Larsson, C., and Sommarin, M.** (1999). Salinity and hyperosmotic stress induce rapid increases in phosphatidylinositol 4,5-bisphosphate, diacylglycerol pyrophosphate, and phosphatidylcholine in *Arabidopsis thaliana* cells. *The Journal of biological chemistry* **274** (53): 38232–38240.
- Quartacci, M.F., Pinzino, C., Sgherri, C., and Navari-Izzo, F.** (1995). Lipid Composition and Protein Dynamics in Thylakoids of Two Wheat Cultivars Differently Sensitive to Drought. *Plant physiology* **108** (1): 191–197.
- Quick, W.P., and Stitt, M.** (1989). An examination of factors contributing to non-photochemical quenching of chlorophyll fluorescence in barley leaves. *Biochimica et Biophysica Acta (BBA) - Bioenergetics* **977** (3): 287–296.
- Ruijter, J.M., Ramakers, C., Hoogaars, W.M.H., Karlen, Y., Bakker, O., van den Hoff, M.J.B., and Moorman, A.F.M.** (2009). Amplification efficiency: linking baseline and bias in the analysis of quantitative PCR data. *Nucleic acids research* **37** (6): e45.
- Sacharz, J., Giovagnetti, V., Ungerer, P., Mastroianni, G., and Ruban, A.V.** (2017). The xanthophyll cycle affects reversible interactions between PsbS and light-harvesting complex II to control non-photochemical quenching. *Nature plants* **3**: 16225.
- Sade, N., Del Mar Rubio-Wilhelmi, M., Umnajkitikorn, K., and Blumwald, E.** (2018). Stress-induced senescence and plant tolerance to abiotic stress. *Journal of experimental botany* **69** (4): 845–853.
- Saheki, Y., and Camilli, P. de** (2017). Endoplasmic Reticulum-Plasma Membrane Contact Sites. *Annual review of biochemistry* **86**: 659–684.
- Sakamoto, W., Miyagishima, S.-Y., and Jarvis, P.** (2008). Chloroplast biogenesis: control of plastid development, protein import, division and inheritance. *The arabidopsis book* **6**: e0110.

- Savaldi-Goldstein, S., and Chory, J.** (2008). Growth coordination and the shoot epidermis. *Current opinion in plant biology* **11** (1): 42–48.
- Schaller, F., Schaller, A., and Stintzi, A.** (2004). Biosynthesis and Metabolism of Jasmonates. *J Plant Growth Regul* **23** (3): 179–199.
- Schapiro, A.L., Voigt, B., Jasik, J., Rosado, A., Lopez-Cobollo, R., Menzel, D., Salinas, J., Mancuso, S., Valpuesta, V., Baluska, F., and Botella, M.A.** (2008). Arabidopsis synaptotagmin 1 is required for the maintenance of plasma membrane integrity and cell viability. *The Plant cell* **20** (12): 3374–3388.
- Schindelin, J., Arganda-Carreras, I., Frise, E., Kaynig, V., Longair, M., Pietzsch, T., Preibisch, S., Rueden, C., Saalfeld, S., Schmid, B., Tinevez, J.-Y., White, D.J., Hartenstein, V., Eliceiri, K., Tomancak, P., and Cardona, A.** (2012). Fiji: an open-source platform for biological-image analysis. *Nature methods* **9** (7): 676–682.
- Schjoerring, J.K., Mäck, G., Nielsen, K.H., Husted, S., Suzuki, A., Driscoll, S., Boldt, R., and Bauwe, H.** (2006). Antisense reduction of serine hydroxymethyltransferase results in diurnal displacement of NH₄⁺ assimilation in leaves of *Solanum tuberosum*. *The Plant journal for cell and molecular biology* **45** (1): 71–82.
- Schopfer, P., and Brennicke, A.** (2010). *Pflanzenphysiologie* (Berlin, Heidelberg: Springer Berlin Heidelberg).
- Seltmann, M.A., Stingl, N.E., Lautenschlaeger, J.K., Krischke, M., Mueller, M.J., and Berger, S.** (2010). Differential Impact of Lipoxxygenase 2 and Jasmonates on Natural and Stress-Induced Senescence in Arabidopsis. *Plant Physiol.* **152** (4): 1940–1950.
- Shaw, P., and Brown, J.** (2012). Nucleoli: composition, function, and dynamics. *Plant physiology* **158** (1): 44–51.
- Sheard, L.B., Tan, X., Mao, H., Withers, J., Ben-Nissan, G., Hinds, T.R., Kobayashi, Y., Hsu, F.-F., Sharon, M., Browse, J., He, S.Y., Rizo, J., Howe, G.A., and Zheng, N.** (2010). Jasmonate perception by inositol-phosphate-potentiated COI1-JAZ co-receptor. *Nature* **468** (7322): 400–405.
- Shi, Y., An, L., Zhang, M., Huang, C., Zhang, H., and Xu, S.** (2008). Regulation of the plasma membrane during exposure to low temperatures in suspension-cultured cells from a cryptophyte (*Chorispora bungeana*). *Protoplasma* **232** (3-4): 173–181.
- Shishova, M.F., and Yemelyanov, V.V.** (2021). Proteome and Lipidome of Plant Cell Membranes during Development. *Russ J Plant Physiol* **68** (5): 800–817.
- Sickler, C.M., Edwards, G.E., Kiirats, O., Gao, Z., and Loescher, W.** (2007). Response of mannitol-producing Arabidopsis thaliana to abiotic stress. *Functional plant biology FPB* **34** (4): 382–391.
- Simidjiev, I., Barzda, V., Mustárdy, L., and Garab, G.** (1998). Role of thylakoid lipids in the structural flexibility of lamellar aggregates of the isolated light-harvesting chlorophyll a/b complex of photosystem II. *Biochemistry* **37** (12): 4169–4173.

- Spurr, A.R.** (1969). A low-viscosity epoxy resin embedding medium for electron microscopy. *Journal of Ultrastructure Research* **26** (1-2): 31–43.
- Stael, S., Wurzinger, B., Mair, A., Mehler, N., Vothknecht, U.C., and Teige, M.** (2012). Plant organellar calcium signalling: an emerging field. *Journal of experimental botany* **63** (4): 1525–1542.
- Steen, C.J., Morris, J.M., Short, A.H., Niyogi, K.K., and Fleming, G.R.** (2020). Complex Roles of PsbS and Xanthophylls in the Regulation of Nonphotochemical Quenching in *Arabidopsis thaliana* under Fluctuating Light. *The journal of physical chemistry. B* **124** (46): 10311–10325.
- Stepien, P., and Johnson, G.N.** (2009). Contrasting responses of photosynthesis to salt stress in the glycophyte *Arabidopsis* and the halophyte *Thellungiella*: role of the plastid terminal oxidase as an alternative electron sink. *Plant physiology* **149** (2): 1154–1165.
- Stintzi, A., Weber, H., Reymond, P., Browse, J., and Farmer, E.E.** (2001). Plant defense in the absence of jasmonic acid: the role of cyclopentenones. *Proceedings of the National Academy of Sciences of the United States of America* **98** (22): 12837–12842.
- Sui, N., and Han, G.** (2014). Salt-induced photoinhibition of PSII is alleviated in halophyte *Thellungiella halophila* by increases of unsaturated fatty acids in membrane lipids. *Acta Physiol Plant* **36** (4): 983–992.
- Sylak-Glassman, E.J., Malnoë, A., Re, E. de, Brooks, M.D., Fischer, A.L., Niyogi, K.K., and Fleming, G.R.** (2014). Distinct roles of the photosystem II protein PsbS and zeaxanthin in the regulation of light harvesting in plants revealed by fluorescence lifetime snapshots. *Proceedings of the National Academy of Sciences of the United States of America* **111** (49): 17498–17503.
- Tasseva, G., Richard, L., and Zachowski, A.** (2004). Regulation of phosphatidylcholine biosynthesis under salt stress involves choline kinases in *Arabidopsis thaliana*. *FEBS letters* **566** (1-3): 115–120.
- Tester, M., and Davenport, R.** (2003). Na⁺ tolerance and Na⁺ transport in higher plants. *Annals of botany* **91** (5): 503–527.
- Troncoso-Ponce, M.A., Cao, X., Yang, Z., and Ohlrogge, J.B.** (2013). Lipid turnover during senescence. *Plant science an international journal of experimental plant biology* **205-206**: 13–19.
- Tuomi, J.M., Voorbraak, F., Jones, D.L., and Ruijter, J.M.** (2010). Bias in the C_q value observed with hydrolysis probe based quantitative PCR can be corrected with the estimated PCR efficiency value. *Methods (San Diego, Calif.)* **50** (4): 313–322.
- Tuteja, N., and Mahajan, S.** (2007). Calcium signaling network in plants: an overview. *Plant signaling & behavior* **2** (2): 79–85.
- Tuteja, N., and Sopory, S.K.** (2008a). Chemical signaling under abiotic stress environment in plants. *Plant signaling & behavior* **3** (8): 525–536.

- Tuteja, N., and Sopory, S.K.** (2008b). Plant signaling in stress: G-protein coupled receptors, heterotrimeric G-proteins and signal coupling via phospholipases. *Plant signaling & behavior* **3** (2): 79–86.
- Umena, Y., Kawakami, K., Shen, J.-R., and Kamiya, N.** (2011). Crystal structure of oxygen-evolving photosystem II at a resolution of 1.9 Å. *Nature* **473** (7345): 55–60.
- Valitova, J.N., Sulkarnayeva, A.G., and Minibayeva, F.V.** (2016). Plant Sterols: Diversity, Biosynthesis, and Physiological Functions. *Biochemistry. Biokhimiia* **81** (8): 819–834.
- van den Brink-van der Laan, E., Killian, J.A., and Kruijff, B. de** (2004). Nonbilayer lipids affect peripheral and integral membrane proteins via changes in the lateral pressure profile. *Biochimica et biophysica acta* **1666** (1-2): 275–288.
- van Eerden, F.J., Melo, M.N., Frederix, P.W.J.M., and Marrink, S.J.** (2017). Prediction of Thylakoid Lipid Binding Sites on Photosystem II. *Biophysical journal* **113** (12): 2669–2681.
- Vick, B.A., and Zimmerman, D.C.** (1984). Biosynthesis of jasmonic Acid by several plant species. *Plant physiology* **75** (2): 458–461.
- Vieler, A., Scheidt, H.A., Schmidt, P., Montag, C., Nowoisky, J.F., Lohr, M., Wilhelm, C., Huster, D., and Goss, R.** (2008). The influence of phase transitions in phosphatidylethanolamine models on the activity of violaxanthin de-epoxidase. *Biochimica et biophysica acta* **1778** (4): 1027–1034.
- Viola, A., and Gupta, N.** (2007). Tether and trap: regulation of membrane-raft dynamics by actin-binding proteins. *Nature reviews. Immunology* **7** (11): 889–896.
- Wada, M.** (2016). Chloroplast and nuclear photorelocation movements. *Proceedings of the Japan Academy. Series B, Physical and biological sciences* **92** (9): 387–411.
- Wallis, J.G., and Browse, J.** (2002). Mutants of Arabidopsis reveal many roles for membrane lipids. *Progress in lipid research* **41** (3): 254–278.
- Wang, K., Hersh, H.L., and Benning, C.** (2016). SENSITIVE TO FREEZING2 Aides in Resilience to Salt and Drought in Freezing-Sensitive Tomato. *Plant physiology* **172** (3): 1432–1442.
- Wang, S., Uddin, M.I., Tanaka, K., Yin, L., Shi, Z., Qi, Y., Mano, J.'i., Matsui, K., Shimomura, N., Sakaki, T., Deng, X., and Zhang, S.** (2014). Maintenance of Chloroplast Structure and Function by Overexpression of the Rice MONOGALACTOSYLDIACYLGLYCEROL SYNTHASE Gene Leads to Enhanced Salt Tolerance in Tobacco. *Plant physiology* **165** (3): 1144–1155.
- Wang, Z., Anderson, N.S., and Benning, C.** (2013). The phosphatidic acid binding site of the Arabidopsis trigalactosyldiacylglycerol 4 (TGD4) protein required for lipid import into chloroplasts. *The Journal of biological chemistry* **288** (7): 4763–4771.
- Wasternack, C.** (2017). A plant's balance of growth and defense - revisited. *The New phytologist* **215** (4): 1291–1294.

- Wasternack, C., and Hause, B.** (2013). Jasmonates: biosynthesis, perception, signal transduction and action in plant stress response, growth and development. An update to the 2007 review in *Annals of Botany*. *Annals of botany* **111** (6): 1021–1058.
- Weise, S.E., Schrader, S.M., Kleinbeck, K.R., and Sharkey, T.D.** (2006). Carbon balance and circadian regulation of hydrolytic and phosphorolytic breakdown of transitory starch. *Plant physiology* **141** (3): 879–886.
- White, D.L., Andrews, S.B., Faller, J.W., and Barnett, R.J.** (1976). The chemical nature of osmium tetroxide fixation and staining of membranes by X-ray photoelectron spectroscopy. *Biochimica et Biophysica Acta (BBA) - Biomembranes* **436** (3): 577–592.
- Wollman, F.A.** (2001). State transitions reveal the dynamics and flexibility of the photosynthetic apparatus. *The EMBO journal* **20** (14): 3623–3630.
- Wu, J., Seliskar, D.M., and Gallagher, J.L.** (2005). The response of plasma membrane lipid composition in callus of the halophyte *Spartina patens* (Poaceae) to salinity stress. *American journal of botany* **92** (5): 852–858.
- Xu, C., Fan, J., and Shanklin, J.** (2020). Metabolic and functional connections between cytoplasmic and chloroplast triacylglycerol storage. *Progress in lipid research* **80**: 101069.
- Yu, C.-W., Lin, Y.-T., and Li, H.-M.** (2020a). Increased ratio of galactolipid MGDG DGDG induces jasmonic acid overproduction and changes chloroplast shape. *The New phytologist* **228** (4): 1327–1335.
- Yu, L., Nie, J., Cao, C., Jin, Y., Yan, M., Wang, F., Liu, J., Xiao, Y., Liang, Y., and Zhang, W.** (2010). Phosphatidic acid mediates salt stress response by regulation of MPK6 in *Arabidopsis thaliana*. *The New phytologist* **188** (3): 762–773.
- Yu, M., Cui, Y., Zhang, X., Li, R., and Lin, J.** (2020b). Organization and dynamics of functional plant membrane microdomains. *Cellular and molecular life sciences CMLS* **77** (2): 275–287.
- Zang, J., Zhang, T., Hussey, P.J., and Wang, P.** (2020). Light microscopy of the endoplasmic reticulum-membrane contact sites in plants. *Journal of microscopy* **280** (2): 134–139.
- Zeng, Y., Chung, K.P., Li, B., Lai, C.M., Lam, S.K., Wang, X., Cui, Y., Gao, C., Luo, M., Wong, K.-B., Schekman, R., and Jiang, L.** (2015). Unique COPII component AtSar1a/AtSec23a pair is required for the distinct function of protein ER export in *Arabidopsis thaliana*. *Proceedings of the National Academy of Sciences of the United States of America* **112** (46): 14360–14365.
- Zhang, J., Liu, H., Sun, J., Li, B., Zhu, Q., Chen, S., and Zhang, H.** (2012a). *Arabidopsis* fatty acid desaturase FAD2 is required for salt tolerance during seed germination and early seedling growth. *PLoS one* **7** (1): e30355.
- Zhang, J.-T., Zhu, J.-Q., Zhu, Q., Liu, H., Gao, X.-S., and Zhang, H.-X.** (2009). Fatty acid desaturase-6 (Fad6) is required for salt tolerance in *Arabidopsis thaliana*. *Biochemical and biophysical research communications* **390** (3): 469–474.

- Zhang, L., Kato, Y., Otters, S., Vothknecht, U.C., and Sakamoto, W.** (2012b). Essential role of VIPP1 in chloroplast envelope maintenance in Arabidopsis. *The Plant cell* **24** (9): 3695–3707.
- Zhang, M., Barg, R., Yin, M., Gueta-Dahan, Y., Leikin-Frenkel, A., Salts, Y., Shabtai, S., and Ben-Hayyim, G.** (2005). Modulated fatty acid desaturation via overexpression of two distinct omega-3 desaturases differentially alters tolerance to various abiotic stresses in transgenic tobacco cells and plants. *The Plant journal for cell and molecular biology* **44** (3): 361–371.
- Zhang, Y., Wang, L., Liu, Y., Zhang, Q., Wei, Q., and Zhang, W.** (2006). Nitric oxide enhances salt tolerance in maize seedlings through increasing activities of proton-pump and Na⁺/H⁺ antiport in the tonoplast. *Planta* **224** (3): 545–555.
- Zhao, Y., Chan, Z., Gao, J., Xing, L., Cao, M., Yu, C., Hu, Y., You, J., Shi, H., Zhu, Y., Gong, Y., Mu, Z., Wang, H., Deng, X., Wang, P., Bressan, R.A., and Zhu, J.-K.** (2016). ABA receptor PYL9 promotes drought resistance and leaf senescence. *Proceedings of the National Academy of Sciences of the United States of America* **113** (7): 1949–1954.
- Zörb, C., Geilfus, C.-M., and Dietz, K.-J.** (2019). Salinity and crop yield. *Plant biology (Stuttgart, Germany)* **21 Suppl 1**: 31–38.
- Zwiewka, M., Nodzyński, T., Robert, S., Vanneste, S., and Friml, J.** (2015). Osmotic Stress Modulates the Balance between Exocytosis and Clathrin-Mediated Endocytosis in Arabidopsis thaliana. *Molecular plant* **8** (8): 1175–1187.

6. Supplements

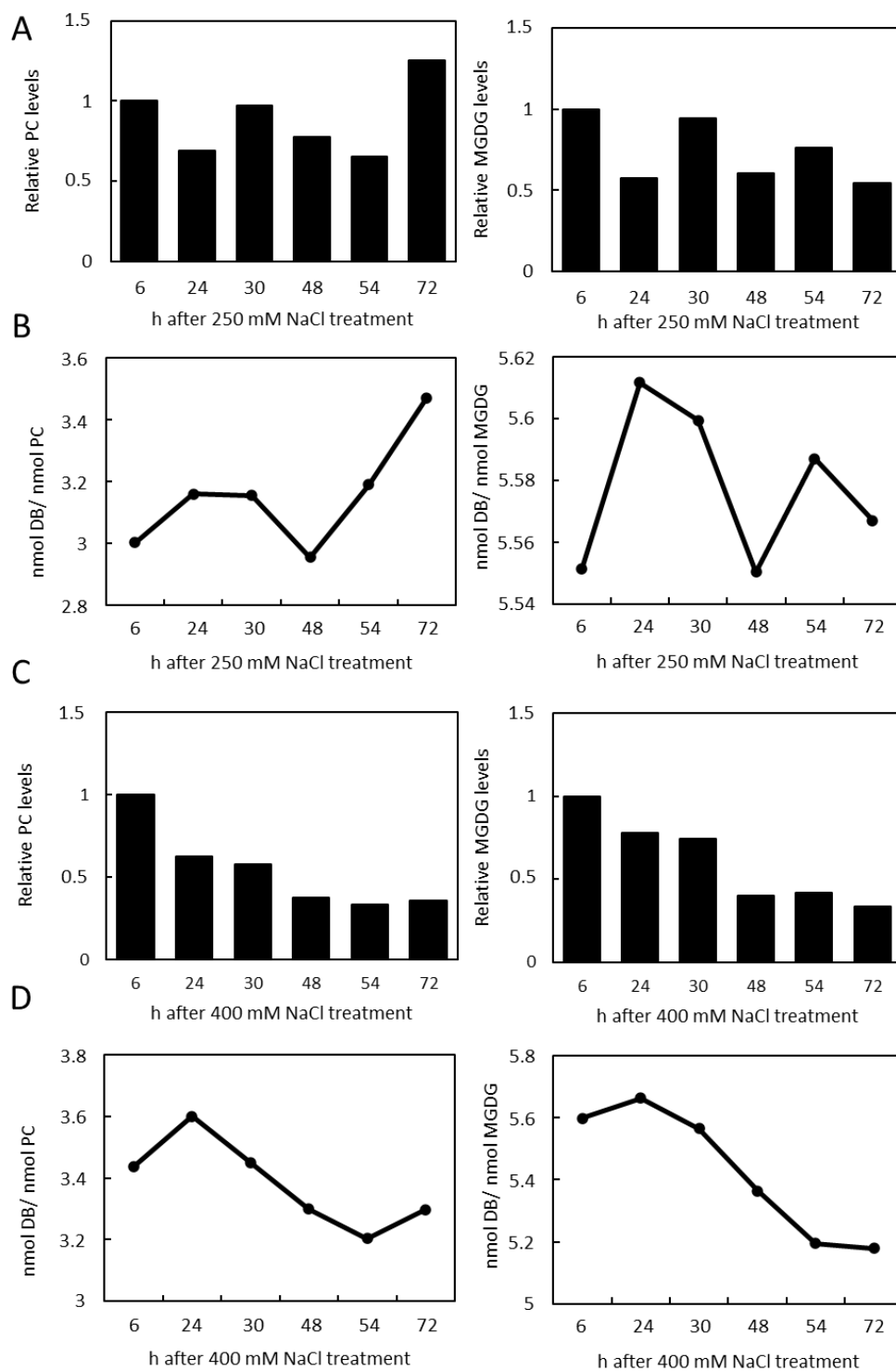


Figure 6.1.: Analysis of PC and MGDG levels of WT after long-term treatment with high salt concentrations.

Seedlings were grown for two-weeks on $\frac{1}{2}$ MS solid media and then transferred on $\frac{1}{2}$ MS solid media containing either 250 (A, B) or 400 (C, D) mM NaCl. Green tissue was harvested after 0, 6, 24, 30, 48, 54 and 72 h of treatment and prepared for lipid extraction. Lipids were extracted, separated into galacto- and

phospholipid fraction by solid phase chromatography. Thin layer chromatography was used for separation into lipid classes and isolation of phosphatidylcholine (PC) and monogalactosyldiacylglycerol (MGDG), and lipid-associated fatty acids were methyl transesterified before measured by gas chromatography. Fatty acid content per lipid was calculated using internal standard tripentadecanoin (15:0, 10 μ g), molar mass of fatty acids and fresh weight (g FW). Displayed are the fatty acid profiles of PC and MGDG after 0, 6, 24, 30, 48, 54 and 72 h after either 250 (A) and 400 (C) mM NaCl treatment of one experiment. Identified fatty acids: blue, 16:0; orange, 16:1 ^{Δ 7}; grey, 16:2 ^{Δ 7,10}; yellow, 16:3 ^{Δ 7,10,13}; light blue, 18:0; green, 18:1 ^{Δ 9}; dark blue, 18:2 ^{Δ 9,12}; brown, 18:3 ^{Δ 9,12,15}. Based on the lipid amounts and fatty acid profiles of each time point the nmol double bonds (DB)/ nmol lipids for PC and MGDG were calculated.

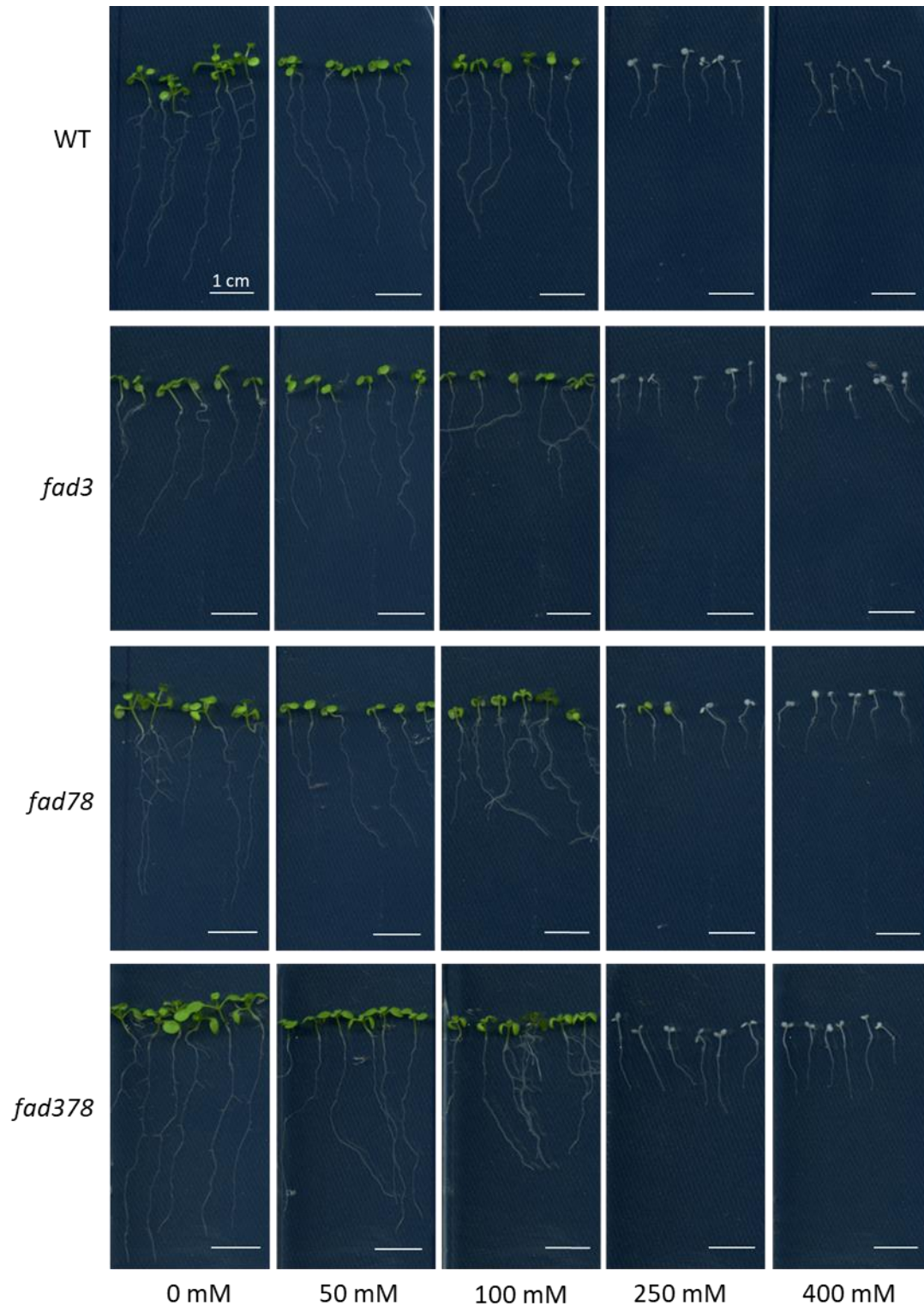


Figure 6.2.: Images of root growth of WT, *fad3*, *fad78* and *fad378* seedlings under salt stress.

Seedlings of WT, *fad3*, *fad78* and *fad378* lines were grown for four days on $\frac{1}{2}$ MS solid media before transferred on $\frac{1}{2}$ MS solid media containing either 50, 100, 250, 400 mM NaCl or no supplements (0). After seven days seedlings were documented.

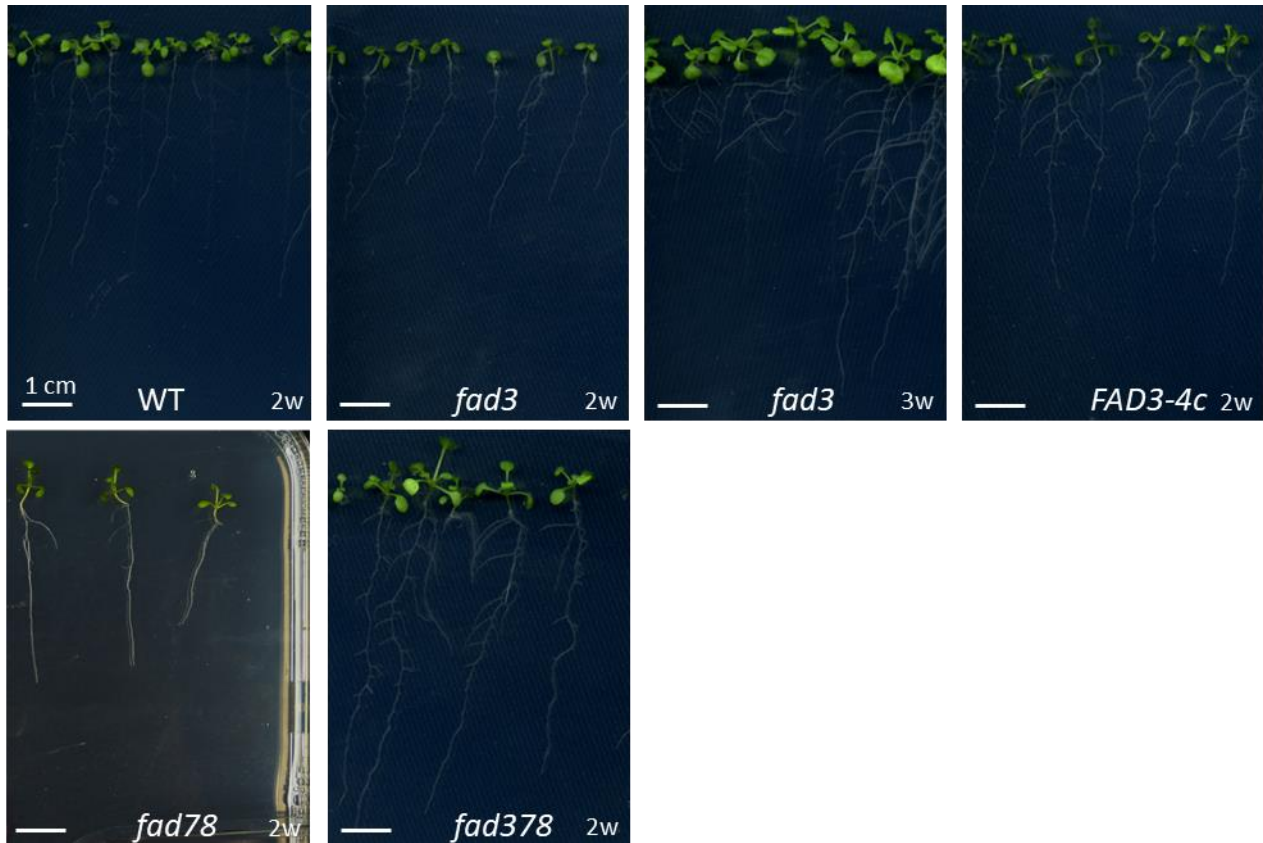


Figure 6.3.: Development of *fad* mutant seedlings.

Seedlings were grown for two weeks (WT, *fad3*, *fad3-4c*, *fad78*, *fad378*) or three weeks (*fad3*) on ½ MS solid media under short-day (8/16 h, light/dark) conditions. Scale bars = 1 cm.



Figure 6.4.: Comparison of plant rosettes between *fad* mutants.

Seedlings of WT and *fad* mutants: *fad3*, *fad78*, *fad378* were grown for two weeks on ½ MS solid media and then individually transferred on soil and grown for another seven weeks under short-day (8/ 16h, light/dark) conditions. Scale bars = 1 cm. Documented were 4-5 individual plants.

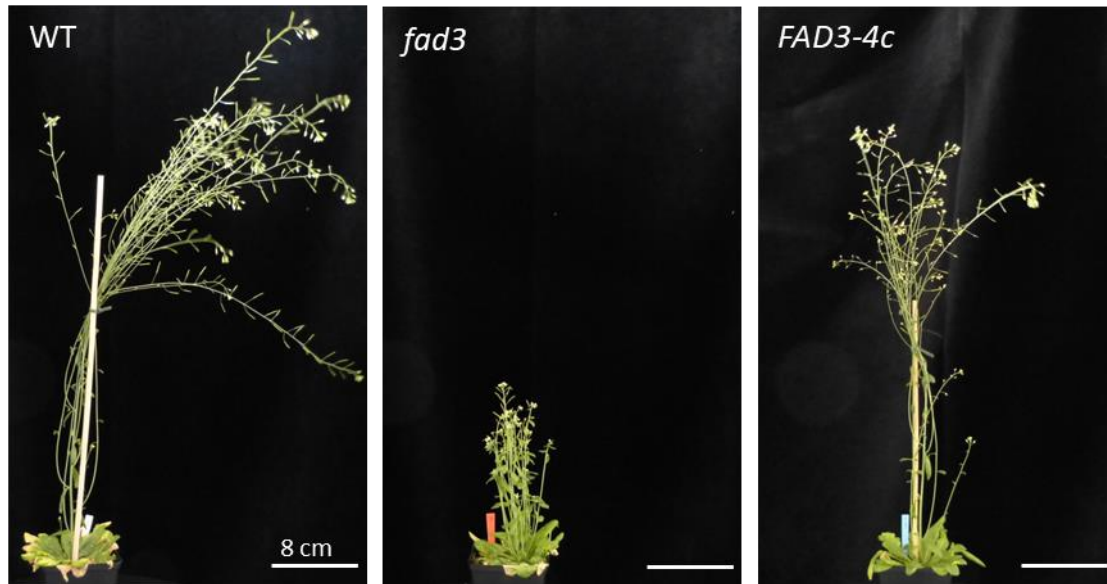


Figure 6.5.: Inflorescence state of WT, *fad3* and complemented *FAD3-4c* line.

Images of two-week-old plants were obtained from Dr. Larissa Launhardt, who also created the complemented *FAD3-4c* line. Plants were grown for two weeks on $\frac{1}{2}$ MS solid media and then individually transferred on soil to grow for seven more weeks on soil under short-day (8 h/ 16 h, light/ dark) conditions. For another five weeks plants have grown under long-day (16 h/ 8 h, light/ dark) conditions to start inflorescence. Scale bars = 8 cm. Number of documented plants: 8-10.



Figure 6.6.: Impaired development of siliques in *fad378* plant line.

Plants were grown for two weeks on $\frac{1}{2}$ MS agar plates and then individually transferred on soil for another 19 weeks under short-day (8 h/ 16 h, light/ dark) conditions. Scale bars = 1 in images showing total flower stem (left). Scale bar = 0.5 cm in magnified images of siliques (right). Documented were four individual plants.

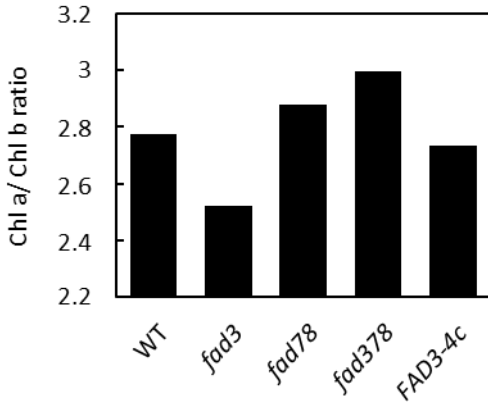


Figure 6.7.: Ratio of chlorophyll a to chlorophyll b in different *fad* mutants.

The absorbance of extracted pigments from seedlings of WT, *fad3*, *fad78*, *fad378* and *FAD3-4c* lines were photometrically measured at 663, 647 and 470 nm. Amount of chlorophyll a (Chl a) and b (Chl b) were calculated according to Lichtenthaler and Buschmann (2001). Averages of Chl a and Chl b from 2-4 independent experiments were used to evaluate Chl a/ Chl b ratio.

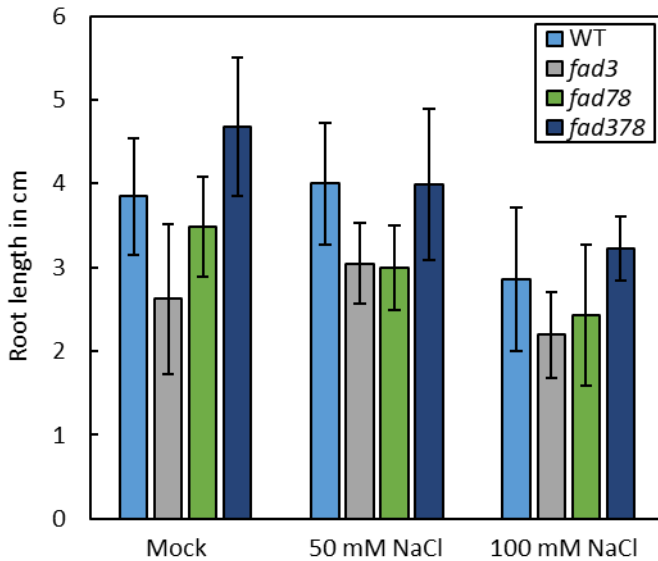


Figure 6.8.: Effect of salt on root growth of Arabidopsis *fad* mutants compared to WT.

Seedlings of WT, *fad3* (grey), *fad78* (green) and *fad378* (dark blue) lines were grown for four days on ½ MS solid media before transferred on ½ MS solid media containing either 50 mM NaCl, 100 mM NaCl or no supplements (mock). After seven days seedlings were documented, and root length measured using ImageJ software. Displayed bar chart shows mean values and standard errors from two independent experiments and 10-12 biological replicates.

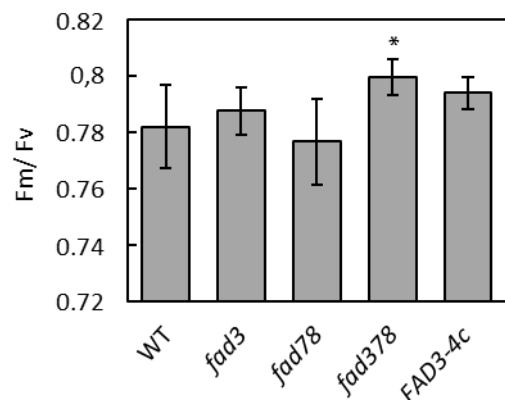


Figure 6.9.: Maximum quantum PSII efficiency in Arabidopsis WT and *fad* mutant seedlings.

First true leaves of seedlings, grown for two-weeks (WT, *fad78*, *fad378*, *FAD3-4c*) or three-weeks (*fad3*), were cut and placed on $\frac{1}{2}$ MS agar plates. Leaves were dark adapted for at least 5 min before starting with saturation pulse for 800 ms and exposed to $2400 \mu\text{mol m}^{-2} \text{s}^{-1}$. A light curve was measured with photosynthetically active radiation (PAR, in $\mu\text{mol m}^{-2} \text{s}^{-1}$) increasing from 14 to 1200 PAR in 15 steps and duration intervals of 30 s by IMAGING-PAM. The parameters Fm and Fv were recorded to calculate maximum quantum PSII efficiency at 0 PAR. Shown are mean values and standard deviations of two-eight independent experiments and 4-15 biological replicates. At least five leaves were measured for every biological replicate. Asterisks were determined using Student's *T*-test (* $P < 0,05$).

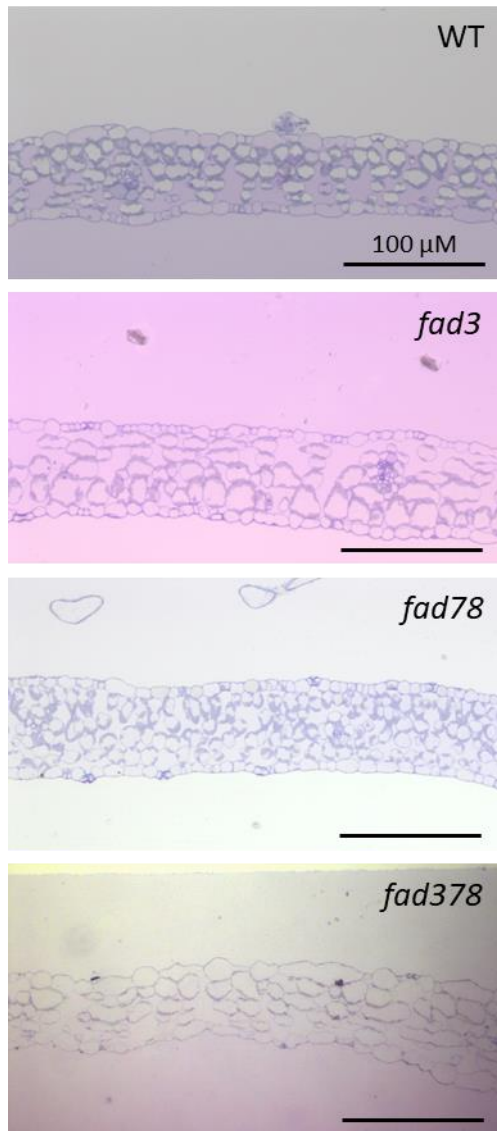


Figure 6.10.: Leaf cross sections of WT, *fad3*, *fad78* and *fad378*.

First true leaves of seedlings, grown for two-weeks (WT, *fad78*, *fad378*, *FAD3-4c*) or three-weeks (*fad3*), were as prepared for ultrastructural analyses Dr. Gerd Hause (Biozentrum Halle). Samples were cut into 1 μm wide slices, fixated on slides and dyed with 1 % toluidine blue solution. Images were acquired using Axioskop 20 (Carl Zeiss Microscopy GmbH, Jena) with the use of a 10 lens and the AxioCam MRc camera (Carl Zeiss Microscopy GmbH, Jena). Scale = 100 μm. Number of analyzed plants: 2-11.

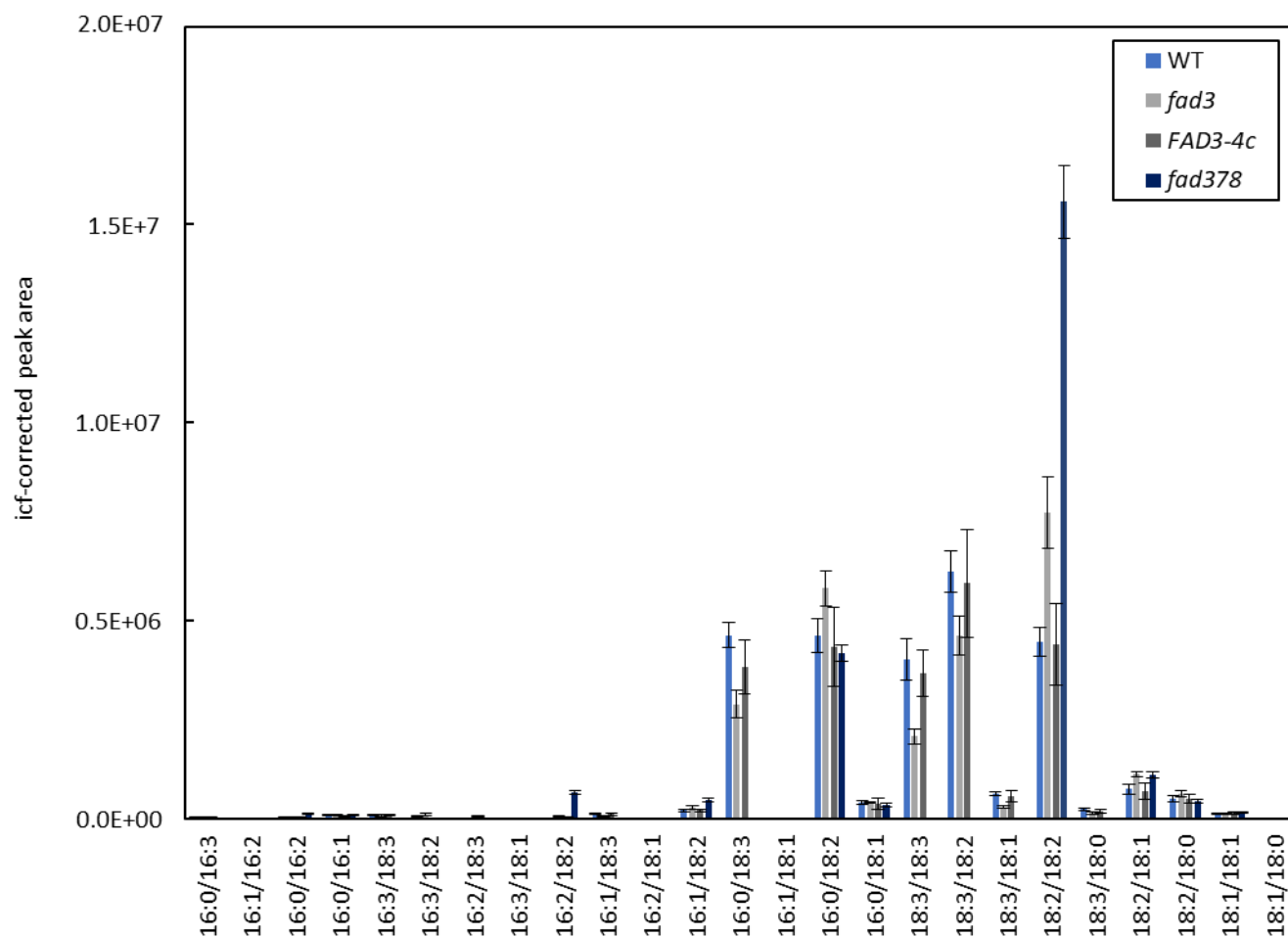


Figure 6.11.: The comparison of fatty acid species associated to PC between WT, *fad3*, *FAD3-4c* and *fad378* plant lines.

Seedlings were grown for two weeks (blue, WT; dark grey, *fad3-4c*; dark blue, *fad378*) or three weeks (grey, *fad3*) on ½ MS solid media and frozen in liquid N₂. Preparation and lipidomics analysis of PC were performed by Dr. Cornelia Herrfurth (Metabolomics Facility, AG Feußner, University Göttingen, Herrfurth et al., 2021) using UPLC-nanoESI-MS/MS. Fatty acid species are displayed with corrected absolute peak area by their isotopic corrected factor (icf) with the naturally occurring proportion of the ¹³C isotopes. Data represent means ± SD of three biological replicates from one experiment.

Statistical analysis

To determine whether the displayed results of salt treated (0.5, 1, 1.5, 2 h) and non-treated (0 min) seedlings or WT and *fad* mutants have the same mean the Student's T-test for a two tailed distribution was performed. If the calculated *p*-values were smaller than *P*<0,05, it is likely that the compared samples do not have the same mean and differ significantly from each other and were marked in the displayed graphs with "*". *P*-values even lower than *P*<0,01 or *P*<0,001 it was marked with "***" or "****", respectively. Values *P* < 0.05 are highlighted in grey.

Table 6.1.: Lipid analysis of WT seedlings after treatment with 50 mM NaCl displayed in Figures 3.3. C, D.

For Student's T-test, results of non-treated (0 h) plants were compared to results of each time point after treatment (0.5, 1, 1.5, 2 h).

	0 h	1 h	1.5 h	2 h
PC – total amount	0.726287378	0.125269685	0.17524598	0.002824324
18:3	0.482841623	0.151520845	0.121819851	0.00072687
18:2	0.800072481	0.158033916	0.272192189	0.011393769
16:0	0.82106776	0.119024264	0.167613821	0.000947268
MGDG – total amount	0.462785348	0.509897636	0.281253589	0.037024432
18:3	0.342431759	0.490434326	0.222374015	0.034415461
16:3	0.74457292	0.649943564	0.569133238	0.193756362
18:2	0.596765292	0.489969188	0.368435087	0.027033165

Table 6.2.: Saturation degree calculated from measured lipid amounts of PC and MGDG displayed in Figure 3.4. B.

The Student's T-test was performed using results of non-treated (0 h) plants were compared to results of each time point after treatment (0.5, 1, 1.5, 2 h).

	0 h	0.5 h	1 h	1.5 h	2h
PC	-	0.52826154	0.904222547	0.36405424	0.782900035
MGDG	-	0.901057801	0.589774106	0.99415497	0.319439261

Table 6.3.: Fatty composition of seeds from *fad3* and complemented line *FAD3-4c* displayed in Figure 3.6. A.

For Student's T-test, results of WT were compared to results of either *fad3* or *FAD3-4c*.

	<i>fad3</i>	<i>FAD3-4c</i>
16:0	0.013908109	0.009167743
16:1 ^{Δ7/9}	0.563941857	0.040168278
18:0	0.927696786	0.177447817
18:1 ^{Δ9}	0.735080962	0.248647478
18:1 ^{Δ11}	0.146737331	0.001966817
18:2 ^{Δ9,12}	4.73188E-18	1.31854E-05
18:3 ^{Δ9,12,15}	1.4409E-28	0.000270104
20:0	0.429366051	0.161476393
20:1 ^{Δ11}	0.057333078	0.002450567
20:1 ^{Δ13}	0.714205672	0.012251662

Table 6.4.: Basal lipid level of PC and MGDG in *fad* mutants displayed in Figures 3.6. B, C and 3.7. A, B.
For Student's T-test, results of WT were compared to results of either *fad3*, *fad78*, *fad378* or *FAD3-4c*.

	<i>fad3</i>	<i>fad78</i>	<i>fad378</i>	<i>FAD3-4c</i>
PC – total amount	0.001078131	0.083997165	0.000133458	0.378273814
18:3	0.032176464	0.121260932	n.d.	0.977032198
18:2	0.000188352	0.002383802	4.48472E-09	0.595819303
16:0	0.002235898	0.41819225	0.016027154	0.274701152
MGDG – total amount	0.007394132	0.899098058	0.158702476	0.073801827
18:3	0.008658784	1.64131E-06	n.d.	0.06122869
18:2	0.003216741	4.42679E-06	9.53941E-16	0.174960388
16:3	0.005744919	3.92196E-07	n.d.	0.027609217

Table 6.5.: Lipid analysis of *fad3* and *fad78* mutants after treatment with 50 mM NaCl displayed in Figure 3.9. A.

For Student's T-test, results of non-treated (0 h) plants were compared to results of each time point after treatment (0.5, 1, 1.5, 2 h).

	Total amount	0.5 h	1 h	1.5 h	2 h
<i>fad3</i>	PC	0.986732904	0.560815895	0.255622773	0.952330672
	MGDG	0.610328547	0.306844615	0.495871873	0.456367804
<i>fad78</i>	PC	0.54719989	0.729342278	0.872992629	0.756048708
	MGDG	0.350305487	0.596651364	0.798778258	0.738967245

Table 6.6.: Saturation degree calculated from measured lipid amounts of PC and MGDG displayed in Figure 3.9. B.

Student's T-test was performed using results of non-treated (0 h) plants were compared to results of each time point after treatment (0.5, 1, 1.5, 2 h).

		0.5 h	1 h	1.5 h	2 h
<i>fad3</i>	PC	0.812630489	0.492196097	0.217154454	0.230863949
	MGDG	0.730142957	0.579016582	0.823922463	0.972680374
<i>fad78</i>	PC	0.538595543	0.26292995	0.13267542	0.281038474
	MGDG	0.025486609	0.031603903	0.052299297	0.035437469

Table 6.7.: Basal concentration of Chl a, Chl b and Carotenoids in *fad* mutants displayed in Figure 3.10.
For Student's T-test, results of WT were compared to results of either *fad3*, *fad78*, *fad378* or *FAD3-4c*.

	<i>fad3</i>	<i>fad78</i>	<i>fad378</i>	<i>FAD3-4c</i>
Chl a	0.247706684	0.000995004	0.036166658	0.268778
Chl b	0.018594764	6.98816E-05	0.008537588	0.342871957

Carotenoids	0.115299594	0.030835529	0.178523553	0.179661
-------------	-------------	-------------	-------------	----------

Table 6.8.: Photosynthetic parameter of WT and *fad* mutants from low to high light as displayed in Figures 6.7.; 3.11.; 3.12.

For Student's T-test, results of WT were compared to results of either *fad3*, *fad78*, *fad378* or *FAD3-4c*.

	in PAR	<i>fad3</i>	<i>fad78</i>	<i>fad378</i>	<i>FAD3-4c</i>
Fm/Fv	0	0.34072832	0.898347819	0.017413939	0.080712265
Fq'/Fm'	52	0.131127598	0.260742461	0.016582706	0.114765565
	170	0.525048781	0.065252137	0.016761734	0.545292857
	580	0.61292316	0.550276355	0.252999208	0.216938035
	950	0.8103797	0.720295809	0.302177597	0.238938485
NPQ	52	0.15555974	0.151943618	0.666627321	0.813255351
	170	0.220693291	0.092788466	0.29223827	0.429379414
	580	0.048832325	0.50149147	0.51181234	0.72846661
	950	0.036661957	0.941454391	0.823279782	0.944979577

Table 6.9.: Photosynthetic parameters of WT under normal conditions and treated with either 50 or 100 mM NaCl as displayed in Figure 3.13. A-D.

For Student's T-test, results of mock treated plants were compared to results of salt treatment of either 50 or 100 mM NaCl.

	in PAR	50 mM NaCl	100 mM NaCl
Fm/Fv	0	1.64654E-06	2.76133E-11
Absorptivity	0	9.65683E-05	2.61303E-18
Fq'/Fm'	52	0.357959856	2.27786E-09
	170	9.56013E-05	3.37566E-19
	580	3.20559E-06	1.00302E-17
NPQ	52	0.00066027	0.000250377
	170	0.000605107	0.773809517
	580	0.37273964	2.09089E-08

Table 6.10.: Root length of WT and *fad* mutants under normal conditions and treated with either 50 or 100 mM NaCl as displayed in Figure 6.6.

For Student's T-test, results of WT under normal growth condition were compared to results of either *fad3*, *fad78*, *fad378* or *FAD3-4c*. And each line under mock treated was compared with results of salt treatment of either 50 or 100 mM NaCl.

	WT	<i>fad3</i>	<i>fad78</i>	<i>fad378</i>
mock	-	1.38752E-05	0.018867409	0.000364554
50 mM NaCl	0.045032064	0.026591326	0.763946013	0.138938736
100 mM NaCl	0.000106486	0.031132348	1.23639E-05	6.48394E-10

Table 6.11.: Transcript level of various genes after treatment with 50 mM NaCl displayed in Figures 3.1. B-D and 3.19.

For Student's T-test, results of non-treated (0 h) plants were compared to results of each time point after treatment (0.5, 1, 1.5, 2 h).

	0.5 h	1 h	1.5 h	2 h
<i>DREB2A</i>	0.045474736	0.741137735	0.807532481	0.9146198
<i>RD29B</i>	0.529832392	0.014525296	0.012074494	0.012108188
<i>FAD2</i>	0.757531634	0.622723611	0.509346553	0.697807372
<i>FAD3</i>	0.507506621	0.333073174	0.266931024	0.39337571
<i>MGD1</i>	0.495709595	0.639651351	0.426427518	0.295847692
<i>S40</i>	0.592012044	0.353812356	0.071276438	0.067289096
<i>SAG13</i>	0.089035009	0.110406296	0.023360214	0.082696795

Table 6.12.: JAZ10 transcript level in roots and shoots in unwounded and wounded seedlings of *fad3* and *FAD3-4c* displayed in Figure 3.17.

For Student's T-test, results of WT were compared to results of either *fad3* or *FAD3-4c*.

	<i>JAZ10</i> expression	<i>fad3</i>	<i>FAD3-4c</i>
roots	wounded	0.565024544	0.162596816
	unwounded	0.737646114	0.898497695
shoots	wounded	0.442545662	0.075592121
	unwounded	0.877211245	0.977808257

Table 6.13.: Basal oxylipin concentrations in WT and *fad* mutants as displayed in figure 3.18.

For Student's T-test, results of WT were compared to results of either *fad3* or *FAD3-4c*.

	JA	dn-OPDA	OPDA	JA-Ile
<i>fad3</i>	0.188503417	0.881689414	0.349918232	0.648236651
<i>fad378</i>	0.015143051	n.d.	0.014504065	n.d.
<i>FAD3-4c</i>	0.010894832	0.729988375	0.747698986	0.053794179

Table 6.14.: Lipid analysis of WT seedlings after treatment with 100 mM NaCl displayed in Figures 3.5.

For Student's T-test, results of non-treated (0 h) plants were compared to results of each time point after treatment (0.5, 1, 1.5, 2 h).

		0.5 h	1 h	1.5 h	2 h
Total amount	PC	0.680782755	0.721271711	0.662656571	0.356455125
	MGDG	0.888269151	0.805585883	0.412546871	0.459018121
Saturation degree	PC	0.526156251	0.647873956	0.802923316	0.889312057
	MGDG	0.751112344	0.836724938	0.435674458	0.516781821

Acknowledgement – Danksagung

Mein erstes und größtes Dankeschön geht an Prof. Ingo Heilmann. Vielen Dank, dass du mir dieses Projekt überlassen hast, auch wenn es sich etwas anders entwickelt hat, als du es dir ursprünglich vorgestellt hattest. Vielen Dank, dass du so viel Offenheit und Verständnis gegenüber meinen Ideen gezeigt hast, ich hoffe, dass es sich irgendwann auszahlen wird. Vielen Dank für die Geduld, die du mir bei Gesprächen entgegengebracht hast, ich weiß, dass es manchmal etwas schwer ist herauszufinden, auf was ich hinauswill. Generell waren die Meetings mit dir immer eine thematische Reise, bei der man am Anfang nie wusste, wo es hingehet und wie man am Ende dort gelandet ist. Dadurch hast du mich nicht nur an deinem Wissensreichtum und den Visionen teilhaben lassen, sondern hast Begeisterung und Motivation versprüht, was oft sehr hilfreich war, um Frustrationsphasen zu überstehen und fokussiert zu bleiben. Und für dein Vertrauen bin ich sehr dankbar, da es für mich selbst oft fehlt.

Meinen (voraussichtlichen) Gutachtern Prof. Kristina Kühn und PD. Rochus B. Franke möchte ich für die Zeit danken, die sie sich genommen haben, um meine Arbeit zu lesen und zu begutachten.

Der „Research Training Group 2498: Communication and Dynamics of Plant Cell Compartments“ und damit der Förderung durch die Deutschforschungsgesellschaft möchte ich für die Finanzierung danken. Den PIs und PhD Studenten innerhalb der GRK-Gemeinschaft möchte ich für den steten Austausch und das konstruktive Feedback gerade auch im Rahmen des regelmäßigen Seminars danken. Des Weiteren hat mir die Förderung ermöglicht, an zahlreichen Workshops und Seminaren teilzunehmen. Einen besonderen Dank möchte ich auch an Dr. Julia Grimmer richten, die als Koordinatorin des GRKs bei administrativen Problemen alles gegeben hat, um diese zu lösen und auch jederzeit ein offenes Ohr hatte.

Meinen Thesis Committee Members Prof. Klaus Humbeck und Dr. Debora Gasperini möchte ich erst einmal dafür danken, dass sie mir viele wertvolle Vorschläge gegeben haben und immer ansprechbar waren. Darüber hinaus bin ich ihnen dafür dankbar, dass sie mich auch experimentell unterstützt haben.

Vielen Dank Debora, dass ich von dir die Samen der *fad378* Mutante bekommen haben und du und Yunjing Ma euch die Zeit genommen habt Verwundungsexperimente an meinen Pflanzenlinien und die darauffolgenden qPCR-Analysen der *JAZ10* Transkript Abundanz durchzuführen.

Vielen Dank an Klaus, dafür dass ich regelmäßig Zugang zu deinem Labor bekommen habe und das Imaging-PAM nutzen durfte. In diesem Bezug vielen Dank an Dr. Olaf Barth, der mich bei den Durchführungen der PAM-Messungen betreut und beraten hat. Die Diskussionen über die Daten waren sehr nützlich für diese Arbeit, besonders in Bezug das Verständnis und die Interpretation.

Prof. Reimund Goss von der Universität Leipzig möchte ich dafür danken, dass er uns bei der Analyse des NPQ-Phänotyps unterstützt hat. Vielen Dank, dass du dir die Zeit genommen hast,

um die meisten der HPLC-Messungen durchzuführen und immer für Fragen und Diskussionen erreichbar warst.

Dr. Gerd Hause möchte ich für die unermüdliche Probenaufbereitung und EM-Aufnahmen meiner Pflanzenlinien danken.

Prof. Ivo Feussner von der Universität Göttingen danke ich für die ausführliche Analyse der Phytohormone und Lipidomics meiner zahlreichen Proben in den Laboren seiner Metabolomics Facility. Hierbei möchte ich noch besonders Dr. Cornelia Herrfurth als Ansprechpartnerin danken, die auch für die Probenaufbereitung und Analysen verantwortlich war.

Dr. Mareike Heilmann möchte ich dafür danken, dass ich sie bei experimentellen Problemstellungen immer fragen konnte. Gerade deine Ideen zu so manchen methodischen Durchführungen waren auf einer Weise clever, dass es für mich immer etwas Erleuchtendes hatte.

Christoph Kastner möchte ich für die tolle, gemeinsame Zeit danken, die schon während meiner Masterarbeit begonnen hatte. Vielen Dank für den starken Kaffee und den inspirierenden Austausch über biologische Vorgänge und Gott und die Welt. Für dein Verständnis, wenn mich mal wieder die Panik im Griff hatte und ich dir die doofsten Fragen gestellt habe. Ein wichtiger Ausgleich zur Arbeit haben für mich die Zock- und Shisha-Abende dargestellt. Danke!

Ich danke Johanna N. meiner Laborplatznachbarin für die vielen lustigen und emotionalen, aber auch professionellen und hilfreichen Labormomente. Vielen Dank, dass ich des Öfteren deinen Platz okkupieren durfte.

Der gesamten AG Heilmann möchte ich für die großartige Gemeinschaft danken, zu der jeder Einzelne beigetragen hat. Vielen Dank für den regelrechten Kuchenmarathon in den letzten Jahren. Ein Tag ohne Kuchen fühlt sich nicht vollkommen an. Vielen Dank Irene für die zahlreichen Hinweise. Vielen Dank an Kristin und Marion für das Ansetzen der meisten Pflanzenmedien und der Hilfe beim Finden von Laborequipment. Vielen Dank an Marta und Angela für die witzigen Situationen und die internationalen Drinking Abende. Ein großes Dankeschön auch an all meine PhD-Kollegen Franzi, Benita, Johanna U, Lennart und Nadine, die meinen Laboralltag bereichern haben. Und Larissa möchte ich nochmal besonders dafür danken, dass sie mir die *FAD3-4c*-Linie hinterlassen hat und ich einen kleinen Teil ihrer Daten in dieser Arbeit verwenden durfte.

Ein großes Dankeschön geht besonders an Anja Hähnel, die sich Tapfer über die Jahre 90 % meiner Vorträge Probe-angehört hat und mir dadurch wertvollen Input gegeben hat und mir vor allem versucht hat zu helfen, meine Vortragsweise durch mehr Übung zu verbessern.

Ich möchte Alex, Georg, Hanna und Sean, den Fehlersuchern und Probelesern dieser Arbeit, danken, dass sie ihr bestmögliches gegeben haben, um die Qualität dieser Arbeit zu verbessern.

Zu guter Letzt möchte ich meinen Freunden und meiner Familie für ihre vielfältige Unterstützung und ihr Verständnis, gerade während der besonders schwierigen Phasen, danken.

Curriculum vitae

Monique Matzner

Date of Birth: 24.04.1993

Place of Birth: Magdeburg

Nationality: German

Education

- Since 08/2019 Ph.D. as a member of the RTG 2498
Communication and Dynamics of Plant Cell Compartments
Martin-Luther-Universität Halle-Wittenberg
Department of Plant Biochemistry (Prof. Dr. Ingo Heilmann)
- 10/2017-07/2019 Master of Science in Biology
Martin-Luther-Universität Halle-Wittenberg
- 10/2013-09/2016 Bachelor of Science in Biology
Martin-Luther-Universität Halle-Wittenberg
- 2011 Abitur
Albert-Einstein-Gymnasium, Magdeburg

Publications

Fratini, Marta; Krishnamoorthy, Praveen; Stenzel, Irene; Riechmann, Mara; **Matzner, Monique**; Bacia, Kirsten et al. (2021): Plasma membrane nano-organization specifies phosphoinositide effects on Rho-GTPases and actin dynamics in tobacco pollen tubes. In: *The Plant cell* 33 (3), S. 642–670. DOI: 10.1093/plcell/koaa035.

Goss, Reimund; Schwarz, Christian; **Matzner, Monique**; Wilhelm, Christian (2021): Influence of the compatible solute sucrose on thylakoid membrane organization and violaxanthin de-epoxidation. In: *Planta* 254 (3), S. 52. DOI: 10.1007/s00425-021-03699-w.

Launhardt, Larissa; **Matzner, Monique**; Heilmann, Mareike; Heilmann, Ingo (2021): Analysis of Phosphoinositides from Complex Plant Samples by Solid-Phase Adsorption Chromatography and Subsequent Quantification via Thin-Layer and Gas Chromatography. In: *Methods in molecular biology* (Clifton, N.J.) 2295, S. 379–389. DOI: 10.1007/978-1-0716-1362-7_21

Erklärung

Hiermit erkläre ich, dass ich die vorliegende Dissertation selbständig und ohne fremde Hilfe verfasst habe, keine anderen als die angegebenen Quellen und Hilfsmittel benutzt habe und die den benutzten Werken wörtlich oder inhaltlich entnommenen Stellen als solche kenntlich gemacht habe.

Des Weiteren erkläre ich, bisher keine vergeblichen Promotionsversuche unternommen zu haben und die Dissertation in der gegenwärtigen bzw. in einer anderen Fassung nicht bereits an einer anderen Fakultät vorgelegt zu haben.

Halle (Saale), _____

Monique Matzner